The Physics of Metals and Metallography, Vol. 76, No. 3, 1993.

THEORY OF METALS

Localized and Itinerant Behavior of Electrons in Metals

S. V. Vonsovskii*, M. I. Katsnel'son*, and A. V. Trefilov**

**Institute of Metal Physics, Ural Division, Russian Academy of Sciences, ul. Kovalevskoi 18, Ekaterinburg, 620219 Russia*

***Kurchatov Institute Russian Scientific Center, pl. Kurchatova 1, Moscow, 123182 Russia*

Received March 30, 1993

CONTENTS

PREFACE

> "An answer to the questions philosophy leaves unanswered is that they should be stated differently."
>
> H.W. Hegel

In this overview, we attempt not so much to set forth finalized, firmly established results of specific studies, as to formulate in clear terms the problems related to the dual (localized-itinerant) nature of electron states in metals. We are aware that many specialists in metal physics may well see no problem here at all (we hope, however, that on reading this review they will receive enough information to change their stand). At present, it is widely believed that, given a powerful computer, one can calculate any physical properties of any metals, alloys, and compounds by state-of-the-art computational methods based on the density functional formalism. Admittedly, this belief rests on a fairly strong foundation supplied by the impressive successes scored in solid-state physics, at least with regard to ideal crystals.

The view that the density functional method is an omnipotent device carries a deep truth. According to Bohr, however, it must have the property that its converse is, likewise, a deep truth (in contrast, of course, to a trivial truth, for which its converse is an obvious falsity). In the case at hand, this deeply truthful converse assertion consists in that the band theory, as accepted at

present (see, for example, [1, 2]), is all but helpless in cases involving rather strong electron-electron interactions. In this sense, one may assert, for example, that a sufficiently narrow band is no band at all and that one should then go over to a "localized" picture. Can one name a specific quantitative measure that would pinpoint where Bloch's description [3] underlying the band theory fails? In a sense (and, of course, to a very rough approximation), one may take as a natural limit the smallest total width W of the energy d band in a pure transition d metal, namely, nickel ($W \approx 5$ eV). Actually, precisely in nickel one runs into a number of sensible troubles related to fairly strong electron correlations, such as poor agreement between calculated and experimental values for spin splitting and photoemission spectra and the occurrence of satellites in the latter. It may be thought that in d metal compounds, with $W \lesssim 4$ eV, correlation effects can cause electrons to show a strong tendency to localization. Indeed, when one comes to the properties of metals at finite temperatures, these effects can be decisive even in pure metals, that is, iron, cobalt, and nickel (see Ch. 4). If, however, a substance contains f electrons, the tendency to localization will *a priori* always exist. Of course, this does not mean to say that the results of a particular band-theoretic calculation for the rare-earth metals or their compounds may not agree with experimental data. However, such an agreement would in most cases be a matter of luck and would generally call for a special theoretical justification in each particular case. Even in cerium, where $4f$ electrons are "delocalized" the most (see Sec. 2.6), the width of the f band is of the order of 2 eV, and many-electron effects are undoubtedly important, for example, in interpreting its photoemission spectra. In the other rare-earth metals, however, the $4f$ levels are seen to have a termlike structure, definitively implying that the corresponding states have a localized, atomlike character.

Thus, in some cases a complete quantitative theory cannot be developed from "first principles," and one is forced to turn to many-electron models (or to combined approaches, such as the band theory in a tight-bonding approximation, explicitly including Hubbard's corrections). We hope that the readers interested in such models will find useful information about relevant methods and approaches in Chs. 5 and 6. On the other hand, the same category of readers will probably likewise benefit from Chs. 3 and 4; which discuss the capabilities offered by the present-day quantitative methods of the band theory. For example, it is not at all easy to explain convincingly in terms of Hubbard's model [4] why $FePd_3$ and $FePt_3$ differ in magnetic structure, but this problem is readily solvable by direct band-theoretic calculations (see Sec. 4.3).

Whereas metal theorists, most likely, will have to be convinced of the validity of the localized electron concept, the converse will probably be true of materials scientists and chemists. They have traditionally been using a language based on the views that atoms preserve their individual identities in metals and alloys and that electron states have, as a consequence, an atomlike character. Therefore, it is quite possible that the attempt we set out to make, to correlate this language with the pseudopotential [6] (see Ch. 2) and band theories [1 - 3, 5] (see Ch. 3), will not be wasted.

Lastly, a few words are in order as regards some important and interesting matters related in a way to the problem of localized and delocalized states but not touched upon in this review.

1. Polarons. In the review, we consider the possibility of electron localization and self-localization (in Sec. 5.7) owing to electron-electron interactions, with the lattice assumed to be "dead." Actually, electron-phonon interaction leading, among other things, to the formation of *polarons* is probably essential for Mott insulators, intermediate-valence systems, and other cases.

2. Disorder and nonperiodicity effects. In the review, we invariably limit ourselves to ideal crystals, thus leaving out important and interesting entities, such as metallic glasses, quasicrystals, and disordered alloys.

3. The actinides. The elements in the $5f$ row of the Periodic System distinctly differ from the $4f$ elements and the transition d metals. As to the pure actinides, the elements from thorium to neptunium (or plutonium?) are, roughly speaking, similar to the $3d$ metals (the $5f$ electrons are delocalized), and the elements from plutonium (or americium?) to the end of the series are similar to the $4f$ elements (the $5f$ electrons are localized). These elements and their compounds were not easy to study for obvious reasons; fortunately, recent years have seen a sizeable increase in accessible experimental findings.

4. Biology. The variable valence of the d elements, usually iron (Fe^{2+} or Fe^{3+}), lies at the basis of many life processes. For example, the reversible transition $Fe^{2+} \leftrightarrows Fe^{3+}$ in the enzymes called cytochromes is essential for cell respiration. The ideas and views developed by physicists in their studies of variable valence in crystals might be highly beneficial when applied in biophysics.

5. Structural phase transitions. Except for a few remarks in Ch. 3, the review does not touch upon the wide range of matters bearing on the relationship that exists between the electronic and crystal structures of metals, lattice stability and structure, and, notably, martensitic transformations. Among others, we have left out the extremely interesting and nontrivial electronic structure of γ-Fe, crucial in the martensitic transformation.

Chapter 1. INTRODUCTION

The gist of the problem of localized and delocalized electron behavior in metals is outlined and its place among the general concepts and problems of physics is defined. The history of the problem is traced from its inception immediately after the advent of solid-state quantum theory to our time.

1.1. Electron Localization and Delocalization: The General Concept

The theory of the metallic state of matter has as its objective to explain, describe, and, ideally, predict the properties of metals, their alloys, and compounds from the general principles reliably and long established by quantum mechanics and statistical physics. In this sense, the theory of metals (and, more broadly, the theory of the condensed state) is of "applied" character in comparison with the divisions of physics that deal with fundamental physical laws and stand at the forefront of science (at present, these are elementary-particle physics, high-energy physics, and some sectors of astrophysics and cosmology). This contraposition is rather arbitrary, and a number of results falling in the class of nature's fundamental laws were obtained through research on metals. Here are a few examples of this "feedback" from applied to "fundamental" forefront physics. The concept of the spontaneous breaking of symmetry, which has its origin in the theory of ferromagnetism and the theory of superconductivity (in works of Bogolyubov, Ginzburg and Landau, and other physicists), is at the same time a pivotal one in the modern physics of elementary particles (for example, it lies at the basis of Weinberg–Salam's theory of electrically weak interaction). The quark confinement, a fundamental concept of strong-interaction physics, has a very close analog in Kondo's problem related to the behavior of a magnetic impurity in a metal. (It is no coincidence that one and the same physicist, K. Wilson, substantially contributed to the solution of both problems). Lastly, resorting to the Mössbauer effect (the recoilless emission of gamma quanta by some atomic nuclei in crystals) offered the first opportunity to verify to a high degree of accuracy the slowdown of time in a gravitational field – a dramatic prediction of the general relativity theory.

In all of these cases, a solid, as a physical entity, displays a substantially many-particle character. It is precisely the interactions of atomic nuclei and electrons in the crystal, though rather simple in themselves (they reduce to the Coulomb law) but not small in magnitude, that make the task of deducing the properties of solids from known laws of physics a challenging and often intractable task.

As to metals, an especial difficulty arises in connection with the electronic subsystem because the problem of motion of atomic nuclei (or, more accurately, ions, which additionally include the electrons of the closed and slightly perturbed inner shells) "decouples itself" owing to the smallness of the so-called adiabatic parameter defined as the ratio of the mass of an electron to that of an atomic nucleus.

In fact, to obtain insight into the properties of a system of interacting electrons means to describe it in terms of effective *non*interacting species ("quasiparticles"). In most cases, this is quite feasible because the quasiparticles are similar to free electrons and differ solely in the magnitude or sign of mass (more accurately, in the form of the dispersion law) and in magnetic moment. This is what we will call the delocalized (itinerant) behavior. If, however, the interaction is sufficiently strong, it may turn out that the properties of a many-electron system can be approximated far better and more accurately if it is visualized as a multiplicity of localized quasiparticles, each of which behaves more like an electron in an isolated atom than a free electron. This is what we will call the localized behavior of electrons. In either case, however, the problem can be simplified only to a certain degree of accuracy. Indeed, it may so happen that electrons behave as delocalized (itinerant) in terms of some properties and as localized in terms of others in the same substance. In still other cases (fortunately, rather rare and exotic, such as one-dimensional chains), the concept of quasiparticles will be inapplicable in either sense. In this review, such cases will be discussed seldom, if at all.

The most "pure" examples of the itinerant and localized behavior of electrons in metals are, respectively, conduction electrons in the alkali metals and the f electrons in the rare-earth metals, except cerium. The transition d metals and especially their compounds abound in examples of the most difficult intermediate case.

From a more general point of view, the essence of the problem involving the itinerant and localized behavior of electrons in metals can be stated as follows. The "itinerant-vs.-localized" contraposition is in fact embedded in the wave–particle dualism of quantum mechanics. The ability of an electron to move without dissipating energy and momentum in an ideal crystal lattice, that is, its delocalized (band) behavior, is purely a wave property related to the diffraction of the electron on the lattice. Owing to the interaction of electrons as species that repel one another by Coulomb's law, the wave can break up, and the electron can be almost trapped in a finite region of space, that is, change to the localized state.

By Bohr's complementarity principle, the wave–particle dualism arises from the fact that one is forced to describe quantum phenomena in a classical language. Such a representation is feasible only if one resorts to mutually complementary pictures (for example, wave and particle). Similarly, one may say that the problem of the localized and itinerant behavior of electrons arises when one attempts to interpret the behavior of a substantially many-particle, strong-interaction system in a "quasielectronic" language.

In theory, one can calculate the properties of some not too complicated many-particle system without resorting to model representations (by, for example, the

quantum Monte Carlo method). Nevertheless, even in such a case, one faces the need to interpret the results thus obtained. The need for such a suggestive language is even more urgent when one considers real systems.

In cases where a purely band-theoretic description is not completely adequate, one has to admit a combination of traits of localized and itinerant behavior. Such a situation sometimes arises with *d* electrons and, even more so, with *f* electrons. Quite often (but not always), it can be demonstratively described as an outcome of the existence of some characteristic time for spin or charge fluctuations, τ_f, such that electrons show an itinerant behavior at $t \gg \tau_f$ and a localized behavior at $t \ll \tau_f$. In other words, the localized state exists for a finite time τ_f and then breaks up.

1.2. The Evolution of Views on Electron States in Metals

The first attempt to obtain insight into why the electrons in the crystal divide into the localized type and the itinerant type was made in the polar model [8 - 11]. In between the early works of Schubin and Vonsovskii in the mid-1930s and the 1960s, one should mention Peierls' fundamental remark that he made during the discussion of de Boer and Verwey's work [12] at a conference in Bristol, Mott's famous work of 1949 [13] on NiO, its "many-electron" discussion by Svirskii and Vonsovskii in 1957 [14] (see also their later works [15 - 17]), and, lastly, Hubbard's model [4], a particular case of the polar model which appeared in 1963 and has been widely used by the scientific community since then. However, no definitive answer was obtained and no unambiguous statement was formulated as to what is the main thing in the problem of Mott insulators (more generally, in the problem of metal–insulator transition) and of the correlations that arise from the polar model treatment (the so-called Hubbard correlations). These matters will be discussed in sufficient detail in the second part of this review.

When considering the general issues of the quantum theory of metals, the question inevitably arises as to why the band theory, despite its explicit one-electron character, is excellent for describing the huge assortment of properties one finds in solids. An opportunity to answer this question presented itself with the advent of Landau's theory of normal Fermi liquid [18], its generalization to the case of electrons in metals [19], and its microscopic verification (see [20]). Within this theory, it is an easy matter to show that the electron correlation does not qualitatively and radically change the thermodynamic and many kinetic properties of the electron Fermi gas; everything reduces solely to a renormalization of various parameters. The physical cause of this somewhat peculiar "insensitivity" to correlation is the fact that in a metal the electronic system is of the Fermi type and obeys the Pauli principle [2]. Thus, the band theory holds as before, with one exception. Now it concerns not only the motion of an electron in a fixed crystal potential, but also a more complex quasiparticle obeying its own dispersion law that determines all observable electronic properties of the crystal.

A relatively small number of entirely new effects show up solely in the high-frequency properties of crystals [21, 22]. Things, however, stand that way only as long as the Fermi liquid remains normal; that is, as long as the basic state of the system undergoes no radical rearrangement. This kind of rearrangement takes place, for example, when the substance changes to the superconducting state, or when magnetic order (ferromagnetic or antiferromagnetic) is established, or when various metal-insulator transitions occur. Interestingly, all of these cases strongly involve metals, alloys, and compounds containing transition (*d* or *f*) elements. It seems reasonable to think that this is probably related to the important trait noted previously in the electronic structure of many of these substances. This trait is a considerable degree of localization, almost complete, first of all, for *f* electrons and at least partial for *d* electrons, so that they retain their "atomlike" character as noted earlier. In a homogeneous electron gas (in the complete absence of localization), magnetic ordering and a metal–insulator transition might occur, at least in principle (the latter in the form of Wigner crystallization). As Monte Carlo calculations [23] showed, however, the corresponding values of electron density are unattainably small. Experience seems to indicate unambiguously that, in the case of, for example, the ferromagnetism of the iron group of metals, the system of *d* electrons displays both a collective (itinerant) and a localized behavior. Perhaps nobody doubts now that the *d* electrons of iron show a noticeable degree of itinerant behavior (see [26]). However, the existence of localized electronic magnetic moments in such a system remains a debatable issue. Here, one faces a question that stems from a well-known experimental fact – the Curie–Weiss law for the paramagnetic susceptibility of Fe, Co, and Ni is observed at above the Curie temperature. If electronic spin magnetic moments displayed a purely collective behavior, the paramagnetic susceptibility would be completely independent of temperature. Sometimes, alternative attempts are made to interpret the fact that the Curie–Weiss law is observed in ferromagnetic 3*d* metals as being related to some particular features in the electronic structure, such as, for example, *sd* hybridization, interaction with phonons, etc. (see, for example, [24]). Recently, Guletskii *et al.* [25] and Clauberg *et al.* [27] reported direct spectral findings, both optical and photoelectric, on this matter. Among other things, they demonstrated that the electronic structure of iron changes only slightly as the specimen passes through the Curie point toward the higher temperatures. This indicates that at $T > T_C$ some analog of Stoner splitting exists, which may be related to the existence of localized magnetic moments.

The situation outlined above indicates that the traditional approaches to correlation effects, notably, Landau's theory of Fermi liquid, may prove inadequate in considering the coexistence of localized and delocalized states in the electronic subsystem of metals. This is associated with two things. First, the exchange splitting of the energy spectrum in the paramagnetic phase violates the key postulate of the Landau theory that there must be a one-to-one correspondence between the states of particles and quasiparticles. Second, it is obviously important to take into account short-wave spin fluctuations because, in real space, localized magnetic moments have an atomlike character. The latter occurrence can be described in semiphenomenological terms within the modern functional integration method, such as the "static" approximation for Hubbard's model (see, for example, [28]). This enables one to relate the usual definition of local magnetic moments in terms of the Curie–Weiss law to the behavior of the electronic spectrum.

Undoubtedly, the development of spin-fluctuation theories markedly advanced the theory of the magnetic properties of metals, notably, magnetic ordering. However, this has not unraveled completely the detailed microscopic mechanism responsible for the fact that *d* electrons display features of both localized and delocalized behavior. Moreover, many questions are raised here by the fact that the original many-particle translation-invariant system is identified with a "disordered alloy" (which is the basis of the static approximation), although such a treatment is fruitful.

The quantitative band theory owes its recent significant headway to the local spin density functional method and partial consideration of correlation effects through the introduction, for example, of exchange-correlation potential [29 - 32]. True, the latter point raises a number of questions that call for further verification, although this method made it possible to calculate several complex parameters of the transition metals and of their compounds, which are in good agreement with the experiment. Among them are equilibrium lattice constants [33], the energy of formation of chemical compounds [34], elastic constants [35], and various magnetic characteristics [36, 37].

In the latter "magnetic" case, when one considers the paramagnetic phase, one essentially invokes the ideology of spin-fluctuation theories, carried over from the conventional Hubbard model [4] to the local spin-density-functional method. This approach, whereby one considers magnetic materials at finite temperatures as disordered alloys, is in fact traceable to Slater's long-time ideas [38].

Yet, for all of its successes, the solid-state quantum theory today faces the question: To what extent does the band theory, even in its "revised" modern form, take care of correlation effects? Here, two priority subquestions stand out. One is, "Can correlation effects, even as weak as they are, lead to qualitatively new effects because of some divergences?" The other is, "Can correlation effects grow so strong that the band theory, corrected as it is, will fail even as a first approximation?"

As to the first subquestion, it is noted in [39 - 41] that, if the electronic density-of-states function $N(\varepsilon)$ has narrow peaks near the Fermi level ε_F (a situation typical of alloys and compounds of the transition, especially 4*d* and 5*d*, metals), the electronic energy spectrum and, in consequence, the thermodynamic properties of the crystals may receive singular contributions as a result of virtual transitions from the peak of the $N(\varepsilon)$ curve to the Fermi level ε_F or back. These "dynamic screening" anomalies are especially accentuated in transitions between closely spaced filled and empty peaks. Formally, these anomalies imply the need to apply nonlocal corrections to the spin density functional [40].

One should bear in mind, however, that anomalous contributions of the same sign as the one-particle contributions related to the peak on the $N(\varepsilon)$ curve primarily serve to expand the domain of the singularity and sometimes to enhance it or to change its character (for more detail, see Ch. 3).

The other subquestion is related to the "catastrophe" of the present-day band theory, similar to those of its predecessors, beginning with the classical Drude–Lorentz theory [2]. Here, too, instead of hailing the truly impressive advances of the modern band theory, one must stress the necessity of a careful search for facts that explicitly contradict it and cannot be done away with through a simple "face-lifting" operation. Two such facts come to one's mind at once. The first, known for a good half-century, is the existence of Mott insulators [42, 43]. The second, of a more recent origin, is related to the discovery of 4*f* and 5*f* compounds, or heavy-electron (fermion) systems [44, 45]. Here, one runs into a new scale of electron energy. Instead of the usual energy bands 1 to 10 eV or 10^4 - 10^5 K wide, one observes narrow peaks just several hundred or even tens of Kelvins across.

Precisely these two important physical problems should serve as case histories through which one can draw the attention of those who wish to give new impetus to the quantum solid-state theory.

On the whole, no solution has yet been found to what is a crucial problem of the quantum theory of condensed system and the subject-matter of this review – the coexistence of localized and collective (delocalized) traits in the behavior of electrons in the transition metals, their alloys and compounds, although it was actually known and formulated more than fifty years ago. On the other hand, further meditations on the subject may do a lot to stimulate the evolution of views on many-particle systems in general, including systems of former valence electrons and the electrons of former *d* and *f* incompletely occupied electron shells in the metallic substances listed above. This review was intended to precisely serve this aim.

1.3. A Guide to the Chapters

As is noted in Sec. 1.1, the need to introduce the concept of localized electron states arises when one encounters rather strong electron–electron interactions. Here, it is important to differentiate between two aspects of the problem. In metals, a special role belongs

to the electrons of the partly filled shells. Therefore, one should consider the interaction of these electrons with those that are part of the ion core, on the one hand, and with one another, on the other. Hence, the first step is to define what the ion core is like and which electrons should be included in it. From the viewpoint of metal physics, the states of the completely filled electron shells are "of no interest" by themselves (except in studies of X-ray and, sometimes, optical spectra). It makes no sense to ask whether these states are of the localized or the delocalized type, because a completely filled band can be described by the Slater determinant built from either Bloch or atomic functions. Actually, the question is, "How do they affect the states of conduction electrons?" Either one of two approaches can be used to answer it. One involves the pseudopotential method, in which the ion core is treated as a "black box" having particular parameters; the other relies on the band theory, in which the core is "disassembled" completely or in part.

Then comes the question of interactions in the system of electrons belonging to unfilled shells. As long as the interactions are not too strong, one may use the band theory within the framework of what is known as the density-functional method. Effects due to a very strong interaction are currently investigated solely within simplified models.

The foregoing sets the pattern for the presentation of material. On the whole, it evolves from weak-interaction to strong-interaction systems.

Chapter 2 investigates the interaction of conduction electrons with ion cores, the applicability of the concept of pseudopotential, and the division of electrons into those belonging to the core and external electrons. It also considers the criterion of a well-defined "rigid" core (the alkali metals), and its limiting inverse – a "soft" core (cerium).

Chapter 3 considers the interaction of localized and delocalized states in terms of the band approach. It explains in detail how the difference between the two states appears in this approach.

Chapter 4 takes up the case of an interaction that is sufficiently strong to result in magnetic ordering and localized magnetic moments. Beginning with Ch. 4, resorting to the concept of localized electron behavior becomes more a matter of necessity, rather than simply of convenience.

The second part of the review, to be published in the next issue of the Journal, consists of three chapters.

Chapter 5 examines *d*-systems with an even stronger interaction and sets forth purely model approaches. It discusses the polar model of Schubin and Vonsovskii and its most popular version, the Hubbard model. Methodologically, the pivotal point is the introduction and use of the atomic representation and of its mathematical implementation, the so-called $\hat{X}$ operators. In strongly correlated (that is, strong-interaction) systems, the states of charge carriers are produced not by the usual Fermi creation and annihilation operators, but by $\hat{X}$ operators that involve a far more complex algebra (commutative and anticommutative relations).

Chapter 6 describes unusual substances, such as intermediate-valence and heavy-fermion systems, in which electrons display their dual "localized–delocalized" nature most strongly. As in Ch. 5, this chapter deals with too "hot" problems and cannot therefore claim in any way that it covers the matter fully. Nonetheless, we hope the readers will be able to pick the basic ideas in this field and to acquire preliminary knowledge that would help them take their bearings in the latest publications on the subject.

Chapter 7 concludes the review. A formal mathematical derivation of the results is not given in all cases. Where, however, it conveys an ideological message, the derivation is given, as a rule, in sufficient detail. The results of specific experiments and calculations are likewise given, solely to illustrate the key points of the presentation, such as when a "flourishing" theory fails completely (as in an attempt to describe Mott insulators within the conventional density functional scheme), or, on the contrary, when a seemingly oversimplified treatment turns out impressively successful (as with the theory of local pseudopotential for the lattice properties of the alkali metals). Each chapter starts with a historical overview and a qualitative presentation of the problem involved and is gradually "formalized."

Of course, it would be a folly to think that a small team of authors could have been able to cover all the problems listed above from all angles and within a limited space. Rather, emphasis in the review is placed on the issues associated with the authors' original works and their own views on the matters.

> "...But let your communication be, Yea, Yea'; Nay, Nay: for whatsoever is more than these cometh of evil."
>
> The New Testament, Matthew 5:37

Chapter 2. THE DIVISION INTO CORE AND DELOCALIZED ELECTRON STATES

2.1. The Ion Core and the Idea of Pseudopotential

Situations are discussed where a line can be drawn between the states of the ion core and conduction electrons with a good measure of unambiguity. Formal criteria are developed, which, when satisfied, permit one to introduce the pseudopotential as a parameter of the ion core independent of the environment (a "rigid" core). In such cases, one can develop a consistent microscopic approach and describe quite successfully a very broad range of properties for a wide gamut of metals. The converse limiting case of a "soft" core is likewise investigated. The relation between the collapse of the wave function, known from atomic physics, and the intermediate valence of cerium is discussed.

The idea to divide the electrons in metals into "core" (or "bound") electrons and "quasifree" (or conduction) electrons falls among the most fundamental ones in solid-state physics. The concept of a free electron gas in metals was first developed as far back as Drude's classical theory; then, within Frenkel's theory of "roaming" electrons; and, lastly, in Pauli and Sommerfeld's model of the ideal Fermi gas [2]. The statement of Bloch's theorem [3] and Wilson's metal-nonmetal criterion made it possible, for the first time ever, to reveal the physical causes of such a division. According to Wilson, this division fits in with the division of electrons into those belonging to partly or fully filled energy bands. A very important step was made by Peierls [5], who proposed a free-electron model, thus establishing the connection between the energy spectrum of quasifree electrons and the Fourier components of the crystal potential $V_{\mathbf{g}}$ (where $\mathbf{g}$ is the reciprocal lattice vector). Arguments supporting the applicability of this approximation to real metals were discussed, among others, by Schubin [48] (see also [11], p. 308) from an analysis of variations in the electric resistance of metals on melting.

It was not until the 1950s - 1960s that the hypothesis about the adequacy of the nearly free-electron model in some metals was directly confirmed after a systematic study of the Fermi surface for many real metals by the de Haas–Van Alphen method. (A great number of specific experiments were made by Shoenberg on the basis of the theory developed by Lifshitz and, independently, by Onsager [49, 50]). From an analysis of these findings, Harrison [6] demonstrated an unexpectedly broad applicability of the nearly free-electron approximation. This seemed more surprising because the real potential of electron-ion interaction in metals cannot obviously be small (at least because it involves bound states). The snag was removed with the advent of the pseudopotential concept [51] at about the same time. Formally, the idea of pseudopotential can be summed up as follows [6, 7, 52].

The properties of a metal are defined by the states in the conduction band, that is, in an energy interval of the order of the Fermi energy ε_F, which is a small fraction of the characteristic energies of the excited core states. Therefore, infinitely many potentials must exist, equally adequate in describing these properties: they must lead to scattering phases coincident solely within this finite energy interval. Among such potentials, one can choose those which have no bound states, that is, significantly weakened at small distances from the nuclei in comparison with the initial potentials of the ions.

An important step in the evolution of the pseudopotential concept was made when it was realized that knowledge of the detailed behavior of the wave functions of conduction electrons "inside" the ion core (that is, at small distances from the nucleus) was immaterial for a description of the properties observed in metals. Noteworthy, the idea (close to that of pseudopotential) that one need not know in detail the character of interaction in order to describe the scattering in a limited range of energies was advanced much earlier by Fermi in connection with the theory of neutron scattering on atomic nuclei [53]. A physical picture thus arises, where the metallic crystal is visualized as a crystal lattice whose sites are occupied by spherically symmetric regions, or ions, "washed by a sea" of electrons only slightly scattered on them. Moreover, the manner in which conduction electrons are scattered by these regions (ions) is determined by a "pseudopotential" whose magnitude depends on which ion occupies which lattice site and not on the crystal environment. The parameters of the pseudopotential can, in theory, be deduced from the calculated properties of the ion (for example, spectroscopically), and the task of describing the properties of the metal thus breaks up into two subtasks. In one, the objective is to "construct" pseudopotential, and in the other, to calculate the characteristics of the metal with this pseudopotential. Supposedly, one is in a position to derive a pseudopotential V_{ps} that would enable one to successfully describe (without any change in the parameters of V_{ps}) all the crystal forms of the metal, as well as the liquid phase, the properties under pressure, and even the properties of alloys and compounds containing this metal. Although this program cannot be implemented in such an all-embracing form, its realization for a series of simple metals has yielded many new physical results.

The idea of constructing V_{ps} can be illustrated best by taking as a very simple example the pseudopotential of the Heine–Abarenkov type [7]:

$$\hat{V}_{ps} = \sum_l \left[A_l \theta(r_0 - r) \hat{P}_l - \frac{Z}{r} \theta(r - r_0) \right], \qquad (2.1)$$

where $\theta(x) = 1$, $x \geq 0$, $\theta(x < 0) = 0$, Z is the charge of the ion (atomic units are used: $\hbar = m = |e| = 1$), $\hat{P}_l$ is the operator of projection onto a subspace of states with the orbital quantum number l, and r_0 is the radius of the ion core. (Schematically, the potential $V_l(r)$ acting upon a state with the specified l is shown in Fig. 2.1). The parameters r_0 and A_l should be specified so as to describe the energy levels ε_{nl} of a free ion (here, n is the principal quantum number). The potential $\hat{V}_{ps}$ in (2.1) is nonlocal (unless the A_l are the same for all l). Because of this, the matrix element of $\hat{V}_{ps}$ on plane waves $\langle \mathbf{k} | \hat{V}_{ps} | \mathbf{k} + \mathbf{q} \rangle$ is a function of both $\mathbf{k}$ and $\mathbf{k} + \mathbf{q}$, and not only of $\mathbf{q}$, as is the case with the usual potential scattering. Moreover, the constants A_l and, in consequence, $\hat{V}_{ps}$, may be chosen energy-dependent. These are first-principle pseudopotentials, because they use solely information about the properties of a free ion (atom) and not about those of the metal itself. At present, far more elaborate techniques are used to construct the first-principle $\hat{V}_{ps}$ (see, for example, [54, 55]), and the properties of metals are calculated *ab initio* by using various $\hat{V}_{ps}$ [54 - 58]. Unfortunately, at present, these approaches cannot be used to calculate the more complex parameters of the crystal, such as thermodynamic

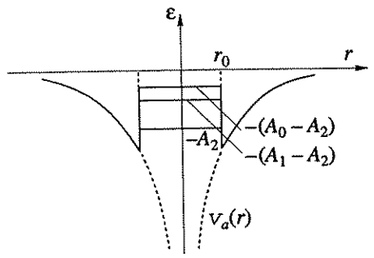

Fig. 2.1. *Illustrating the Heine–Abarenkov pseudopotential ($A_{l>2} = A_2$); $v_a(r)$ is the atomic potential.*

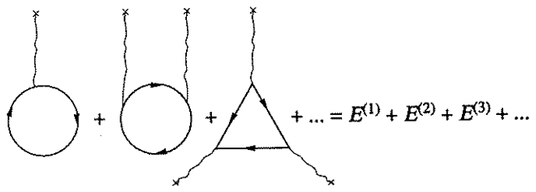

Fig. 2.2. *Diagrams for $E^{(1)}$, $E^{(2)}$, and $E^{(3)}$, with electron–electron interaction neglected.*

properties and anharmonicity effects. The point is that they involve a prohibitive amount of computations, which presume, among other things, a self-consistent solution of the Schrödinger equation with $\hat{V}_{ps}$ at every step.

In some cases, however, it proves more efficient to use a far simpler approach, based on the theory of perturbations in $\hat{V}_{ps}$. As already noted, the almost free-electron approximation often proves quite good in describing the shape of the Fermi surface (in any case, for simple metals). This prompted Harrison [6], in the early 1960s, to make an attempt at calculating the total energy of the metal and the associated quantities (for example, pressure and bulk modulus) in the form of a series expansion in $\hat{V}_{ps}$. His results appeared fairly encouraging, and this stimulated rapid advances in the relevant theory [6, 7]. This was stated in a most consistent form and with due regard to many-electron effects and higher order perturbations in $\hat{V}_{ps}$ (up to the third order) in [46]. We give the derivation of the expansion for the total energy E of the metal in the case of a nonlocal $\hat{V}_{ps}$ that is independent, however, of the energy of the electron.

The series expansion of E in terms of V_{ps} takes the form

$$E = E^{(i)} + E^{(0)} + E^{(1)} + E^{(2)} + \ldots, \qquad (2.2)$$

where $E^{(n)}$ ($n = 1, 2, \ldots$) is the energy of the nth order with respect to V_{ps}, and $E^{(i)}$ is the Madelung energy of electrostatic interaction between point ions in a homogeneous electron gas that ensures electroneutrality

$$E^{(i)} = -\frac{Z^2\alpha_M}{2\Omega_0^{1/3}}. \qquad (2.3)$$

Here, Z is the charge of the ion; Ω_0 is the volume per atom; α_M is a structure-dependent factor (see, for example, [6]);

$$E^{(0)} = Z\frac{3}{5}\varepsilon_F - \frac{3}{4\pi}k_F + E_c(r_s), \qquad (2.4)$$

is the energy of a homogeneous electron liquid ($\varepsilon_F = k_F^2/2$), and $E_c(r_s)$ is its correlation part, dependent on $r_s = (3\Omega_0/4\pi Z)^{1/3} = (9\pi/4)k_F^{-1}$ (the first two terms describe the kinetic energy of the free-electron gas and the exchange energy in the Hartree–Fock approximation [2]). At present, the following interpolation formula is believed to be most adequate for $E_c(r_s)$:

$$E_c(r_s) = \begin{cases} -\dfrac{Z}{2}\dfrac{0.1471}{1 + 1.1581\sqrt{r_s} + 0.3446 r_s}, & r_s \geq 1, \\ \dfrac{Z}{2}\left[\dfrac{0.0311}{r_s} + 0.0014\,(1 + \ln r_s) - 0.0108\right], & r_s < 1, \end{cases} \qquad (2.5)$$

derived from numerical calculations [23] by the quantum Monte Carlo method. On neglecting electron–electron interaction, the diagrammatic expressions for $E^{(n)}$ ($n = 1, 2, 3$) take the form shown in Fig. 2.2, where the full line represents the electronic Green's function [20], and the wavy line with a cross represents V_{ps}. Consideration of the electron–electron Coulomb interaction (the dashed line) in the graph for $E^{(1)}$ leads to the replacement of the free-electron Green's function G_0 by its exact equivalent G and to the following result [46]:

$$E^{(1)} = \sum_{\mathbf{k}} V_{\mathbf{k},\mathbf{k}} n_{\mathbf{k}}, \qquad (2.6)$$

where $n_{\mathbf{k}}$ is the exact distribution function of electrons with a quasimomentum $\mathbf{k}$ [for free electrons, $n_{\mathbf{k}}^0 = \theta(k_F - |\mathbf{k}|)$]. For a local pseudopotential [$V_{\mathbf{k},\mathbf{k}+\mathbf{q}} = V_{ps}(\mathbf{q})$], we have

$$E^{(1)} = \frac{bZ}{\Omega_0}; \qquad (2.7)$$

$$b = \Omega_0 \lim_{\mathbf{q}\to 0}\left[V_{ps}(\mathbf{q}) + \frac{4\pi Z}{\Omega_0 q^2}\right]. \qquad (2.8)$$

Here, b is the "forward" scattering amplitude minus the Coulomb term balanced out owing to electroneutrality; for the hydrogen atom (a point ion), $b = 0$.

Consideration of electron–electron interaction in $E^{(2)}$ brings with it various inserts in the diagrams and the need to take the sum over the series shown in Fig. 2.3, where the shaded rectangle $\hat{\Gamma}$ (see Fig. 2.4) is the scattering amplitude of a particle and a hole, irreducible in terms of the "longitudinal" Coulomb interaction, and $\hat{\tilde{v}}$ (see Fig. 2.5) is the scattering amplitude of a particle and a hole, irreducible in terms of both particle–hole and longitudinal Coulomb interactions [59]. For a local pseudopotential,

$$R(q) = |V_{ps}(q)|^2\Pi(q), \quad T(q) = V_{ps}(q)\Pi(q).$$

Explicit expressions for energy in the case of a nonlocal $\hat{V}_{ps}$ can be obtained only in what is known as the local field approximation [46], where it is assumed that $\hat{\tilde{v}}$ depends solely on the transmitted 4-momentum $q = (\omega, \mathbf{q})$ (where $\mathbf{q}$ is the wave vector and ω is the frequency subsequently assumed to be $\omega = 0$), and not on all terminal 4-momenta. With this approximation, one is in a position to reduce the integral equation shown diagrammatically in Fig. 2.4 to an algebraic one. Then, one has

$$\Gamma(\mathbf{q}) = \frac{\tilde{v}(\mathbf{q})}{1 - \tilde{v}(\mathbf{q})\Pi_0(\mathbf{q})}, \qquad (2.9)$$

where $\Pi_0(\mathbf{q})$ is the Lindhardt polarization operator (an "empty loop") equal (see, for example, [7]) to

$$\Pi_0(\mathbf{q}) = \sum_{\mathbf{k}} \frac{n_{\mathbf{k}} - n_{\mathbf{k}+\mathbf{q}}}{\varepsilon_{\mathbf{k}+\mathbf{q}}^0 - \varepsilon_{\mathbf{k}}^0} = \frac{k_F}{\pi^2}\left[\frac{1}{2} + \frac{4k_F^2 - q^2}{8k_F q}\ln\left|\frac{2k_F + q}{2k_F - q}\right|\right], \qquad (2.10)$$

where k_F is the Fermi wave vector, and $\varepsilon_{\mathbf{k}}^0 = k^2/2$ is the energy of an electron. The function $\tilde{v}(\mathbf{q})$ is usually written as

$$\tilde{v}(\mathbf{q}) = v_c(\mathbf{q})G(\mathbf{q}), \qquad (2.11)$$

where $v_c(\mathbf{q}) = 4\pi/q^2$ is the Fourier component of Coulomb electron–electron interaction, and for the function $G(\mathbf{q})$ various approximate expressions are known to exist. For example, in a most fitting approximation [60], the expression for $\Pi(\mathbf{q})$, related to $G(\mathbf{q})$ by (2.12) (see below), is found by adding together diagrams up to the second order with respect to $v_c(\mathbf{q})$, and the result thus obtained is then corrected using the exact asymptotics for $\mathbf{q}$ tending to zero.

Consider the exact electron polarization operator $\Pi(\mathbf{q})$ (see Fig. 2.4), which appears in Fig. 2.3. From Fig. 2.5 and subject to (2.11), one has $\Pi = \Pi_0 - \Pi_0 v \Pi_0 + \ldots$, that is,

$$\Pi(\mathbf{q}) = \frac{\Pi_0(\mathbf{q})}{1 - v_c(\mathbf{q})G(\mathbf{q})\Pi_0(\mathbf{q})}. \qquad (2.12)$$

Then, introducing the permittivity

$$\varepsilon(q) = 1 + v_c(q)\Pi(q) \qquad (2.13)$$

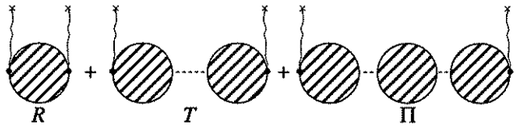

Fig. 2.3. *Diagrams for $E^{(2)}$ with allowance for electron–electron interaction.*

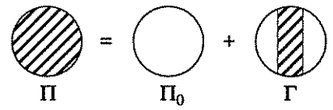

Fig. 2.4. *Expression for the polarization potential Π in terms of particle and hole scattering amplitude Γ.*

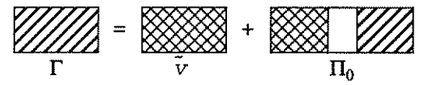

Fig. 2.5. *Expression for Γ in terms of the "twice irreducible" amplitude $\tilde{v}$.*

and "elementary" blocks

$$R_0(\mathbf{q}) = \sum_{\mathbf{k}} |V_{\mathbf{k},\mathbf{k}+\mathbf{q}}|^2 \frac{n_{\mathbf{k}}^0 - n_{\mathbf{k}+\mathbf{q}}^0}{\varepsilon_{\mathbf{k}+\mathbf{q}}^0 - \varepsilon_{\mathbf{k}}^0}; \qquad (2.14)$$

$$n_{\mathbf{k}}^0 = \theta(k_F - |\mathbf{k}|),$$

$$T(\mathbf{q}) = \sum_{\mathbf{k}} V_{\mathbf{k},\mathbf{k}+\mathbf{q}} \frac{n_{\mathbf{k}}^0 - n_{\mathbf{k}+\mathbf{q}}^0}{\varepsilon_{\mathbf{k}+\mathbf{q}}^0 - \varepsilon_{\mathbf{k}}^0}, \qquad (2.15)$$

we have

$$R = R_0 + T_0\Gamma T_0, \quad T = T_0 + T_0\Gamma\Pi_0. \qquad (2.16)$$

As a result, for the contribution $E^{(2)}$ described by the sequence of diagrams in Fig. 2.3, one has

$$E^{(2)} = -\frac{\Omega_0}{2}\sum_{\mathbf{g}}{}' |S(\mathbf{q})|^2 F(\mathbf{q}),$$

$$F(\mathbf{q}) = R(\mathbf{q}) - v_c(\mathbf{q})G(\mathbf{q})\frac{|T(\mathbf{q})|^2}{\varepsilon(\mathbf{q})}; \qquad (2.17)$$

$$R(\mathbf{q}) = R_0(\mathbf{q}) + \frac{v_c(\mathbf{q})G(\mathbf{q})|T_0(\mathbf{q})|^2}{1 - v_c(\mathbf{q})G(\mathbf{q})\Pi_0(\mathbf{q})},$$

$$T(\mathbf{q}) = \frac{T_0(\mathbf{q})}{1 - v_c(\mathbf{q})G(\mathbf{q})\Pi_0(\mathbf{q})},$$

where $\mathbf{g}$ are the vectors of the reciprocal lattice (the prime on the sum implies that $\mathbf{g} \neq 0$), and

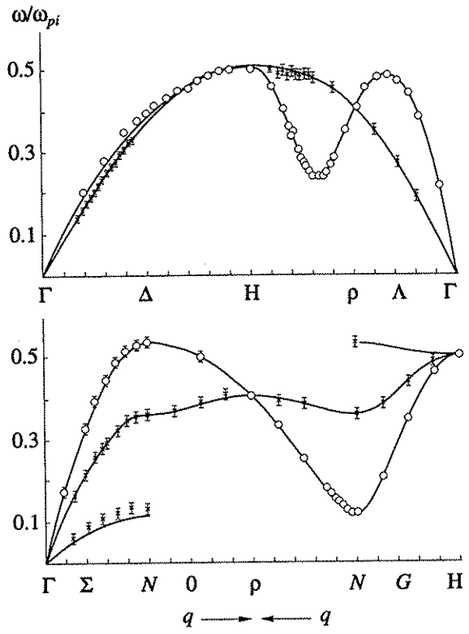

Fig. 2.6. *Phonon spectrum of sodium. The full lines are calculated dispersion curves, and the dots represent experimental data. The frequency ω is expressed in units of plasma ionic frequency ω_{pi} (for Na, $\hbar\omega_{pi}$ = 342.8 K).*

$S(\mathbf{q}) = \frac{1}{\nu}\sum_{j=1}^{\nu-1} e^{i\mathbf{q}\boldsymbol{\rho}_i}$ is the structure factor ($\boldsymbol{\rho}_i$ are the basis vectors in a unit cell with ν atoms). The expressions for local $\hat{V}_{ps}$ are greatly simplified

$$E^{(2)} = -\frac{\Omega_0}{2}\sum_{\mathbf{g}} |S(\mathbf{q})|^2 F(\mathbf{q}),$$

$$F(\mathbf{q}) = |V_{ps}(\mathbf{q})|^2 \frac{\Pi(\mathbf{q})}{\varepsilon(\mathbf{q})}; \qquad (2.18)$$

$$R_0(\mathbf{q}) = |V_{ps}(\mathbf{q})|^2 \Pi_0(\mathbf{q}),$$

$$T_0(\mathbf{q}) = V_{ps}(\mathbf{q})\Pi_0(\mathbf{q}).$$

This is an exact expression for local $\hat{V}_{ps}$ (that is, it can be derived without resorting to the local-field approximation [46]).

The higher order diagrams with respect to $\hat{V}_{ps}$, shown in Fig. 2.2, may be discarded if $|V_{ps}(\mathbf{q})| \ll \varepsilon_F$. Then, one has a closed expression for the total energy of the metal, (2.2) - (2.6), (2.18). By differentiating it with respect to deformation parameters, or atom displacements, one can obtain the applicable equation of state, elastic constants, phonon spectra, thermodynamic parameters, etc. Let us see how successful this program can be when applied to several specific metals.

2.2. Pseudopotential, Valence, and Chemical Bonding in Metals

When discussing the applicability of the pseudopotential concept to real entities, it is natural to begin with the alkali metals. They may be regarded as a base reference from the viewpoint of the simplicity of chemical bonding. Their electronic structure is ultimately simple, and the experimentally determined Fermi surface comes very close to spherical [61]. Under normal pressures, they have a bcc structure typical of metals near the melting point. Lithium and sodium undergo a low-temperature phase transition to a hcp (9*R*) structure [62]. For this reason, they can be used as an example on which to verify how accurately the properties of various crystalline phases are described with the aid of a "unified" pseudopotential. Lastly, because the alkali metals have a low melting point and a high compressibility (a relatively small bulk modulus), their properties were well studied in the liquid phase and under heavy compressions.

Following the suit set by Vaks and Trefilov [63], consider the simplest model, that of a local pseudopotential of the Animalu–Heine type (ξ = 0.03)

$$V_{ps}(q) = -\frac{4\pi Z}{\Omega_0 q^2}\left[\cos qr_0 - \nu\left(\frac{\sin qr_0}{qr_0} - \cos qr_0\right)\right] \times \exp\left(-\xi\left(\frac{q}{2k_{F_0}}\right)^4\right). \qquad (2.19)$$

Leaving out the last factor (introduced to improve the convergence in calculating the sums over the reciprocal lattice; k_{F_0} is the Fermi momentum at zero pressure and temperature), (2.19) is the Fourier transform of the local potential (2.1)

$$V_{ps}(r) = \frac{Z\nu}{r_0}\theta(r_0 - r) - \frac{Z}{r}\theta(r_0 - r). \qquad (2.20)$$

In contrast to the transition metals, the alkali metals pose no problem with the choice of the charge (valence) of the ion; it is $Z = 1$. It is important to dwell on the choice of the parameters ν and r_0. Generally speaking, the form of the pseudopotential defined by (2.19) and (2.20) is clearly too oversimplified for one to be able to determine the parameters from the properties of a free atom (ion). The point is that this is a local pseudopotential, whereas all known techniques for constructing first-principle pseudopotentials lead to nonlocal V_{ps}. However, one may relax accuracy requirements for a description of detail in the electronic spectrum if one limits oneself to the lattice properties (pressure, phonon spectrum, elastic constants, etc.) deducible in the final analysis from the total energy – a quantity integrated with respect to the electronic spectrum. If, furthermore, one opts to determine ν and r_0 by the physically reasonable procedure of fitting to the experimental values of physical properties, one may expect to make up for inaccuracies in the original statement of the model. Then the validity test for the model would be its ability to describe the largest possible range of lattice properties for the same values of these two parameters. As is shown in [63], for the alkali metals, the optimal procedure of determining V_{ps} is the one proposed earlier in [46]

$$p(\Omega_0) = 0; \quad C_{44} = C_{44}^{\exp}, \qquad (2.21)$$

where Ω_0 is the experimentally found volume (per atom) at zero pressure p, and C_{44} and $C_{44}^{\exp}$ are the calculated and experimental values of one of the shear moduli. For the screening function $G(q)$ [see (2.12)], the best choice is the approximation used in [60]. Note that, with the other simple local expressions reported for $V_{ps}(q)$ and $G(q)$ in the literature, the properties of the alkali metals are described less successfully than with the model (2.19).

It was shown in [63, 65 - 67] that, within the proposed model, the largest possible set of atomic, thermodynamic, and anharmonic properties of the alkali metals can be described with an accuracy in no way inferior to state-of-the-art experiments. Among other things, the investigators were able to calculate such fine properties of the crystal lattice as the thermal expansion coefficient, anharmonic frequency shifts and damping of phonons, the heat of the martensitic structural transition in sodium, the structure factor, and the thermodynamic properties of the liquid phase, and to derive the equation of state at finite temperatures. The most illustrative of the results are given in Figs. 2.6 through 2.15.

Against the background of the overall precision of the experiment, one's attention is immediately drawn to the qualitatively improper behavior of the phase diagram for lithium under pressure (in contrast to sodium) (see Fig. 2.12). The physical causes of this occurrence will be discussed in Ch. 3. Another point worthy of mention is the discrepancy between theory and experiment in the equation of state for sodium under a pressure of about 1 Mbar and, similarly, for other alkali metals (Fig. 2.11). Quite likely, such pressures might cause changes in the very properties of the ion core (see Sec. 2.4).

One is prompted to wonder if it is not a lucky chance that the lattice properties can be described so well within the framework of such a simple model. The answer is "no." For one reason, this success by itself supports the possibility of using V_{ps} as a characteristic of an individual ion. Why this is so will be discussed in Sec. 2.4. For another, what is involved is a specific form of the pseudopotential (2.20) with the ion core having a "sharp edge" at $r = r_0$ [because of the smallness of the smoothing exponential factor in (2.19)]. Figure 2.16 gives the electron density distribution ρ(**r**) in metallic sodium obtained by first-principle band-theoretic calculations [68]. As is seen, the hypothesis that the ion core has a sharp edge is physically tenable. Finally, one is concerned with the applicability of the

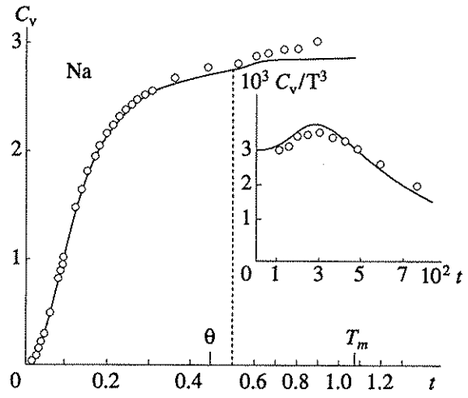

Fig. 2.7. *Heat capacity of bcc sodium. The full lines are calculated curves, and the dots represent experimental data. $t = T/\hbar\omega_{pi}$; θ is the Debye temperature, T_m is the melting point (for Na, θ = 152.5 K, T_m = 370.7 K).*

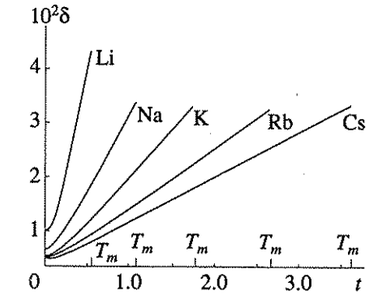

Fig. 2.8. *Mean-square displacement of atoms, $\overline{x^2(T)}$, in the alkali metals in relative units: $\delta(T) = 4\overline{x^2(T)}/d^2(T)$, where d(T) is the nearest-neighbor distance with allowance for thermal expansion; $t = T/\hbar\omega_{pi}$; the curves are drawn as far as T_m of the corresponding metals.*

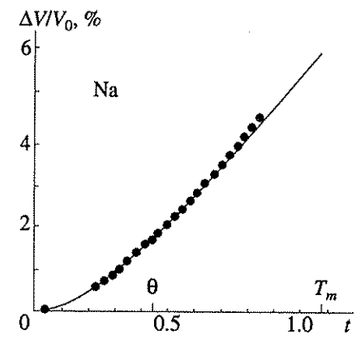

Fig. 2.9. *Thermal expansion of sodium, $\Delta V/V_0 = (V(T) - V_0)/V_0$, where V_0 is the atomic volume (V_0 = 254.5 a.u.). The full lines represent calculated data, and the dots, experimental data.*

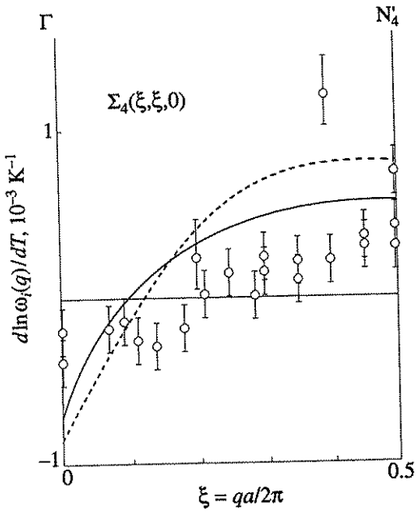

Fig. 2.10. *Derivative of the relative frequency shift $d\ln\omega_i/dT$ with respect to temperature for the phonons of the $\Sigma_4(q, q', 0)$ branch in the bcc phases of sodium and lithium. The full line is the theoretical curve for sodium, the dashed line is the theoretical curve for lithium; circles represent experimental data.*

theory of perturbations in V_{ps}. This is validated by the fact that an explicit calculation of contributions of the third order with respect to V_{ps}, discarded in the model in question, proves their smallness [69]. Note that, from the viewpoint of the nature of chemical bonding, the third and higher order pseudopotential terms describe the effects associated with nonpairwise ion interaction, that is, with covalency [7]. In this sense, the applicability of the model in question to the alkali metals implies the possibility of introducing pairwise potentials $\varphi(r)$ (see Fig. 2.13). These are, however, strongly dependent on electron density, that is, volume – a feature that sets metals apart from, for example, ionic crystals. This explains, among other things, why metals violate the Cauchy relations for the elastic constants [46].

Experience with calculations by the perturbation theory in terms of local pseudopotential demonstrates its limited capabilities in the sense that, for all metals, except the alkali metals, it either fails completely or describes only some of the lattice properties and to a significantly lower accuracy than for sodium. For example, in the case of Ca and Sr, one of the shear moduli calculated within this model even turns negative [70], whereas in the case of Al, a poor result is obtained for the bulk modulus [46]. For Pb, as follows from our calculations, the discrepancy between the theoretical and experimental values of some phonon frequencies is as great as 25%. In some cases, it is possible to find out why the model gives a poor fit and to remove the causes. In Ca, for example, the discrepancy is traceable to the rearrangement of the electronic spectrum near the Fermi surface because it touches the faces of the Brillouin zone (see Ch. 3); after proper care was taken of the corresponding contributions to the total energy, the description of the lattice properties becomes fairly accurate, even within the pseudopotential model [70]. In most cases, however, the causes of the impediments are not so easy to remove. Thus, for the transition metals, one does not even know the exact valence of ions, Z, or, in other words, to what extent the *d* electrons must be regarded as being part of the ion core or treated as quasifree. This might sound somewhat naive because the present-day band theory need not know this distinction at all. However, this kind of skepticism will remain justified as long as first-principle approaches are unable to yield as diverse information, for example, as shown in Figs. 2.6 through 2.15. That is why attempts are still being made to construct efficient pseudopotential models for the transition metals. As Vaks *et al.* [71] and Greenberg *et al.* [72] showed, it is possible to apply to the transition metals Ti, Zr, Ni, Cu, Fe, and Ir a model that uses a pseudopotential of the type (2.19) and takes into account $\hat{V}_{ps}$ terms up to the second order. This model gives a fairly accurate description of the equilibrium volume, phonon spectra, and structure factor in the liquid phase for some, generally nonintegral, values of Z (see Table 2.1). An important fact is that the properties of fcc metals (Ni, Cu, and Ir) are described significantly better than those of bcc metals (α–Fe, β–Ti, and β–Zr), whereas in the case of polymorphous metals (for example, Ti and Zr), the properties of the hcp phase are defined better than those of the bcc phase. In turn, among the fcc metals, the properties of a 5*d* metal (Ir) are described substantially better than those of the 3*d* metals. Finally, a successful description of all the properties of the above metals, except Ir, is feasible for $Z \approx 2$, and those of Ir for $Z = 4.5$. The last point may be regarded as an indication that, when it comes to describing the lattice properties, the 3*d* electrons in the 3*d* metals behave as the "core" electrons because $Z = 2$ roughly corresponds to the number of *s* and *p* electrons. This fact deserves a more detailed discussion.

Table 2.1. Effective ion charge in the pseudopotential description of the properties of the transition and noble metals

Metal	Z
Ti	2.0
Zr	2.0
Fe	1.95
Ni	1.50
Cu	1.50
Ir	4.50

Figure 2.17 gives the density distribution for *s*, *p*, and *d* electrons in metallic vanadium as found by band-theoretic calculations [68]. As should be expected, the *d* electrons are concentrated predominantly in a region closest to the nucleus. If one takes as the edge of the ion

core that of the muffin-tin sphere, $r = r_{MT}$ (see, for example, [2]) and finds the number of "free" electrons by spreading the corresponding electron density $\rho(r_{MT})$ over the unit cell

$$Z^* = \rho(r_{MT})\Omega_0, \qquad (2.22)$$

one will obtain values of Z^* fairly close to those found by the pseudopotential method (see Table 2.1). Noteworthy, as direct calculations show, the value of $\rho(r_{MT})$ in the 3*d* metals is mainly determined by *s* and *p* electrons, and in Ir also in part by *d* electrons because the 5*d* electrons are significantly more delocalized in space than the 3*d* electrons.

The relative proximity of the *d* electrons to the nucleus is, however, only a part of the story. As follows from band-theoretic calculations (see, for example, the results reported by Ho *et al.* [73] for niobium and shown in Fig. 2.18), the fraction of the electron density $\rho(\mathbf{r})$ associated with *d* electrons is strongly anisotropic and mainly concentrated along preferred directions in space. Therefore, one may roughly take that the *s* and *p* electrons in the transition metals provide the metallic component of chemical bonding and the *d* electrons are responsible for covalent bonding. The latter is more favorable for the bcc structure, which admits partitioning into two sublattices, than for the close-packed structures, which do not admit such partitioning. In the latter case, not only the bonding, but also antibonding orbitals become inevitably filled, thus implying that some of the chemical bonds "jut out" into emptiness. This is the reason why the transition metals with a band filled about half-full have a bcc structure (the bonding orbitals are filled, and the antibonding orbitals are empty). By contrast, in the close-packed structures the "covalent" component of chemical bonding makes a relatively small contribution and the "metallic" component can be described in terms of pseudopotential theory. Of course, this is a rather crude reasoning and may only be regarded as explaining the difference in results between band-theoretic and pseudopotential calculations. As is seen, only band-theoretic calculations can yield quantitative values of occupancy for states of different symmetries, their hybridization, etc.

In the case of bcc metals, a simple empirical criterion can be proposed for the degree of covalence of chemical bonding. If the covalence is negligibly small, the lattice properties can be described in terms of pairwise central forces with a potential $\varphi(R)$, where R are the lattice vectors. Then (assuming zero pressure *p*) for the two shear moduli C_{44} and $C' = 1/2(C_{11} - C_{12})$ in cubic structures, one has

$$C_{44} = \frac{1}{\Omega_0}\sum_{\mathbf{R}}\frac{R_x^2R_y^2}{R^4}\left(R^2\frac{\partial^2\varphi}{\partial R^2} - R\frac{\partial\varphi}{\partial R}\right), \qquad (2.23)$$

$$C = \frac{1}{\Omega_0}\sum_{\mathbf{R}}\frac{R_x^2(R_x^2 - R_y^2)}{R^4}\left(R^2\frac{\partial^2\varphi}{\partial R^2} - R\frac{\partial\varphi}{\partial R}\right), \qquad (2.24)$$

and one can see that in the case of the bcc structure the first coordination shell makes a zero contribution to C'.

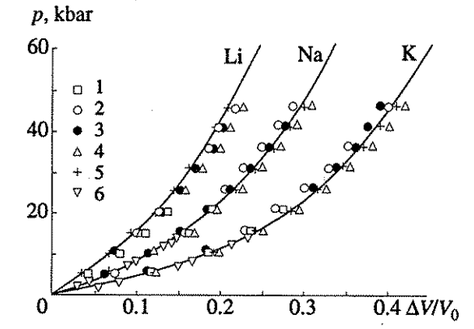

Fig. 2.11. *Equation of state p(V, T) for the alkali metals at T = 295 K. $\Delta V = V - V_0$. The full lines represent calculated data, and the dots, various experimental data.*

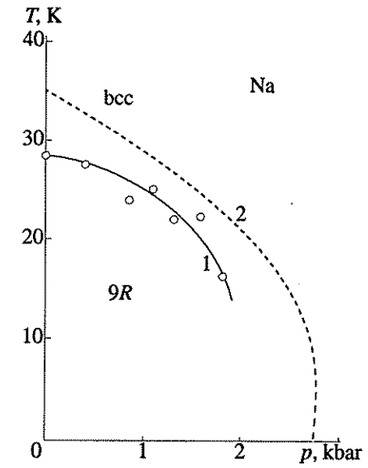

Fig. 2.12. *Phase diagram for sodium. The starting temperature of the martensitic transformation. $M_s(p)$: (1) experiment, (2) calculation.*

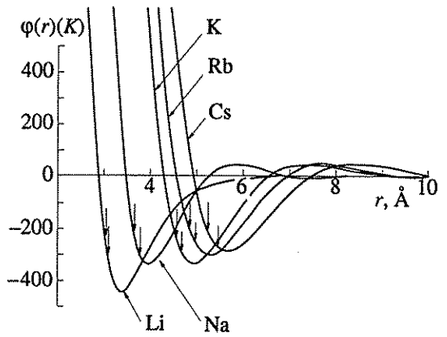

Fig. 2.13. *Pair potentials $\varphi(r)$ for liquid alkali metals. The solid arrows indicate the position of the nearest neighbors in the bcc lattice with the same atomic volume V(T) for $T = T_m$, the dashed arrows for T = 0; r is in angstroms, and $\varphi(r)$ in Kelvins.*

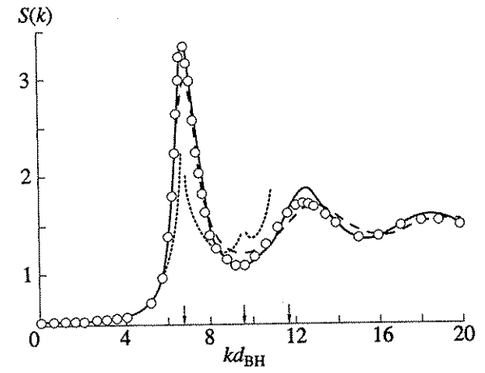

Fig. 2.14. *Structure factor S(k) in liquid sodium for $T = T_m$. The full and dashed lines represent calculation in the Percus–Yevick and hyperchain approximation; the dots represent experiment. The dotted line represents the phonon contribution to S(k) in the bcc phase of sodium averaged over the angles of the vector k for $T = T_m$. The arrows indicate the position of the first three nearest neighbors in the reciprocal lattice. $d_{BH} = \int_0^\sigma dr\,[1 - exp\,(-\varphi(r)/T_m)]$ is the effective diameter of the solid sphere after Barker-Henderson; σ is the first zero of the potential $\varphi(r)$.*

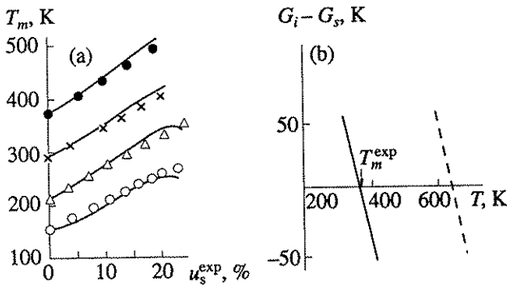

Fig. 2.15. *(a) Melting curves $T_m(u_s)$ of the alkali metals; u_s^{exp} is the experimental value of compression. For clarity, the result for every next heavier metal is shifted 50 K downward with respect to the previous lighter metal. The values on the T axis are given for Na; for K they should be reckoned as T + 50 K, for Rb as T + 100 K, and for Cs, as T + 150 K. The full lines represent calculation, and the dots, experiment (a) and (b). (b) Temperature dependence of the difference between the Gibbs thermodynamic potentials G(p, T) in the liquid (G_l) and solid (G_s) phases of sodium (expressed in Kelvins) at p = 0. The solid curve represents the Weeks–Chandler–Anderson approximation; dashed curve, the hard-sphere approximation using a diameter that provides the free energy minimum.*

Because $\varphi(R)$ drops with distance rather quickly (see Fig. 2.13), it necessarily follows that $C' \ll C_{44}$. Indeed, for sodium, $C_{44} \simeq 62$ kbar and $C' \simeq 7.4$ kbar. If, however, $C' \simeq C_{44}$ (as in W, Mo, the bcc phase of Ti, and Zr) or even if $C' > C_{44}$ (as in Nb), then the importance of covalent bonding effects is obvious. Similarly, it can be shown that for bcc metals the consequence of using the pair central force model in the nearest-neighbor approximation is a minimum on the longitudinal branch of the phonon spectrum in the ⟨111⟩ direction of the Brillouin zone near the point $\mathbf{Q}_0 = \frac{2\pi}{a}(\frac{2}{3}, \frac{2}{3}, \frac{2}{3})$ (where a is the lattice constant) and the frequencies of longitudinal (L) and transverse (T) phonons are in the ratio $\omega_L(\mathbf{Q}_0) : \omega_T(\mathbf{Q}_0) = 1 : 2$ (see Fig. 2.6). The absence of such a minimum or a strong deviation from the 1 : 2 ratio are likewise indicative of covalent-bond effects (a strong pseudopotential and the need to consider many-particle forces).

After a brief discourse on a specific pseudopotential model, we now proceed to discuss general conditions that permit one to divide electrons into "inner" and "outer" and to introduce pseudopotential. Before we do that, we need to examine some of the properties of metallic ions and to estimate the real values of their characteristic parameters. This is what we are going to do in the section that follows.

2.3. Polarizability of Metal Ions

The crucial question of pseudopotential theory is the possibility of a "rigorous" division of electrons into inner and outer. In such a division, the ion core, which includes all inner electrons, is treated as a "black box" that can be described by a certain definite set of parameters – the same under any conditions. Actually, when conduction electrons experience a Coulomb interaction with ion cores, the latter are polarized. Among other things, this changes the asymptotics of electron interaction at long distances r. In addition to the Coulomb interaction $-Z/r$, a contribution of the type $-\alpha(0)/r^4$ appears, where $\alpha(0)$ is the static polarizability of the ion. On its part, the polarizability of the ion may strongly vary with the medium in which it is placed – an action that can by itself cast doubt on the validity of the idea of a black box with fixed parameters. Moreover, the polarizability of ion cores leads to direct van der Waals interactions between ions, not accounted for in the simple pseudopotential approach. To take one's bearings in this mix of issues, one must above all take at least a rough "microscopic" inventory of the ion core and to estimate its principal parameters.

The simplest integrated characteristic of the ion core is dynamic polarizability $\alpha(\omega)$. In this section, taking as a guide the atomic calculations reported in [74], we will discuss a number of important properties of $\alpha(\omega)$ with special reference to the ions of the metals in the first two groups of the Periodic System. This will yield characteristic energy scales that can be used as points of departure for the microscopic verification of pseudopotential theory discussed in Sec. 2.4.

To begin with, let us recapitulate a few definitions and some of the general properties of $\alpha(\omega)$. In the self-

consistent field approximation, the ionic polarizability $\alpha(\omega)$ is defined by the well-known expression

$$\alpha(\omega) = 2\sum_{\nu\mu} \frac{f_\nu(1-f_\mu)}{\omega_{\mu\nu}^2 - \omega^2} |\langle\nu|\hat{x}|\mu\rangle|^2 \omega_{\mu\nu}, \qquad (2.25)$$

where $|\nu\rangle$ and ε_ν are the one-electron wave functions and state energies of the ion, f_ν is the Fermi distribution function, $\hat{x}$ is the coordinate operator, and $\omega_{\mu\nu} = \varepsilon_\mu - \varepsilon_\nu$ is the frequency of transitions from the $|\nu\rangle$ state to the $|\mu\rangle$ state. The overall properties of the generalized susceptibility [75] suggest the following important sum rules:

$$\alpha(\omega) \sim -\frac{Z_t}{\omega^2}, \quad \omega \to \infty, \qquad (2.26)$$

where Z_t is the total number of electrons in the ion core, and

$$\frac{1}{\pi}\int_0^\infty d\omega\alpha(i\omega) = \frac{1}{3}\langle r_{ml}^2\rangle, \qquad (2.27)$$

where $\langle r_{ml}^2\rangle = 3\sum_{\mu\nu} f_\mu(1-f_\nu)|x_{\mu\nu}|^2$ is the average of the many-electron operator of the squared radii of electrons in the ion at zero temperature. For purposes of estimation, the approximate Kirkwood formula for the diamagnetic susceptibility of an ion (an atom) [76] is often used

$$\chi_d \equiv -\frac{1}{6c^2}\langle r^2\rangle = -\frac{1}{4c^2}\sqrt{Z_t\alpha(0)}, \qquad (2.28)$$

where c is the velocity of light. This formula will immediately follow from (2.27) if one assumes for $\alpha(i\omega)$ the Lorentz approximation

$$\alpha(i\omega) = \frac{\alpha(0)}{1 + \frac{\omega^2}{\omega_0^2}}, \qquad (2.29)$$

and determines ω_0 from the condition (2.26): $\omega_0 = (Z_t/\alpha(0))^{1/2}$, and, taking advantage of the electron-gas approximation, sets $\langle r_{ml}^2\rangle = 3\sum_\nu \langle\nu|x^2|\nu\rangle f_\nu$. Interestingly, for one electron in the external potential, the Cauchy inequality

$$\left(\sum_i x_i y_i\right)^2 \le \left(\sum_i x_i^2\right)\left(\sum_i y_i^2\right),$$

with

$$x_i = [|\langle\nu|\hat{x}|\mu\rangle|^2|\omega_{\mu\nu}|]^{1/2}$$

and

$$y_i = \left[\frac{|\langle\nu|\hat{x}|\mu\rangle|^2}{|\omega_{\nu\mu}|}\right]^{1/2}$$

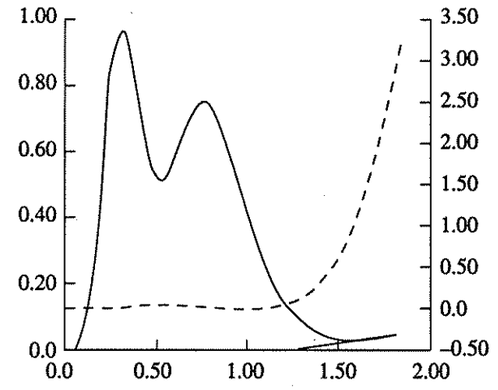

Fig. 2.16. *The full curve represents the distribution of the radial density of charge $4\pi\rho(r)r^2$ in an atom of Na in the metal according to band-theoretic calculations [68] (the left scale, in atomic units). The dashed curve shows the difference of radial densities in an atom of the metal and in a free atom (the right scale, multiplied by 100).*

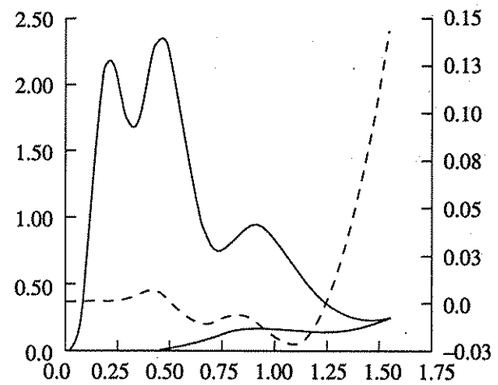

Fig. 2.17. *The full curve represents the distribution of the radial density of charge in an atom of V in the metal according to band-theoretic calculations (the left scale). The dashed curve shows the difference of the radial densities between an atom in the metal and a free atom (the right scale).*

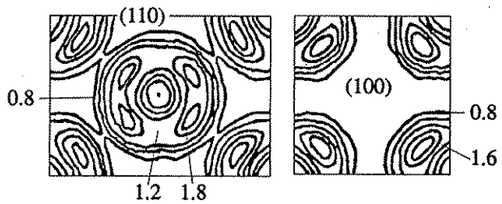

Fig. 2.18. *The distribution of the charge density $\rho(r)$ in Nb in ⟨110⟩ and ⟨100⟩ crystal planes [73]. Decimal numbers stand for the values of $\rho(r)$ at the corresponding lines (in atomic units). The values of ρ are normalized per one electron in a unit cell.*

Table 2.2. Calculated results for light elements

Element		Calculated values					Data on α(0)			
		$\omega_{1\to2}$	$\Delta\alpha_{1\to2}$	$\langle r^2\rangle_{1\to2}$	$\langle r^2\rangle$	α_r	Free ion	Ion in a metal	In ionic crystals	In solutions
$n=1$	Li^+	2.3	0.09	0.3	1	0.2	0.2	0.2		0.17
	Be^{++}	4.5	0.03	0.2	0.5	0.06				0.05
$n=2$	Na^+	1.1	0.12	0.2	7	2	1.1	1.2	2.8	1.2
	Mg^{++}	1.9	0.05	0.1	5	1	0.5	0.6	1.2	0.6

Note: $1\to2$ stands for $ns\to(n+1)p$ transitions; $\langle r^2\rangle_{1\to2} = (3/2)\Delta\alpha_{1\to2}\omega_{1\to2}$.

implies that $\langle r^2\rangle \le (3/2)\sqrt{\alpha(0)}$ ($Z_i = 1$). In contrast to $\langle r^2_{ml}\rangle$, the quantity $\langle r^2\rangle$ defines the diamagnetic susceptibility of an ion [76].

To obtain microscopic estimates for the characteristics of free ions, Katsnel'son *et al.* [74] used the approximations of Band *et al.* [77] and calculated the contributions of the individual transitions to the polarizability of the ions of the metals in the first two groups of the Periodic System within the relativistic version of the self-consistent $X\alpha$ method. In the relativistic case, $|\nu\rangle = |nlj\rangle$, where $j = l \pm 1/2$ is the quantum number of the total moment. After summation over the projections of the total moment, the contribution to α(0) from the transitions $|nl\rangle \to |n'l'\rangle$ ($l' = l \pm 1$) takes the form [81]

$$\Delta\alpha_{nl\to n'l'} = \frac{2}{3}\sum_{\substack{j=l\pm1/2\\ j'=l'\pm1/2}} \frac{|\langle nlj|r|n'l'j'\rangle|^2}{\omega_{n'l'j',nlj}} W_{j',j}, \tag{2.30}$$

$$W_{j',j} = \begin{cases} (j'+\frac{1}{2})(j'+\frac{3}{2})/(j'+1), & j' = j-1,\\ (2j'+1)/4j'(j'+1), & j' = j,\\ (j'-\frac{1}{2})(j'+\frac{1}{2})/j', & j' = j+1. \end{cases}$$

In calculating both the frequencies of transitions and the matrix elements, Katsnel'son *et al.* [74] used Slater's transition-state approximation [38]. That is, the population of the orbitals was assumed equal to the arithmetic mean of the populations in the initial and final states (for example, in the case of a transition from the filled *np* shell to the empty *nd* shell, calculations were done in the $np^{5.5}nd^{0.5}$ configuration, etc.). Also, they calculated $\langle r^2\rangle$ and Kirkwood's polarizability

$$\alpha_r = \frac{4}{9Z_i}\langle r^2\rangle^2, \tag{2.31}$$

which would be the same as α(0) if (2.28) were exact. The basic results of the calculations done by Katsnel'son *et al.* [74] are given along with known experimental [79, 80] and calculated [78] total polarizabilities in Tables 2.2 through 2.4 (all values are given in atomic units).

The metals in question divide quite naturally into three groups. Among the light metals, except perhaps Li and Be (see Table 2.2), one can isolate no particular transitions that might be responsible for the principal contribution to polarizability. Most likely, the latter is determined by transitions to the continuous spectrum. Kirkwood's formula gives a fairly good approximation for static polarizability in the sense that α_r is close to calculated or experimental values of α(0). In these metals, the polarizability is very small, and its effect on their properties is insignificant, which is why we will not discuss them.

In the second group, which includes the heavy alkali and alkaline-earth metals (see Table 2.3), the contribution to the total polarizability α from the $np \to nd$ transitions (where *n* is the principal quantum number of the shell to be filled last) is practically the same as the α calculated by Nieminen and Puska [78] (for K, Rb, and Cs) or found from the optical properties of ionic crystals (Ca, Sr, Ba). In the first three cases, the corresponding contribution is seen to be somewhat greater than the calculated α for the free ion. This is of course traceable to the fact that Katsnel'son *et al.* [74] and Nieminen and Puska [78] used different computational techniques. Anyhow, it is seen that for the Subgroup Ia elements, beginning from potassium, and for the Subgroup IIa elements, beginning from calcium, almost all values of α for the ion are determined by one selected group of $np \to nd$ transitions. It is to be stressed that for heavy elements (with $Z \gtrsim 48$) it is essential to consider relativistic effects, such as the frequency splitting of the transitions. Kirkwood's rule, $\alpha(0) \approx \alpha_r$, is poorly satisfied for K^+ and Rb^+ and a good deal better for Cs^+ and alkaline-earth ions. As is seen from Table 2.3, the polarizability of heavy free ions is from 0.7 to 0.75 of α_r, and that of an ion in a metal, $0.8\alpha_r$. These correlations can be used to assess the polarizability of the ions for which experimental and calculated values of α(0) are not available. According to Nieminen and Puska [78], the difference in polarizability between ions in a metal and in a vacuum is not very great (being about 10%). Therefore, one should expect that in the alkali and alkaline-earth metals the factor responsible for a decisive

Table 2.3. Calculated results for heavy alkali and alkaline-earth metals

Element		Calculated values							Data on α(0)			
		$\omega_{1\to2}$	$\Delta\alpha_{1\to2}$	$\omega_{3\to4}$	$\Delta\alpha_{3\to4}$	$\sum r^2_{i\to j}$	$\langle r^2\rangle$	α_r	Free ion	Ion in a metal	In ionic crystal	In solutions
$n=3$	K^+	0.75(0.01)	5.9	0.66(0.01)	0.75	7.4	20	10	5.7	6.2	9.0	5.7
	Ca^{++}	0.97(0.02)	4.7	1.02(0.04)	0.35	7.4	16	6	–	–	4.8	3.2
$n=4$	Rb^+	0.64(0.03)	8.9	0.54(0.04)	1.66	9.8	33	13	9.4	10	13	9.6
	Sr^{++}	0.83(0.04)	7.7	0.80(0.04)	0.85	10	27	9	–	–	8.4	6.3
$n=5$	Cs^+	0.51(0.06)	18	0.44(0.06)	3.18	16	53	23	16	18	23	17
	Ba^{++}	0.65(0.08)	15	0.64(0.08)	1.74	16	45	17	–	–	15	12
$n=6$	Fr^+	0.50(0.2)	20	0.42(0.2)	6.42	19	68	24	–	–	–	–
	Ra^{++}	0.64(0.2)	16	0.59(0.2)	3.60	19	59	18	–	–	–	–

Note: $1\to2$ stands for $np\to nd$ transitions; $3\to4$, $np\to(n+1)s$ transitions; $\sum r^2_{i\to j} = 3/2(\alpha_{1\to2}\omega_{1\to2} + \alpha_{3\to4}\omega_{3\to4})$. In the columns here and in Table 2.4, $\omega_{i\to j}$ are the average values of the corresponding transition frequencies; the figures in brackets are the difference between the maximum and minimum values due to relativistic effects.

Table 2.4. Calculated results for Subgroup Ib and IIb elements

Element		Calculated values									Data on α(0)			
		$\omega_{1\to2}$	$\Delta\alpha_{1\to2}$	$\omega_{3\to4}$	$\Delta\alpha_{3\to4}$	$\omega_{5\to6}$	$\Delta\alpha_{5\to6}$	$\sum r^2_{i\to j}$	$\langle r^2\rangle$	α_r	ω_{pe}	Free ion	Ion in a metal	In ionic crystals	In solutions
$n=3$	Cu^+	0.28(0.01)	5.6	2.6(0.1)	0.02	–	–	2.5	21	7	0.4	–	–	11	3
	Zn^{++}	0.58(0.01)	1.6	3.0(0.1)	0.02	–	–	1.5	16	4	0.5	–	–	6	2
$n=4$	Ag^+	0.33(0.02)	7.2	2.1(0.2)	0.06	0.62(0.02)	0.38	4.1	37	13	0.3	–	–	16	12
	Cd^{++}	0.57(0.03)	3.1	2.4(0.2)	0.06	1.0(0.03)	0.65	3.8	30	9	0.4	5.3	13	11	8
$n=5$	Au^+	0.31(0.06)	12	2.2(0.6)	0.12	0.59(0.06)	0.70	6.5	50	14	0.3	–	–	–	–
	Hg^{++}	0.51(0.07)	5.5	2.5(0.7)	0.11	0.93(0.07)	1.3	6.5	43	11	0.4	–	–	–	–

Note: $1\to2$ stands for $nd\to(n+1)p$ transitions; $3\to4$, $np\to(n+1)s$ transitions; $5\to6$, $nd\to nf$ transitions; $\sum r^2_{i\to j} = 3/2(\alpha_{1\to2}\omega_{1\to2} + \alpha_{3\to4}\omega_{3\to4} + \alpha_{5\to6}\omega_{5\to6})$; ω_{pe} is the plasma frequency in the free-electron model. Note the proximity of $\omega_{1\to2}$ and ω_{pe}. For the metals in Tables 2.2 and 2.3 all $\omega_{i\to j}$ are markedly greater than ω_{pe}.

contribution to the static ionic polarizability α(0) and the related properties is the proximity of the empty *d* band to the Fermi level. At the same time, the corresponding contributions to $\langle r^2\rangle$ are not so great (see Table 2.3).

Into the third group, one may class the Subgroup Ib and IIb elements (see Table 2.4). In them, one observes the same tendency: as one moves down the Periodic System, the α(0) of ionic crystals approaches the calculated α_r. An important contribution to α(0) comes from the $nd \to (n+1)d$ transitions (where *nd* is the *d* shell that is filled last), beginning from Ag^+, the $nd \to nf$ transitions come to play a prominent role. The frequencies of the $nd \to (n+1)p$ transitions are then of the order of the plasma frequency of conduction electrons, ω_{pe}.

Thus, as should be expected, whereas no significant change occurs in the properties of alkali and alkaline-earth ions when they are placed in a metal (in any case, at not too high pressures), this appears doubtful for the Subgroup Ib and IIb elements. The point is that the large contribution to α(0) from the $nd \to (n+1)p$ transition at a frequency close to ω_{pe} implies the possibility of a strong ("resonance") interaction between inner and outer electrons.

In summary, it may be concluded that the alkali and alkaline-earth metals have two natural smallness parameters related to the properties of an ion in a metal.

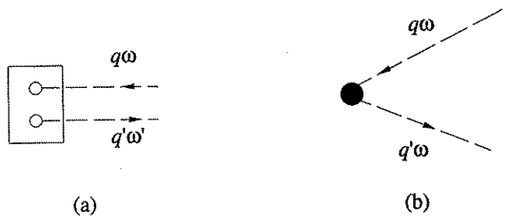

Fig. 2.19.

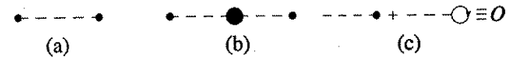

Fig. 2.20.

One is the "energy" parameter $\eta = \omega_{pe}/\omega_0$, where ω_0 is the characteristic frequency of core excitation (in the case at hand, this is, for example, the frequency of the $np \to nd$ transition), and the other is the "space" parameter $\kappa = 4\pi\alpha(0)/\Omega_0$. When one uses the values of $\alpha(0)$ calculated by Nieminen and Puska [78], the parameter κ in the case of the alkali metals ranges from 0.02 for Li to 0.3 for Cs. In the approximation (2.29), these parameters are not independent. Noting that $\omega_{pe} = (4\pi Z/\Omega_0)^{1/2}$ and $\omega_0 = (Z_t/\alpha(0))^{1/2}$,

$$\eta = \left(\frac{Z\kappa}{Z_t}\right)^{1/2}. \tag{2.32}$$

Because usually $Z/Z_t \ll 1$, then $\eta \ll 1$ even for $\kappa \sim 1$. We will use this estimate in the next section.

2.4. The Effects of the Nonpoint Nature of Ions in the Total Energy of a Metal

For simple metals, as was pointed out earlier (see Sec. 2.3), one may take advantage of the fact that ion cores are small in comparison with the interionic distance and that the characteristic energies of conduction electrons are small in comparison with the excitation energy of core electrons. That is, one may assume that

$$\kappa \ll 1, \quad \eta \ll 1. \tag{2.33}$$

Subject to the above inequalities and drawing upon the findings reported in [82], we will give the microscopic derivation of the expression for the total energy of a metal. Using this as an example, we will then discuss the possibility of introducing pseudopotential.

We write the complete Hamiltonian of the electron-ion system of a metal as

$$\hat{H} = \hat{H}_0 + \hat{H}'; \quad \hat{H}_0 = \hat{H}_{0e} + \sum_{\mathbf{R}} \hat{h}_{\mathbf{R}}, \qquad \hat{H}' = \hat{H}_{ee} + \hat{H}_{ii} + \hat{H}_{ei}. \tag{2.34}$$

Here, $\hat{h}_{\mathbf{R}}$ is the Hamiltonian of the Rth ion; $\hat{H}_{0e}$ is the Hamiltonian of free electrons;

$$\hat{H}_{ee} = \frac{1}{2}\sum_{\mathbf{q}} v_c(\mathbf{q})\hat{\rho}_e(-\mathbf{q})\hat{\rho}_e(\mathbf{q}),$$

$$\hat{H}_{ii} = \frac{1}{2}\sum_{\mathbf{q},\mathbf{R}} v_c(\mathbf{q})\hat{\rho}_i^R(-\mathbf{q})\hat{\rho}_i^R(\mathbf{q}),$$

and

$$\hat{H}_{ei} = \sum_{\mathbf{q},\mathbf{R}} v_c(\mathbf{q})\hat{\rho}_i^R(\mathbf{q})\hat{\rho}_e(\mathbf{q})$$

are the Hamiltonians of electron–electron, ion–ion, and electron–ion interactions, respectively; and $\hat{\rho}_i^R(\mathbf{q})$ and $\hat{\rho}_e(\mathbf{q})$ are the Fourier components of the charge density of the Rth ion and conduction electrons, respectively. Owing to the smallness of an ion, we may write $\hat{\rho}_i^R$ as

$$\hat{\rho}_i^R = e^{i\mathbf{qR}}(Z + i\mathbf{q}\hat{\mathbf{d}}_{\mathbf{R}} + \ldots), \tag{2.35}$$

where Z is the charge of the ion and $\hat{\mathbf{d}}_{\mathbf{R}}$ is the dipole moment operator. We choose $\hat{H}_0$ in (2.34) to be the zero Hamiltonian and $\hat{H}'$ to be a perturbation. As in Sec. 2.1, the electronic Green's function in the diagrams will be represented by a solid line, and $v_c(\mathbf{q})$, by a dashed line. The additional element introduced by Rehr *et al.* [83] is the dipole vertex $i\mathbf{q}\hat{\mathbf{d}}_{\mathbf{R}}$. We will designate it by an unfilled circle. When averaging diagrams with such unfilled circles over the ground state $\hat{H}_0$, we will bear in mind that $\langle\hat{\mathbf{d}}_{\mathbf{R}}\rangle = 0$. Averaging two $\hat{\mathbf{d}}_{\mathbf{R}}$ operators at one site yields their causal Green's function [83, 84]

$$\alpha(t) = -i\langle 0|\hat{T}d_{\mathbf{R}}^x(t)d_{\mathbf{R}}^x(0)|0\rangle. \tag{2.36}$$

Thus, to the graph in Fig. 2.19a, where the rectangle denotes averaging over the ground state $\hat{h}_{\mathbf{R}}$, there corresponds an expression

$$(-i\mathbf{q}')\ (i\mathbf{q})\ \frac{\alpha(\omega)}{\Omega_0}e^{i(\mathbf{q}-\mathbf{q}')\mathbf{R}}\delta(\omega-\omega'), \tag{2.37}$$

where $\alpha(\omega)$ is the Fourier transform of the function (2.36). After summation over $\mathbf{R}$, we replace the term $\exp[i(\mathbf{q}-\mathbf{q}')\mathbf{R}]$ in (2.37) with the structure factor. Subsequently, the corresponding expression will be represented by a filled circle (Fig. 2.19b). We consider contributions of the zero, first, and second order in κ to the total energy E.

The zeroth approximation is described by the graph of Fig. 2.20a and the expression [compare with (2.3)]

$$E_{\mathrm{M}} = -\frac{1}{2}\sum_{\mathbf{g}\neq 0} Z^2 v_c(\mathbf{g})|S(\mathbf{g})|^2 = -\frac{Z^2\alpha_{\mathrm{M}}}{2\Omega_0^{1/3}}. \tag{2.38}$$

The first-order contribution in κ is shown in Fig. 2.20b, and

$$\Delta E_{\mathrm{M}} = \frac{Z^2}{2}\sum_{\mathbf{g}\neq 0}\sum_{\mathbf{g}'\neq 0}\mathbf{g}\mathbf{g}' v_c(\mathbf{g})v_c(\mathbf{g}')S(\mathbf{g})S^*(\mathbf{g}') \times \int_{-\infty}^{\infty}\frac{d\omega}{2\pi}\alpha(i\omega) = 0. \tag{2.39}$$

The contribution with $\mathbf{g} = 0$ vanishes because of electroneutrality (see Fig. 2.20c). Thus, in a system with an inversion center, the polarized ions do not screen the direct ion–ion interaction E_M. All contributions to E_M of higher order κ can be likewise shown to be zero.

In an analysis of the first-order-in-κ contribution to E, one has to take into account the effect of polarized ions on the electron-gas energy E_0. Because of this, filled circles are inserted in the dashed lines in the diagrams. For example, the graph of Fig. 2.21a corresponds to the first-order correction in terms of κ to the Fock energy. Let us demonstrate that the summation over all inserts in the dashed lines (both ionic and electronic) results in the replacement of $v_c(\mathbf{q})$ by $v_c(\mathbf{q})/\varepsilon_{\mathrm{tot}}(\mathbf{q}, i\omega)$, where

$$\varepsilon_{\mathrm{tot}}(\mathbf{q}, i\omega) = \varepsilon_e(\mathbf{q}, i\omega) + \frac{4\pi}{\Omega_0}\alpha(i\omega) \tag{2.40}$$

is the total permittivity, and $\alpha(i\omega)$ is the polarizability of the ion with allowance for local-field effects; for the cubic lattices

$$\alpha(i\omega) = \alpha(i\omega)/\left[1 - \frac{4\pi}{3\Omega_0}\alpha(i\omega)\right]. \tag{2.41}$$

To demonstrate, the series of diagrams shown in Fig. 2.22a (with a zero momentum transfer at each vertex) is readily summed to give

$$\tilde{v}_c(\mathbf{q}, i\omega) = \frac{v_c(\mathbf{q})}{\varepsilon_e(\mathbf{q}, i\omega)} - \frac{q^2\alpha(i\omega)}{\Omega_0}\left[\frac{v_c(\mathbf{q})}{\varepsilon_e(\mathbf{q}, i\omega)}\right]^2 + \ldots = \frac{v_c(\mathbf{q})}{\varepsilon_e(\mathbf{q}, i\omega) + 4\pi\alpha(i\omega)/\Omega_0}. \tag{2.42}$$

Between two dotted lines with momentum $\mathbf{q}$ one can insert any number of lines with a nonzero momentum transfer at each dipole vertex. The simplest diagram of this type is shown in Fig. 2.22b. The contributions of these diagrams correspond to local-field effects. For simplicity, let us neglect the screening action of conduction electrons on these effects. Then the expression corresponding to the diagram of Fig. 2.22b takes the form

$$\left[\frac{4\pi\alpha(i\omega)}{\Omega_0}\right]^2\frac{q^\alpha q^\beta}{q^2}\sum_{\mathbf{q}\neq 0}\frac{(\mathbf{q}+\mathbf{g})^\alpha(\mathbf{q}+\mathbf{g})^\beta}{|\mathbf{q}+\mathbf{g}|^2}. \tag{2.43}$$

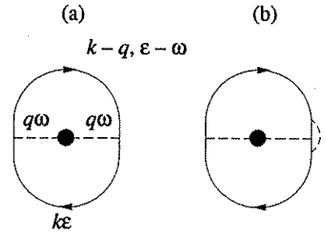

Fig. 2.21.

By writing the sum over $\mathbf{g}$ as

$$S_{\alpha\beta} \equiv \sum_{\mathbf{g}}{}'\frac{(\mathbf{q}+\mathbf{g})^\alpha(\mathbf{q}+\mathbf{g})^\beta}{|\mathbf{q}+\mathbf{g}|^2} = -\frac{\partial^2}{\partial\rho_\alpha\partial\rho_\beta}\sum_{\mathbf{g}}{}'\frac{e^{i(\mathbf{q}+\mathbf{g})\rho}}{|\mathbf{q}+\mathbf{g}|^2}\Bigg|_{\rho=0}, \tag{2.44}$$

we obtain

$$S_{\alpha\beta} = -\frac{1}{4\pi}\frac{\partial^2}{\partial\rho_\alpha\partial\rho_\beta} \times \left[\Omega_0\sum_{\mathbf{R}}\frac{e^{i\mathbf{qR}}}{|\boldsymbol{\rho}+\mathbf{R}|} - \int d\mathbf{r}\frac{e^{-i\mathbf{qr}}}{|\mathbf{r}+\boldsymbol{\rho}|}\right]_{\rho=0}. \tag{2.45}$$

Then for cubic lattices ($S_{\alpha\beta} = -\delta_{\alpha\beta}/3$) the expression (2.43) takes the form

$$-\frac{4\pi}{\Omega_0}\alpha(i\omega)\frac{4\pi}{\Omega_0}\alpha(i\omega). \tag{2.46}$$

By the same token, we find that summation over all diagrams with a nonzero momentum transfer at the dipole vertex between two $v_c(\mathbf{q})$ lines is equivalent to the replacement of $\alpha(i\omega)$ in (2.42) by $\tilde{\alpha}(i\omega)$:

$$\tilde{\alpha}(i\omega) = \alpha(i\omega)\left[1 + \frac{4\pi\alpha(i\omega)}{3\Omega_0} + \left(\frac{4\pi\alpha(i\omega)}{3\Omega_0}\right)^2 + \ldots\right] = \frac{\alpha(i\omega)}{1 - \frac{4\pi\alpha(i\omega)}{3\Omega_0}}, \tag{2.47}$$

which corresponds to the application of the usual local-field correction. It can be shown that consideration of electron screening effects in a local field yields the result

$$\tilde{\alpha}(i\omega) = \frac{\alpha(i\omega)}{1 - \frac{4\pi}{3\Omega_0}\alpha(i\omega)\left\{1 + \sum_{\mathbf{g}}{}'[1 - \varepsilon_e^{-1}(\mathbf{g}, i\omega)]\right\}}, \qquad \varepsilon_e(q, i\omega) = 1 + \frac{4\pi}{q^2}\Pi(q, \omega), \tag{2.48}$$

obtained by Sturm [85] in a different way.

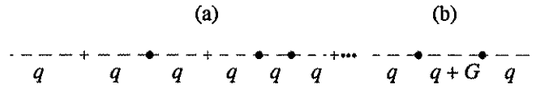

Fig. 2.22.

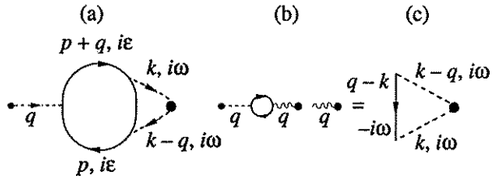

Fig. 2.23.

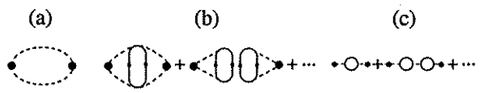

Fig. 2.24.

For a further examination of the first-order-in-κ correction to E, we take advantage of the smallness of κ and η and limit ourselves to the diagrams containing one filled circle each. In the diagram of Fig. 2.21, we may neglect the energy ε in comparison with $\omega \sim \omega_0$ in the upper line because $\eta \ll 1$. It is likewise seen that the main contribution to the integral of $\mathbf{q}$ comes from $q \sim \omega_0^{1/2}$, which is why we may neglect κ ($\kappa \ll q$). Then the expression corresponding to Fig. 2.21a, with allowance for the screening effect $v_c(\mathbf{q})$, takes the form

$$E_a = \frac{1}{2}\sum_{\sigma}\int\frac{d\mathbf{k}}{(2\pi)^3}\int_{-\infty}^{\infty}\frac{d\varepsilon}{2\pi i}e^{i\varepsilon o}G_0(i\varepsilon, \mathbf{k}) \times \int_{-\infty}^{\infty}\frac{d\omega}{2\pi}\int\frac{d\mathbf{q}}{(2\pi)^3}\left(\frac{4\pi}{q^2\varepsilon_e(0, i\omega)}\right)^2\frac{q^2\alpha(i\omega)}{i\omega + q^2/2} = \delta b 2\int\frac{d\mathbf{k}}{(2\pi)^3}\int_{-\infty}^{\infty}\frac{d\varepsilon}{2\pi}e^{i\varepsilon o}G_0(i\varepsilon, \mathbf{k}). \quad (2.49)$$

Here, $G_0(i\varepsilon, \mathbf{k})$ is the unperturbed Green's function, and

$$\delta b = \frac{1}{2}\int_{-\infty}^{\infty}\frac{d\omega}{2\pi}\frac{\alpha(i\omega)}{\varepsilon_e^2(0, i\omega)}\int\frac{d\mathbf{q}}{(2\pi)^3}\left(\frac{4\pi}{q^2}\right)\frac{1}{i\omega + q^2/2} = -2\int_0^{\infty}\frac{d\omega\alpha(i\omega)}{\sqrt{\omega}}\left(\frac{\alpha^2}{\omega^2 + \omega_{pe}^2}\right)^2. \quad (2.50)$$

In (2.49) and (2.50), we retained the ω dependence in $\varepsilon_e(q, i\omega)$ because it leads to the corrections on the order of $\eta^{1/2}$. By contrast, consideration of the $\mathbf{q}$ dependence and the retention of (ε, k) in comparison with $(\omega, \mathbf{q})$ yield the contribution on the order of η. Any inserts in the diagram of Fig. 2.21a (see, for example, Fig. 2.21b) give rise to small factors on the order of η, and we will neglect them. As a result, at the lower orders in κ and η, the total contribution from ionic polarizability to the structurally independent part of the energy is

$$E^{(1)} = \frac{\delta b Z}{\Omega_0}. \quad (2.51)$$

To calculate the pairwise interaction energy of non-point ions, we first turn to the diagram of 2.23a. At the lowest order of η, we replace $G_0(i\varepsilon - i\omega, \mathbf{p} + \mathbf{q} - \mathbf{k})$ by $G_0(-i\omega, \mathbf{q} - \mathbf{k})$, and the diagram takes the form shown in Fig. 2.23b, where the wavy line corresponds to the $J(\mathbf{q})$ block in Fig. 2.23b:

$$J(\mathbf{q}) = -\frac{1}{2}\int_{-\infty}^{\infty}\frac{d\omega}{2\pi}\alpha(i\omega)\int\frac{4\pi}{k^2\varepsilon_e(0, i\omega)} \times \frac{4\pi}{(\mathbf{k} - \mathbf{q})\,\varepsilon_e(0, i\omega)}\frac{\mathbf{k}(\mathbf{k} - \mathbf{q})}{-i\omega + \frac{1}{2}(\mathbf{q} - \mathbf{k})^2}, \quad (2.52)$$

and the energy correction is

$$\Delta E = -\frac{Z}{\Omega_0}\sum_{\mathbf{g}}{}'\frac{v_c(\mathbf{g})}{\varepsilon_e(\mathbf{q}, 0)}J(\mathbf{g})\Pi_0(\mathbf{g})|S(\mathbf{g})|^2. \quad (2.53)$$

Here and elsewhere, the dotted line represents the screened Coulomb interaction $v_c(\mathbf{q})/\varepsilon_e(\mathbf{q}, i\omega)$. Any inserts affecting the internal electronic energy of the block in Fig. 2.23c give rise to additional factors of the order of ω^{-1}. Therefore, the "bold-facing" of the diagram in Fig. 2.23a due to the electron-electron interaction at the lower order of η reduces to the replacement of $\Pi_0(\mathbf{g})$ in (2.53) by the exact $\Pi(\mathbf{g})$.

We now turn to computing the second-order contributions in terms of κ to the pair ion interaction energy. The simplest graph shown in Fig. 2.24a describes the usual van der Waals interaction

$$E_{\mathrm{VdW}} = -\frac{1}{2\Omega_0}\sum_{\mathbf{g}}{}'\int\frac{d\mathbf{q}}{(2\pi)^3}\int_{-\infty}^{\infty}\frac{d\omega}{2\pi}\alpha^2(i\omega) \times [\mathbf{q}(\mathbf{q} + \mathbf{g})]^2\frac{v_c(\mathbf{q})}{\varepsilon_e(\mathbf{q}, i\omega)}. \quad (2.54)$$

On excluding the self-action, the expression (2.54) can be reduced to the form

$$E_{\mathrm{VdW}} = \sum_{\mathbf{R}}{}'E_{\mathrm{VdW}}(\mathbf{R}), \quad (2.55)$$

where

$$v_{\mathrm{VdW}}(\mathbf{R}) = -\int_0^{\infty}\frac{d\omega}{2\pi}\alpha^2(i\omega) \times \left[\left(\frac{\partial^2 V_c(\mathbf{R}, i\omega)}{\partial R^2}\right)^2 + \frac{2}{R^2}\left(\frac{\partial V_c(\mathbf{R}, i\omega)}{\partial R}\right)^2\right], \quad (2.56)$$

and

$$V_c(\mathbf{R}) = \int\frac{d\mathbf{q}}{(2\pi)^3}v_c(\mathbf{q})\frac{e^{i\mathbf{q}\mathbf{R}}}{\varepsilon(\mathbf{q}, i\omega)} \quad (2.57)$$

is the potential of the screened Coulomb interaction. This expression was first derived by Rehr *et al.* [83]. They estimated the contribution (2.55) to the energy of Cu, Ag, and Au; it was found to be significant. The expressions (2.56) and (2.57) provided the basis for further inquiry. The investigation of the expression (2.56) undertaken by Mahanty and Taylor [86] demonstrated that consideration of space dispersion in $\varepsilon(\mathbf{q}, i\omega)$ yielded two added terms in comparison with the usual $1/R^6$ terms. One varied as $[\exp(-R/R_d)]/R^{5/2}$ (where R_d is on the order of the screening radius), the other behaved as $\cos^2(2k_FR)/R^{5/2}$ (where k_F is the Fermi momentum), and both were found to be small. Consideration of the frequency dependence $\varepsilon_e(0, i\omega) = 1 + \omega_{pe}^2/\omega^2$ (where ω_{pe} is the electronic plasma frequency) for the noble metals was found to be significant. A similar conclusion was drawn by Rehr *et al.* [83] who calculated (2.56) by numerical methods. Considering solely the ω dependence in $\varepsilon_e(\mathbf{q}, i\omega)$, we have

$$v_{\mathrm{VdW}}(R) = -\frac{C}{R^6}; \quad C = \frac{3}{\pi}\int_0^{\infty}d\omega\alpha^2(i\omega)\left(\frac{\omega^2}{\omega^2 + \omega_{pe}^2}\right)^2. \quad (2.58)$$

To find the total energy of pairwise interaction, we need to calculate the contributions shown in Fig. 2.24b and 2.24c. Their sum, together with the first-order terms, is the same as the usual second-order contribution in terms of pseudopotential [see (2.18)]

$$E^{(2)} = -\frac{\Omega_0}{2}\sum_{\mathbf{g}}{}'\frac{\Pi(\mathbf{g})}{\varepsilon(\mathbf{g})}|V(\mathbf{g})|^2|S(\mathbf{g})|^2,$$

provided that

$$V_{ps}(\mathbf{q}) = \frac{1}{\Omega_0}[Zv_c(\mathbf{q}) + J(\mathbf{q})]. \quad (2.59)$$

Thus, a "pseudopotential" naturally arises when the energy is consecutively expanded in terms of κ and η.

If one abandons the dipole approximation (2.35) and constructs the perturbation theory in terms of the Hamiltonian $\hat{H}_{ei}$, then the expression $\mathbf{q}\mathbf{q}'\alpha(\omega)$ in (2.37) will be replaced by $\chi(\mathbf{q}, \mathbf{q}'; \omega)$, which is the Fourier transform of the causal Green's function of the total ion density ρ^i:

$$\chi(\mathbf{q}, \mathbf{q}'; \omega) = -i\sum_{\mathbf{R}}\int_{-\infty}^{\infty}dte^{i\omega t} \times \left\langle 0\left|\hat{T}\delta\rho_{\mathbf{R}}^i(\mathbf{q}, t)\delta\rho_{\mathbf{R}}^i(-\mathbf{q}, 0)\right|0\right\rangle, \quad (2.60)$$

$$\delta\rho_{\mathbf{R}}^i(\mathbf{q}, t) = \rho_{\mathbf{R}}^i(\mathbf{q}, t) - F_{\mathbf{R}}(\mathbf{q}), \quad F_{\mathbf{R}}(\mathbf{q}) = \left\langle 0\left|\rho_{\mathbf{R}}^i(\mathbf{q}, 0)\right|0\right\rangle, \quad (2.61)$$

and Z is replaced by $Z - F_{\mathbf{R}}(\mathbf{q})$ (where F is the form-factor of the Rth ion). As a result, the expression for E_{M} is complicated because one takes into account the non-point property of ions. As will be recalled [87], this leads (in the case of spherically symmetric ions) to the appearance of additional terms of the order of $\exp(-\gamma R)$ in the ion–ion interaction energy. Terms of the same order come about owing to the effects of electron–electron exchange interaction at different sites; they can be taken into account in, for example, the Heitler–London method [87, 88]. As a result, (2.55) is extended to include the term due to the Born–Mayer interaction, $E_{\mathrm{BM}} = \sum{}'v_{\mathrm{BM}}(R)$. As a rule, for $v_{\mathrm{BM}}(R)$, one uses the approximation $v_{\mathrm{BM}}(R) = A\exp(-\gamma R)$. In the end, the total energy can be written as

$$E = E_\Omega + E_{\mathrm{M}} + E^{(2)} + E_{\mathrm{VdW}} + E_{\mathrm{BM}}; \quad E_\Omega = E^{(0)} + E^{(1)}. \quad (2.62)$$

Here, $E^{(1)}$ takes the form of (2.51), and δb is defined by an expression of the type (2.50) [considering that $\alpha(i\omega) \to q^{-2}\chi(\mathbf{q}, \mathbf{q}; i\omega)$] and by an additional term

$$\delta b_R = \lim_{q\to 0}\frac{4\pi}{q^2}[Z - F_R(\mathbf{q})] = \frac{2\pi}{3}\langle 0|r^2|0\rangle = 2\int_0^{\infty}d\omega\alpha(i\omega). \quad (2.63)$$

The rate of fall of $\chi(\mathbf{q}, \mathbf{q}'; i\omega)$ with $\mathbf{q}$ is then determined by the ionic radius R_i. If the parameter $\lambda = R_i/R_a$ (where R_a is the interionic distance) is not small and $\eta \ll 1$, then in Fig. 2.21a one can neglect ε in comparison with ω, but one cannot neglect $|\mathbf{k}|$ in comparison with $|\mathbf{q}|$. Then, instead of (2.51), one obtains

$$E^{(1)} = \Omega_0\int\frac{d\mathbf{k}}{(2\pi)^3}n_{\mathbf{k}}V_{\mathbf{k},\mathbf{k}}; \quad (2.64)$$

$$V_{\mathbf{k},\mathbf{k}} = \frac{1}{2\Omega_0}\int_{-\infty}^{\infty}\frac{d\omega}{2\pi}\int\frac{d\mathbf{q}}{(2\pi)^3}\chi(\mathbf{q}, \mathbf{q}; i\omega) \times \left[\frac{4\pi}{q^2\varepsilon_e(\mathbf{q}, i\omega)}\right]^2 G_c(\mathbf{k} - \mathbf{q}, -i\omega) + \frac{\delta b_R}{\Omega_0}. \quad (2.65)$$

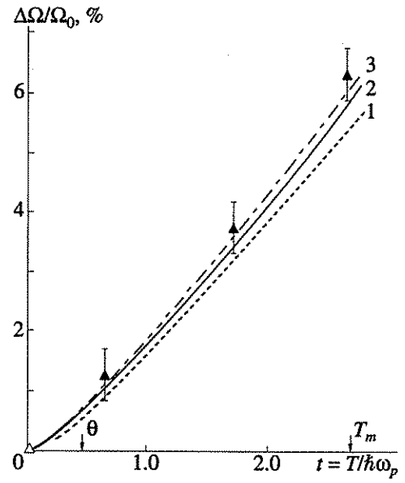

Fig. 2.25. *Thermal expansion of Rb (Ω is the atomic volume): (1) calculation by the pseudopotential theory; (2) calculation with allowance for E_{BM}; and (3) calculation with allowance for E_{BM} and E_{VdW}. The dots stand for the experimental data.*

Equation (2.64) is the same as the usual expression for $E^{(1)}$ in the case of nonlocal pseudopotential (2.6), and (2.65) is a microscopic expression for the diagonal matrix elements of the latter. It is thus seen that the pseudopotential owes its local character to the smallness of λ and η, and that (2.50) holds only for $(\eta)^{1/2} \ll \lambda$.

The analysis presented above implies that, in the case of λ, $\eta \ll 1$, all effects associated with the nonpoint nature of the ion can be accommodated within the usual local pseudopotential scheme extended to include E_{BM} and E_{VdW}. To form a quantitative estimate of these interactions, Katsnel'son and Trefilov [82] calculated the atomic properties of K, Rb, and Cs with allowance for E_{BM} and E_{VdW}. Benedek [89] calculated the parameters A and γ of the Born–Mayer interaction for K and Rb, using atomic calculations by the Hartree–Fock method, and Upadhayaya *et al.* [90] found them for Cs by extrapolation. Upadhayaya *et al.* [90] found the constant C in E_{VdW} by (2.58), where $\alpha(i\omega)$ was determined by applying the numerical procedure of analytic continuation to the function Im $\alpha(\omega)$ derived from optical data for the corresponding metals. The calculations performed by Katsnel'son and Trefilov [82] demonstrate that the elastic constants, the Debye temperature expressed in their terms, and the phonon spectra of the alkali metals are only slightly sensitive to the addition of E_{BM} and E_{VdW}. On the contrary, the inclusion of v_{BM} and v_{VdW} causes appreciable changes in the volume derivatives of the elastic constants and the associated Grüneisen parameters. For example, dB/dp (where B is the bulk modulus) for Rb decreases 7%. The effect of v_{VdW} and v_{BM} on the phonon frequencies $\omega_{\nu k}$ is insignificant, being 1 or 2%. In the microscopic Grüneisen parameters $\gamma_{\nu k} = -\partial \ln \omega_{\nu k}/\partial \ln \Omega$, the effects are far stronger. In this case, the change is 5% for K, 25% for Rb, and 16% for Cs. Moreover, consideration of v_{BM} and v_{VdW} causes an increase in $\gamma_{\nu k}$. As is seen from Fig. 2.25, the values of thermal expansion $\Delta\Omega(T)/\Omega_0$ calculated with allowance for v_{BM} and v_{VdW} occur at elevated temperatures markedly closer to their experimental counterparts than when these interactions are neglected (as an example, the results for Rb are given).

The above analysis demonstrates that, when one takes into consideration both E_{BM} and E_{VdW}, this has a negligible effect on the calculated properties of the alkali metals, except the Grüneisen parameters, which are especially sensitive to the strong volume dependence of these interactions.

This fact actually completes the proof that the theory of pseudopotential is fully applicable to metals with a "rigid" core ($\eta \ll 1$).

2.5. The "Soft" Core Case

As follows from the previous sections, the concept of the ion core in a metal may be regarded as well-defined if the core is rigid, that is, if it is characterized by high excitation energies in comparison with the characteristic energies of conduction electrons ($\eta \ll 1$). Furthermore, the very procedure of introducing the concept of core states consists in that one should go on "stripping" the ion until the minimal core excitation energy satisfies the condition of smallness (2.33). In the transition and noble metals, where $\eta \lesssim 1$ and even the ion charge Z is not defined quite well (see Secs. 2.2 and 2.3), it is natural to abandon all attempts to divide the electrons (at least, d electrons) into core electrons and collective electrons, and to go over to a purely band-theoretic description. Then, even if it is possible to introduce pseudopotential at all (see, for example, [54]), its use is, in effect, a technical device that helps one to carry out band-theoretic calculations [57, 58]. Therefore, the concept of an ion core is, one might think, applicable solely when it is rigid. Otherwise, its states diffuse into fairly broad bands and hybridize with the states of conduction electrons. This appears to be exactly the case with, for example, the pure d metals (among the transition metals, the narrowest $3d$ band about 5 eV wide exists in nickel). For, for example, the $4f$ metals and their compounds, however, the concept of an ion core can have a clear-cut meaning even if the core is "soft"; that is, it has excited states with an energy ω_0 small in comparison with the characteristic energies of conduction electrons ($\eta \gg 1$):

$$\omega_0 \ll E_F, \omega_{pe}. \tag{2.66}$$

On their part, the states, transitions between which give rise to these excitations, may not diffuse into a band owing to the strong Coulomb repulsion of f electrons. Why this is so will be discussed in Chs. 5 and 6. From simple physical considerations it is almost obvious that if the overlap of the f wave functions on different atoms is rather small, the f states will be characterized by the

quantum numbers of a free atom even in a metal (the terms $|LSJ\rangle$, where L, S, and J are the orbital, spin, and total moments of the f shell, split into sublevels by weak crystal fields [91]). Then one can identify ω_0 either with the splitting of the basic term in a crystal field or, if it is not degenerate, as in the case of a "Van-Vleck" Sm^{++} ion for which $J = 0$, with the distance to the next term (for a free Sm^{++} ion, $\omega_0 \simeq 410$ K [92]). The level splitting in the f subsystem in a crystal field and its effect on the properties of the f metals are discussed in a review [91].

Thus, situations can exist where the ion core may be regarded as soft [in the sense of the inequality (2.66)] and still remain well definable. Let us see how conduction electrons can be affected by scattering on so readily excitable ions.

To begin with, let us determine the contribution to the "self" energy of a conduction electron, $\Sigma(\mathbf{k}, \varepsilon)$, described by the graph of Fig. 2.26

$$\Sigma(\mathbf{k}, \varepsilon) = \frac{1}{\Omega_0}\int \frac{1}{(2\pi)^3}\int_{-\infty}^{\infty}\frac{d\omega}{2\pi i}\left(\frac{4\pi e^2}{p^2+\lambda^2}\right)^2 \times \frac{\chi(\mathbf{p}, \mathbf{p}; \omega)}{\varepsilon - \omega - \xi_{\mathbf{k}-\mathbf{p}} + i\delta \operatorname{sgn} \xi_{\mathbf{k}-\mathbf{p}}}, \quad \xi_{\mathbf{k}} = \varepsilon_{\mathbf{k}} - \varepsilon_F, \tag{2.67}$$

where we put $\varepsilon(\mathbf{p}, \omega) \simeq 1 + \lambda^2/\mathbf{p}^2$ and $\lambda^2 = 4me^2/\pi k_F$ because only small ω are of importance. Suppose for simplicity that $k_F R_i \ll 1$, where R_i is the ionic radius. Then we can approximate the function $\chi(\mathbf{p}, \mathbf{p}; i\omega)$ by its value for $|\mathbf{p}|$ tending to zero

$$\chi(\mathbf{p}, \mathbf{p}; \omega) \simeq p^2\alpha(\omega) = p^2\frac{c\omega_0}{\omega_0^2 - \omega^2 - i\delta}, \tag{2.68}$$

where $\alpha(\omega)$ is the dipole polarizability, and the contribution of the transition with a small ω_0 is identified; c is proportional to the corresponding oscillator force. We next calculate the frequency integral in (2.67) [upon insertion of (2.68)], while assuming for definiteness that $\varepsilon \geq 0$

$$I(\varepsilon, \xi) = \int_{-\infty}^{\infty}\frac{d\omega}{2\pi}\frac{1}{\varepsilon - \omega - \xi + i\delta \operatorname{sgn} \xi}\frac{1}{\omega_0^2 - \omega^2 - i\delta} = \frac{1}{2\omega_0}\frac{1}{\varepsilon - \xi - \omega_0 + i\delta \operatorname{sgn} \xi}. \tag{2.69}$$

On inserting (2.69) in (2.67) and integrating with respect to $\mathbf{p}$ ($\beta_0 = me^2/\pi k_F \lesssim 1$), we have

$$\Sigma(\mathbf{k}, \varepsilon) \simeq \frac{me^2}{k}\frac{c}{\Omega_0}\ln\left[\frac{(k+k_F)^2+\lambda^2}{(k-k_F)^2+\lambda^2}\right]\ln\left|\frac{\varepsilon - \omega_0}{\varepsilon + \omega_0}\right|. \tag{2.70}$$

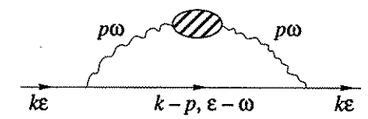

Fig. 2.26.

Equation (2.70) implies that in the lowest order perturbation theory Σ diverges for $\varepsilon = \pm\omega_0$. Moreover, the jump of the distribution function at the Fermi level [20] is

$$Z^* = \left[1 - \frac{\partial\Sigma(k_F, \varepsilon)}{\partial\varepsilon}\bigg|_{\varepsilon=0}\right]^{-1} \simeq \left[1 + \frac{2me^4}{k_F\omega_0}\frac{c}{\Omega_0}\ln\left(1 + \frac{1}{\beta_0}\right)\right]^{-1} \tag{2.71}$$

and, therefore, the effective mass $m^*/m \sim Z^{*-1}$ of conduction electrons contains corrections on the order of ω_0^{-1}, which may become large for small ω_0.

In structure, equation (2.70) is similar to the one describing the interaction of a conduction electron with a dispersionless phonon [93].

The corresponding contribution to the total energy (or, more accurately, to the thermodynamic potential Ω) is defined by the graph of Fig. 2.21a. Standard manipulations yield

$$\delta\Omega = \frac{m^2e^2c}{\pi^2}\ln\left(1 + \frac{1}{\beta}\right)\omega_0\ln\left|\frac{E_F}{\omega_0}\right| \tag{2.72}$$

and one thus finds that the total energy is not analytic in ω_0. Similar results were reported in [39] and [40]. For a specific case where ω_0 is the splitting between the levels of an ion in a crystal field, the result $m^*/m \sim \omega_0^{-1}$ was discussed in detail by Fulde and Loewenhaupt [91]. According to them, such a renormalization of the effective mass is significant in, for example, Pr. As was noted earlier, a rare-earth ion with an f level split in a crystal field is a most illustrative example of a soft core.

Because the renormalization of $\hat{\Sigma}$, especially near $\varepsilon = \pm\omega_0$, is not small, the question arises about the role of the higher order interaction between inner and outer electrons.

This question was examined by Irkhin and Katsnel'son [94] for a contact interaction model described by the Hamiltonian

$$\hat{H} = \sum_{\mathbf{k}}\xi_{\mathbf{k}}\hat{c}_{\mathbf{k}}^+\hat{c}_{\mathbf{k}} - \omega_0 S^z + \mathbf{J}\hat{\mathbf{S}}\sum_{\mathbf{k},\mathbf{k}'}\hat{c}_{\mathbf{k}}^+\hat{c}_{\mathbf{k}'}, \tag{2.73}$$

where $\hat{S}$ are the "pseudospin" operators ($S^z = 1/2$ is the ground state of an ion and $S^z = -1/2$ is its excited state); the terms with $\hat{S}^{\pm}$ describe inelastic scattering processes. This Hamiltonian describes the simplest model situation where the ground state of an ion is a weakly split doublet (ω_0 is the splitting energy). As Irkhin and Katsnel'son [94] showed, all of the key results obtained

with this model hold in the more general case as well. Scattering processes where the pseudospin flips (that is, the ion moves from the ground to the excited state), describable by the interaction constants J_x and J_y, lead in the lowest order perturbation theory to results similar to (2.70) and (2.71). Using the renormalization-group method, Irkhin and Katsnel'son calculated and summed up the divergent contributions to $\Sigma(\mathbf{k}, \varepsilon)$ and the Ω potential for the higher orders in $|\mathbf{J}|$. Without going into technical details of these rather tedious computations, we will dwell on the idea of the procedure and the most important results thus obtained.

With second-order perturbations with respect to $\mathbf{J}$, there appear contributions to $\Sigma(\varepsilon)$

$$\Sigma^{(2)}(\varepsilon) = \frac{1}{2}\langle S^z\rangle J^+J^-\sum_{\mathbf{q}}\left(\frac{f_{\mathbf{q}}}{\varepsilon-\xi_{\mathbf{q}}+\omega_0}-\frac{f_{\mathbf{q}}}{\varepsilon-\xi_{\mathbf{q}}-\omega_0}\right)$$
$$= \frac{1}{2}\langle S^z\rangle J^+J^-N_F\ln\left|\frac{\varepsilon-\omega_0}{\varepsilon+\omega_0}\right|, \qquad (2.74)$$

which are singular for ε tending to $\pm\omega_0$ and similar to (2.70). Here, $J^\pm = J_x \pm iJ_y$, $N_F = N(\varepsilon_F)$ is the density of states at the Fermi level, and

$$\langle S^z\rangle = \frac{1}{2}\tanh\frac{\omega_0}{2T} \qquad (2.75)$$

is the average value of the pseudospin. For $T \ll \omega_0$, $\langle S^z\rangle = 1/2$. Similar divergencies arise in the next higher orders of perturbations with respect to $N_F|\mathbf{J}|$. Thus, direct calculations up to the third order, inclusive, for $T = 0$ yield

$$\Sigma^{(3)}(\varepsilon) = \frac{N_F}{4}J^+J^-\left[\ln\left|\frac{\varepsilon-\omega_0}{\varepsilon+\omega_0}\right|\right.$$
$$\left.+N_FJ_z\left(\ln^2\left|\frac{\varepsilon-\omega_0}{\omega_0}\right|+\ln^2\left|\frac{\varepsilon+\omega_0}{\omega_0}\right|+\ldots\right)\right]. \qquad (2.76)$$

This implies that, for ε tending to $\pm\omega_0$, the perturbation theory ceases to be applicable, and one has to carry out summation over all divergent terms of the series. Most conveniently this can be done by "a poor man's scaling," that is, the renorm-group method's simplest form proposed by P. Anderson [95].

The structure of the perturbation series (2.76) implies that the singularities at ε tending to $-\omega_0$ and to $+\omega_0$ may be regarded independently (there are no divergent "cross" terms of the type $\ln|(\varepsilon-\omega_0)/\omega_0|\ln|(\varepsilon+\omega_0)/\omega_0|$). For the subsequent discussion, it is likewise important that there are no terms divergent at the very Fermi level (of the type $\ln|\varepsilon/\omega_0|$). Let us consider one of the singularities at ε tending to $\pm\omega_0$. *Because our task is to carry out summation over the most* singular terms in each order of $N_F|\mathbf{J}|$, the answer we are interested in must not depend on the exact truncation parameter in (2.76) (for example, on the replacement $\ln^2|(\varepsilon\pm\omega_0)/\omega_0| \to \ln^2|(\varepsilon\pm\omega_0)/2\omega_0|$) and will lead to the appearance of less singular additional terms. Consider the quantity

$$\xi(\omega_0) = \frac{1}{N_F}\sum_{|\xi_{\mathbf{q}}|<\omega_c}\frac{f_{\mathbf{q}}}{\varepsilon-\xi_{\mathbf{q}}\mp\omega_0}, \qquad (2.77)$$

where summation is carried out over a layer of thickness ω_c near ε_F. We reduce the thickness of the layer by going over from ω_c to $\omega_c - \delta\omega_c$. In the case at hand, the rationale of the scaling hypothesis is briefly this: after one "discards" some degrees of freedom, the remaining degrees of freedom can be described (in the sense of their behavior at ε tending to $\pm\omega_0$) by a Hamiltonian of the form (2.73) but, possibly, with modified parameters: $\mathbf{J} \to \mathbf{J} - \delta\mathbf{J}$. This change can be calculated by the perturbation theory. For ε tending to ω_0, the result takes the form

$$\delta J^\pm = 0; \quad \delta J^\mp = \pm N_FJ^\mp J^z\frac{\delta\omega_c}{\omega_c};$$
$$\delta J^z = \mp\frac{1}{2}N_FJ^+J^-\frac{\delta\omega_c}{\omega_c}. \qquad (2.78)$$

The final step is to go over from the equations (2.78) to the differential equations of the renorm group for the effective interaction constants $\mathbf{J}_{\text{eff}} \equiv \mathbf{J}(\omega_c)$

$$\frac{\partial J^\pm_{\text{eff}}}{\partial\xi} = 0; \quad \frac{\partial J^\mp_{\text{eff}}}{\partial\xi} = \pm N_FJ^\pm_{\text{eff}}J^z_{\text{eff}};$$
$$\frac{\partial J^z_{\text{eff}}}{\partial\xi} = \mp\frac{1}{2}N_FJ^+_{\text{eff}}J^-_{\text{eff}} \qquad (2.79)$$

and to analyze their behavior at ξ tending to infinity as ε tends to $\pm\omega_0$. Precisely this behavior will determine the character of the singularity in $\Sigma(\varepsilon)$ at ε tending to $\pm\omega_0$. Equations (2.79) are easy to solve

$$J^z_{\text{eff}} = J_0\frac{\exp(\mp J_0N_F\xi)-K}{\exp(\mp J_0N_F\xi)+K}, \qquad (2.80)$$

where

$$J_0 \equiv |\mathbf{J}|, \quad K \equiv \frac{J_0-J^z}{J_0+J^z},$$

and

$$J^+_{\text{eff}}J^-_{\text{eff}} = \frac{4J_0^2K\exp(\mp J_0K\xi)}{[\exp(\mp J_0N_F\xi)+K]^2} \to 0. \qquad (2.81)$$

Thus, the singularity in $\Sigma(\varepsilon)$ is weakened because the effective constant J^+J^- in (2.74) goes to zero

$$\ln\left|\frac{\omega_0}{\varepsilon\mp\omega_0}\right| \to \left(\frac{\varepsilon\mp\omega_0}{\omega_0}\right)^{J_0N_F}. \qquad (2.82)$$

We now turn to the renormalization of the effective mass m^*/m near the Fermi level ($\varepsilon = 0$). The result of

the second-order perturbation theory, stemming from (2.74),

$$\frac{m^*}{m} \sim \frac{1}{Z^*} = 1+\frac{N_FJ^+J^-}{2\omega_0} \qquad (2.83)$$

[compare with (2.71)] remains valid even if one takes into account the higher order perturbations in $N_F(\mathbf{J})$. This follows from the structure of the series expansion of $\Sigma(\varepsilon)$ in (2.76), which may be written as

$$\Sigma(\varepsilon) = \sum_{n=2}^{\infty}(N_F|\mathbf{J}|)^nF_n\left(\frac{\varepsilon}{\omega_0}\right), \qquad (2.84)$$

where, as is shown in [94], the functions $F_n(x)$ are regular (which is very important!) for x tending to zero. Then we have

$$\frac{\partial\Sigma(\varepsilon)}{\partial\varepsilon} = \frac{1}{\omega_0}\sum_{n=2}^{\infty}(N_F|\mathbf{J}|)^nF'_n(0), \qquad (2.85)$$

and the result (2.83) holds for $N_F|\mathbf{J}| \ll 1$ and an arbitrary ω_0.

Thus, in the soft core case, the energy spectrum of conduction electrons has significant singularities. Notably, the renormalization of the effective mass at the Fermi level can, in theory, be as significant as one may wish.

Quite naturally, the question arises about the reverse effect of conduction electrons on the excited states of the ion core. That is what we proceed to discuss.

Ordinarily, for the Green's pseudospin function $D(\omega)$ that describes these excitations in the lowest order of perturbation, one obtains the following expression:

$$D_0(\omega) = \frac{1}{\omega-\omega_0+i\Gamma(\omega)}, \qquad (2.86)$$

where (at $J^+ = J^- = J_\perp$ and $\omega \ll E_F$)

$$\Gamma(\omega) = \frac{\pi}{4}J_\perp^2\sum_{\mathbf{k}}(f_{\mathbf{k}'}-f_{\mathbf{k}})_{(\omega<\varepsilon_F)}\delta(\varepsilon_{\mathbf{k}'}-\varepsilon_{\mathbf{k}}+\omega)$$
$$\simeq \frac{\pi}{4}N_FJ_\perp^2\omega \qquad (2.87)$$

is the damping of local excitations owing to interaction with conduction electrons. Higher order corrections lead to a strong renormalization of $D_0(\omega)$ due to Anderson's "orthogonality catastrophe" (see [96]). The essence of this catastrophe is that a change in the state of the core (and, generally, of the scattering center) brings about a radical rearrangement of the many-electron system, which tends to suppress the change that caused it. As with the X-ray spectra of metals [96], the orthogonality catastrophe changes the analytic properties of $D(\omega)$ by transforming a pole into a branch cut

$$D(\omega) \simeq -E_F^{-\alpha}[-D_0(\omega)]^{-1+\alpha}, \qquad (2.88)$$

where $\alpha = (N_FJ^z)^2$. This must, among other things, lead to an asymmetric shape of the core excitation spectrum

$$g(\omega) = -\frac{1}{\pi}\text{Im}D(\omega) \simeq \frac{1}{\pi E_F^\alpha}\left\{\Gamma(\omega)+\alpha(\omega_0-\omega)\right.$$
$$\left.\times\left[\frac{\pi}{2}+\text{atan}\frac{\omega-\omega_0}{\Gamma(\omega)}\right]\right\}[(\omega-\omega_0)^2+\Gamma^2(\omega)]^{-1+\frac{\alpha}{2}} \qquad (2.89)$$

compared with the symmetric Lorentz line that results when one disregards the many-electron effects. Another manifestation of the orthogonality catastrophe is a decrease in the average thermodynamic potential $\langle S^z\rangle$ in comparison with 1/2 at $T = 0$ (a partial occupation of the upper level)

$$\langle S^z\rangle = \frac{1}{2}\left(\frac{\omega_0}{E_F}\right)^\gamma, \quad \gamma = \frac{1}{2}(J_\perp N_F)^2. \qquad (2.90)$$

Finally, one can calculate a "singular" contribution (for ω_0 tending to zero) to the Ω potential, equal, according to the perturbation theory, to

$$\delta\Omega \simeq \frac{1}{2}\gamma\omega_0\ln\left|\frac{E_F}{\omega_0}\right| \qquad (2.91)$$

[compare with (2.72)], or, when one considers the higher order terms, to

$$\delta\Omega = -\frac{1}{2}\omega_0\left(\frac{\omega_0}{E_F}\right)^\gamma. \qquad (2.92)$$

Unfortunately, the real numerical values of the power exponents α and γ for specific systems cannot yet be estimated. By way of explanation, note that (2.92) can be derived from (2.90) by use of the Hellmann–Feynman theorem

$$\frac{\partial\Omega}{\partial\omega_0} = \left\langle\frac{\partial\hat{H}}{\partial\omega_0}\right\rangle = -\langle S^z\rangle. \qquad (2.93)$$

Thus, the interaction of conduction electrons with low-lying excitations can substantially change the properties of both the electrons and of the excitations and give rise to contributions, nonanalytic in terms of ω_0, to the thermodynamic potential of the system. In the next chapter, we will discuss physically similar contributions to the properties of metals ("screening anomalies"), which arise even when low-lying energy excitations are of a purely "band" origin.

2.6. The Collapse of f Electrons and Intermediate Valence

Situations where the very state of the ion core changes in response to changes in external parameters is of particular interest. This above all concerns intermediate-valence systems [92, 97]. These are some compounds of Ce, Sm, Eu, Tm, and Yb, in which some of the *f* electrons become delocalized.

Several standpoints were advanced as regards the state of *f* electrons in intermediate-valence systems. According to the most widely accepted one, some of the *f* electrons change to the *d* states owing to hybridization and/or exciton processes [92, 97 - 100]. Accord-

Table 2.5. Level energies, mean squares of wave-function radii, and potential parameters for two Ce configurations (in atomic units)

Configuration	Exchange	$\langle r^2\rangle_{f^-}$	$\langle r^2\rangle_{f^+}$	ε_{f^-}	ε_{f^+}	$\langle r^2\rangle_{p^-}$	$\langle r^2\rangle_{p^+}$	ε_{p^-}	ε_{p^+}	W
$4f^1_{5/2}5d^1_{3/2}6s^2$	$X\alpha$	1.57	1.61	0.230	0.217	3.27	3.60	0.939	0.835	
	BH	2.83	3.35	0.248	0.235					0.040
$4f^2_{5/2}6s^2$	$X\alpha$	3.79	9.11	0.051	0.041	3.46	3.83	0.844	0.748	
	BH	7.64	8.16	0.070	0.060					0.078

Note: The subscript "p" labels the states of the filled 5_p shell, $X\alpha$ stands for the exchange after Slater [38], and BH, after Barth and Hedin [110].

Table 2.6. Parameters of the effective f potential in the $4f^15d^16s^2$ and $4f^26s^2$ configurations of cerium and the $5f^36d^17s^2$ and $5f^47s^2$ configurations of uranium (in atomic units)

Element	Configuration	$r_0^{(1)}$	$r_{\min}^{(1)}$	$U_{\min}^{(1)}$	$r_0^{(2)}$	$r_{\max}$	$U_{\max}$	$r_0^{(3)}$	$r_{\min}^{(2)}$	$U_{\min}^{(2)}$
Ce	$4f^1_-$	0.250	0.370	−5.62	1.445	2.38	0.172	6.0	12.0	−0.041
	$4f^2_-$	0.252	0.371	−5.33	1.270	2.095	0.207	6.0	12.0	−0.041
U	$5f^3_-$	0.114	0.185	−43.29	1.844	2.762	0.140	6.0	12.0	−0.042
	$5f^4_-$	0.117	0.185	−43.15	1.724	2.614	0.162	6.0	12.0	−0.042

ing to another point of view, intermediate-valence systems are Kondo lattices with high Kondo temperatures [101]. It is thus presumed that the f electrons in these systems are completely localized and that the singularities showing up in their electronic spectra near the Fermi level are of many-electron origin. These matters are discussed in detail in Ch. 6.

Recently, however, a growing popularity was gained by Johansson's idea [102] about the special nature of intermediate valence in α-Ce and, according to Finkel'shtein [103], in compounds of Ce with transition metals. The rationale of Johansson's idea is this. In the intermediate-valence systems based on Sm, Eu, and some other rare-earth elements, the $4f$ electron becomes partly delocalized because it changes to the $5d$ state. By contrast, the more likely cause for such a development in the case of Ce is a change in the character of the $4f$ states themselves – the transition from the localized to the itinerant behavior due to the overlap of the f functions at different sites; that is, a Mott transition in the $4f$ subsystem. Johansson's hypothesis, advanced on the basis of thermochemical findings, has of late been confirmed by many spectroscopic studies [103 - 105] and band-theoretic calculations [106]. The latter demonstrate a significant increase in the width of the f band that occurs as one goes over from the lattice constant corresponding to γ-Ce to the lattice constant of α-Ce. At the same time, the occupancy of f- and d-symmetry states changes insignificantly. A good deal of interest is evoked by the microscopic nature of the mechanism responsible for the fact that the $4f$ electron in Ce becomes itinerant. Inquiry into this matter can offer an opportunity to demonstrate the fruitfulness of some ideas from atomic physics in their application to solid-state physics.

Finkel'shtein [103] supposes that the state of tetravalent Ce (without localized $4f$ electrons) corresponds to the $4f^2$ rather than the $4f^0$ atomic configuration. He further supposes that the change of $4f$ electrons to the itinerant behavior upon transition from the $4f^15d^16s^2$ configuration (configuration A) to the $4f^26s^2$ configuration (configuration B) is related to what is known as the "infiltration" of f electrons through the centrifugal barrier. This results in an abrupt change in (the collapse of) the radius and energy of the f state in response to a small perturbation in the atomic parameters [107]. Kamyshenko *et al.* [108] investigated the collapse phenomenon in Ce and some other f elements on the basis of atomic calculations.

By "collapse" we mean a sudden change in the characteristics of the f state in response to a small change in potential (here, this change refers to a change in the configuration and not in the charge on the nucleus [107]). The collapse is accompanied by a drastic reduction in the radius and energy of the corresponding state. The underlying cause of this phenomenon is the "two-well" character of the atomic potential for the f electron and the centrifugal barrier (Fig. 2.27). It occurs when conditions present themselves for a bound state to exist in the inner potential well where the electron moves from the outer well. As is seen from Fig. 2.28 [109], the collapse causes an abrupt decrease in the energy of the $4f$ state as one goes across the Periodic System. Calculations done by Kamyshenko *et al.* (see Table 2.5) confirm that configurations A and B do differ markedly in the mean-square radius $\langle r^2\rangle_{4f}$ and the energy ε_{4f} of the f level. On the other hand, the self-consistent effective potentials for the f electrons differ only slightly (see Table 2.6). Thus, on moving from B to A, the f electron suffers a collapse.

The collapse of the f electron in Ce leaves the other core states almost unaffected. For example, $\langle r^2\rangle_{5p}$ in configuration A is almost exactly the same as it is in configuration B. An important question is how the collapse affects various characteristics of the $4f$ states, both atomic and those governing their behavior in solids. To test Johansson's hypothesis that an increase in the direct overlap of the $4f$ functions at different states plays a decisive role when cerium and its intermetallic compounds change to an intermediate-valance state, measurements were made of the width W of the canonical (that is, unhybridized) $4f$ band. The collapse was found to be accompanied by a significant decrease in the width of the canonical $4f$ band.

A few words are in order as regards the calculations reported in [108]. The atomic calculations were made within the relativistic version of the self-consistent X_α method for $\alpha = 0.7$ adjusted for the Latter correction so as to ensure a correct asymptotic behavior of the potential acting on the electron at a large distance r from the nucleus (see [108]). Calculations were also made, in which the $X\alpha$ potential was replaced by the potential from [110]. As is seen, although the parameters of the "inflated" state are rather sensitive to such a replacement and to spin-orbital interaction (see the ± indices in the tables), a collapse does take place with either of the spin projections and is independent of the choice of the exchange-correlation potential ($X\alpha$ or BH, see Table 2.5). Note, however, that with $\alpha = 1$, no collapse occurs [108]. The width W of the canonical (that is, unhybridized) band was calculated within O.K. Andersen's linearized band theory (for more detail, see [108]).

Another interesting issue is the rearrangement that occurs in the core as a result of a collapse. Quantitatively, it can be estimated in terms of the overlap parameter of Slater determinants $|\Phi\rangle$ developed from the core functions φ_ν in configurations A and B,

$$\langle\Phi_A|\Phi_B\rangle = \det S_{\nu\nu'},$$

$$S_{\nu\nu'} = \langle\varphi_\nu^A|\varphi_{\nu'}^B\rangle.$$

Our calculations show that the overlap of the old and new functions associated with the same orbital state are very nearly unity: $S(5p, 5p) \simeq 0.9997$ and even $S(4f, 4f) \simeq 0.98$.

Thus, one may neglect the effect of collapse on core states, and its practically only consequence is the increased overlap of the $4f$ wave functions at different centers, as revealed by the increased width of the canonical $4f$ band.

The spectroscopy of $3d$ photoelectrons in mixed-valence intermetallic compounds of cerium, such as $Ce_{24}Ce_{11}$ [111] and $CeRu_2$ [112] demonstrates the existence of a triple-peak structure associated by Abbati *et al.* [111] and by Schlapbach *et al.* [112] with the ground state of the Ce ion in these substances. Under Finkel'shtein's hypothesis confirmed by Kamyshenko *et al.*, the so-called f^0 configuration (free from localized f electrons) is in fact related genetically to the f^2 atomic configuration. Then the peak identified by Abbati *et al.* and Schlapbach *et al.* with the contribution from the f^2

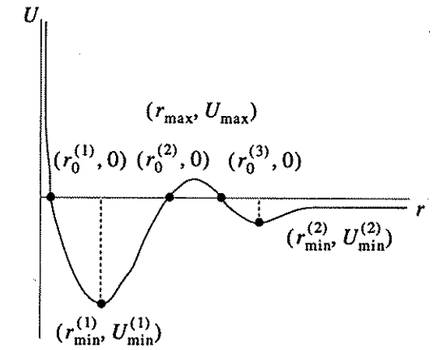

Fig. 2.27. *Schematic view of the effective potential for an f electron. The parameter values are given in Table 2.6.*

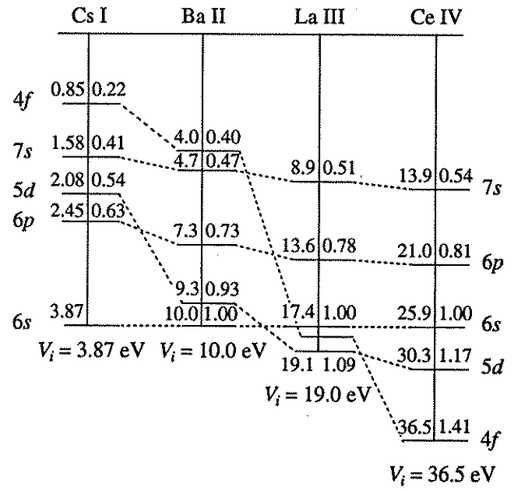

Fig. 2.28. *Changes in the electron bonding energy in various orbital states in the series of isoelectron ions Cs I (Cs^0)–Ba II (Ba^+)–La III (La^{++}), Ce IV (Ce^{+++}). The energy is given in eV on the left and in units of the binding energy of the 6s electron on the right of the vertical line [109].*

configuration should naturally be assigned to the final-state effects. Finkel'shtein calculated the states of the Ce atom in the $4f^25d^16s^2$ configuration with a hole in the $3d_{5/2}$ subshell. Moreover, $\langle r^2\rangle_{4f} \simeq 1.3$, which is even smaller than in configuration A. Thus, in contrast to configuration B, both f electrons in the final state with a core hole are localized and can give rise to an additional peak in photoelectron spectra. This conclusion will remain valid even if, in keeping with Slater's transition-state method [38], one takes into account the "hole effect" by calculating the configuration

$$3d^{3.5}_{5/2}3d^6_{7/2}\ldots 4f^{1.5}5d^16s^2 \qquad (\langle r^2\rangle_{4f} \simeq 1.4).$$

In the case of Ce, the calculations done to date permit one to validate and interpret the conjectures Johans-

Table 2.7. Energy, mean square of radii and potential parameters for Pr and Nd (in atomic units)

Element	Configuration	Exchange	$\langle r^2 \rangle_{f^-}$	ε_{f^-}	Potential parameters
Pr	$4f^2_{5/2}5d^1_{3/2}6s^2$	Xα	1.41	0.261	0.019
		BH	1.42	0.278	
Pr	$4f^3_{5/2}6s^2$	Xα	2.32	0.070	0.044
		BH	2.14	0.093	
Nd	$4f^3_{5/2}5d^1_{3/2}6s^2$	Xα	1.28	0.287	
			–	–	
Nd	$4f^4_{5/2}6s^2$	Xα	1.88	0.088	

Table 2.8. Energies of f levels and mean squares of wavefunction radii for two configurations each of U, Np, and Pu (in atomic units)

Element	Configuration	$\langle r^2 \rangle_{f^-}$	ε_{f^-}
U	$5f^3_{5/2}6d^1_{3/2}7s^2$	2.814	0.147
	$5f^4_{5/2}7s^2$	4.743	0.058
Np	$5f^4_{5/2}6d^1_{3/2}7s^2$	2.460	0.182
	$5f^5_{5/2}7s^2$	3.417	0.076
Pu	$5f^5_{5/2}6d^1_{3/2}7s^2$	2.203	0.216
	$5f^6_{5/2}7s^2$	2.814	0.096

son advanced with regard to the character of changes in its electronic structure in intermediate-valence systems. In the case of the actinides, they can yield entirely new results.

Importantly, a collapse by itself is not a sufficient condition for intermediate valence to occur by Johansson's mechanism. For example, as one can see from Table 2.7, which presents calculated results for Pr (and Nd), a transition from the f^3 to the f^2 configuration is likewise accompanied by a collapse (although less pronounced than in Ce). Nevertheless, even in the delocalized state, the width of the f band is too small for the f electron to become itinerant (the width W is about the same order of magnitude as for Ce in configuration A and substantially smaller than for Ce in configuration B). Here, a significant factor is the absolute value of $\langle r^2 \rangle_{4f}$, with which, as one can see from Table 2.5, the width W correlates.

In a U atom, the excited $5f^47s^2$ configuration, nearest in terms of energy to the ground $5f^36d^17s^2$ configuration [113] corresponds, as in Ce, to the transition of the d electron to the f state and not the other way around (in contrast to, say, Sm). This prompts one to suppose that in U compounds the intermediate-valence mechanism must be of the Ce type; that is, it must be associated with the "inflation" of the wave function in consequence of the transition from the f^3 to the f^4 state. To verify this supposition and to investigate the collapse phenomenon in the 5f states, Kamyshenko *et al.* [108] calculated U atoms in the two configurations, and also Np and Pu atoms. The results are given in Table 2.8. Compared with the 4f electrons, the collapse is seen to be less pronounced and disappears more gradually as one moves across the Periodic System. Still, it does happen, at least in the case of U (upon the transition from the f^4 to the f^3 configuration). This permits one to suppose that in the U-based intermediate-valence system the nature of intermediate valence is, as in the case of Ce, more likely related to the fact that the f electrons become itinerant, than to their transition to the d state. The parameters of the f potential for Ce and U are given in Table 2.6.

2.7. Conclusion

This chapter focused on the concept of pseudopotential, a detailed inquiry into the conditions under which this concept can be introduced, and the demonstration of its high efficiency in cases where these conditions are satisfied. The pseudopotential theory of simple metals is a relatively rare example of a consistent microscopic description of a many-particle system. It enables one to advance, step by step, all the way from the summation of Feynman diagrams to the numerical calculation of, say, anharmonic effects and the melting curve, and to compare calculation with experiment. This explains why we have covered all of these matters in fair detail.

What follows is a summary of the most fundamental ideas and results.

1. The possibility of introducing pseudopotential as an intrinsic characteristic of the ion core can be justified in rigorous terms if the core excitation energy ω_0 is large in comparison with the conduction-electron plasma frequency ω_{pe} (a rigid core). Among the alkali metals, even singly charged ions satisfy this requirement, which is why the pseudopotential V_{ps} is relatively weak, and it is legitimate to apply the perturbation theory in terms of V_{ps}. This allows one to calculate the fine characteristics of the solid and liquid phases with high accuracy. In the noble metals, however, one has to "strip bare" all of the d shell in order to satisfy the condition $\omega_0 \gg \omega_{pe}$. As a result, V_{ps} will be so strong that its introduction will actually offer no advantage over a complete band-theoretic calculation.

2. The soft core case, $\omega_0 \ll \omega_{pe}$, can hold, for example, in rare-earth compounds, where ω_0 is the local-excitation energy of the f shell. Now the interaction of conduction electrons with the core gives rise to substantial anomalies in the electronic spectrum, notably, to a significant increase in the effective mass.

3. Cerium supplies an interesting example of a situation where an analysis of ion core properties enables one to get deep insight into the properties of the metal. The mixed valence of α-Ce is apparently related to the "swelling" of the wave function of the 4f electron as it changes from the $4f^15d^1$ to the $4f^2$ configuration.

Chapter 3. DENSITY-OF-STATES PEAKS: AN ANALOG OF LOCALIZATION IN THE BAND-THEORETIC APPROACH

Anomalies in the physical properties of the transition metals, their alloys, and compounds are discussed. In many cases, a common factor responsible for these anomalies can be identified – the existence of electronic density-of-states peaks near the Fermi level. In turn, these peaks may arise owing to the localized behavior of the electrons and to the geometry of the crystal lattice; in the latter case they can appear even with almost free electrons. As the results reported herein imply, an analysis of electronic density-of-states and of its behavior with changes in external parameters can be an efficient tool with which one can qualitatively explain and predict the anomalous properties of metals.

3.1. On the Nature of Narrow Peaks in the Electronic Density-of-States

Thus far, we set the ion core against the system of quasifree conduction electrons treated as a single entity. Actually, even within the one-electron approximation, these quasifree electrons "live" in the crystal lattice and, in consequence, have properties strongly different from those of the "truly" free electrons. Small groups of electronic states near so-called critical points, $\mathbf{k} = \mathbf{k}_c$, where the electron velocity $\mathbf{v}(\mathbf{k})$ goes to zero, can also play a special role in the properties of a metal. In this sense, such electronic states come closer in some properties to "localized" states, although they remain delocalized ("Blochlike") in strict terms. More specifically, this implies that they can make a significant and strongly energy-dependent contribution to the electronic density-of-states $N(E)$. This situation stands midway between the "smooth" behavior $N(E) \sim E^{1/2}$ for free electrons and the "diffuse" δ-like contribution to $N(E)$ from quasilocalized states (see, for example, [2]). It is the density-of-states $N(E)$ and, especially, its behavior near the Fermi level E_F that govern many properties of a metal. From the viewpoint of an analysis of the form of $N(E)$, the degree of localization of particular states in real space is a special case of the question about the role of small groups of electronic states responsible for singularities in $N(E)$. That is what we are going to discuss in this chapter.

As regards the degree of the localized and delocalized (itinerant) behavior of electrons we are concerned with, there is a "naïve" belief that narrow $N(E)$ peaks directly reflect strong electron localization in real space, whereas a broad energy band is associated with a "truly itinerant" behavior. As early as 1953, van Hove [114] demonstrated that, given any two- or three-dimensional lattice, $N(E)$ singularities would arise within each energy band for purely topological causes. Those are van Hove singularities associated with points $\mathbf{v}(\mathbf{k}_c) = 0$. Three-dimensional lattices have root-type, one-sided van Hove singularities: $\delta N(E) \sim [\pm(E - E_c)]^{1/2}\theta(\pm(E - E_c))$, where E_c is the singular point of the spectrum, $\theta(x > 0) = 1$ and $\theta(x < 0) = 0$.

These singularities are rather weak ($\partial N(E)/\partial E$ diverges) and, generally, one ought not to expect any sudden "peaks" or "crevasses" in $N(E)$. On the other hand, specific band-theoretic calculations revealed very narrow and abrupt peaks in $N(E)$ in the conduction band even in some simple metals (Ca, Sr, Li, and some others), where, it would seem, one has no reason at all to expect electron localization. Such a situation is even more typical of many classes of metal compounds (see the discussion in [39]).

Thus, whether or not the degree of electronic-state localization is related to the presence of narrow $N(E)$ peaks is not a very simple question. A need, therefore, exists to inquire into the possibility of their purely geometrical origin (that is, one conditioned on the crystal structure). A most illustrative example of such an inquiry into the "geometrical enhancement" of van Hove singularities is Gor'kov's model [116, 117] for compounds with the A-15 structure (such as V_3Si and Nb_3Sn). In these compounds one can, however, isolate "quasi-one-dimensional" motifs – chains of (V or Nb) atoms running in three mutually perpendicular directions. As Weber [118] demonstrated, with these compounds one may speak of a noticeable localization of electron density $\rho(\mathbf{r})$ in real space, but along the chains rather than on atoms. On the other hand, in Ca and Sr, which have an fcc lattice and a nearly spherical Fermi surface [119, 120], the narrow $N(E)$ peaks come as a surprise. A detailed study into the origin of these peaks was undertaken in [70]. Van Hove singularities arise from points where the group velocity $\mathbf{v}_n(\mathbf{k}) = \partial E_n(\mathbf{k})/\partial \mathbf{k}$ goes to zero (here, E_n is the electron energy and $\mathbf{k}$ is the quasimomentum). The calculation of $E_n(\mathbf{k})$ and $\mathbf{v}_n(\mathbf{k})$ performed in [70] showed that near the Fermi level E_F the fcc and bcc phases of Ca and Sr exhibit extended segments where $|\mathbf{v}_n(\mathbf{k})|$ is small (see Figs. 3.1 and 3.2). In the bcc lattice of Ca, these are some of the P–N and N–H lines, and in the fcc lattice of Sr, these are some of the X–U, U–L, L–K, K–U, and K–W lines. All of these lines lie at the boundaries of the Brillouin zone (Fig. 3.3); by virtue of symmetry, $(\mathbf{v}_n(\mathbf{k}))_\perp = 0$ on the Γ–N and N–H lines (where $(\mathbf{v}_n)_\perp$ [sign: perpendicular] are the velocity components in the perpendicular direction). If such a line has two van Hove singularities closely spaced in terms of energy, they will show up in $N(E)$ as an almost single "quasi-two-dimensional" singularity.

Consider this matter in more detail with reference to [70]. (For the density of phonon states, a similar enhancement in van Hove singularities was discussed earlier by Gilat [163].) Assume that along some segment in $\mathbf{k}$ space we have $(\mathbf{v}_n)_\perp = 0$. Then, near that segment we can write $E(\mathbf{k})$ as

$$E(\mathbf{k}) = E_0 + \gamma\xi(k_1) + \frac{k_2^2}{2m_2(k_1)} + \frac{k_3^2}{2m_3(k_1)}, \qquad (3.1)$$

where, for definiteness, the coordinates of the segment are defined as $k_2 = k_3 = 0$ and $k_a \le k_1 \le k_b$, where k_a and

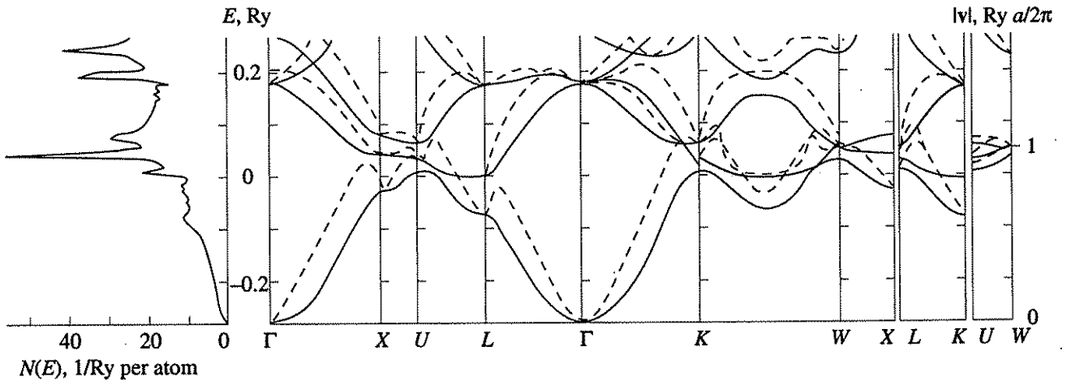

Fig. 3.1. *Energy spectrum of the fcc phase of calcium. The electronic density of states is given on the left, the dispersion curves E(k) (full lines) on the right. The dashed curves represent E(k) + v(k), where v(k) is the group velocity in Ry a/2π. To the van Hove singularities there corresponds the merger of the full and dashed lines.*

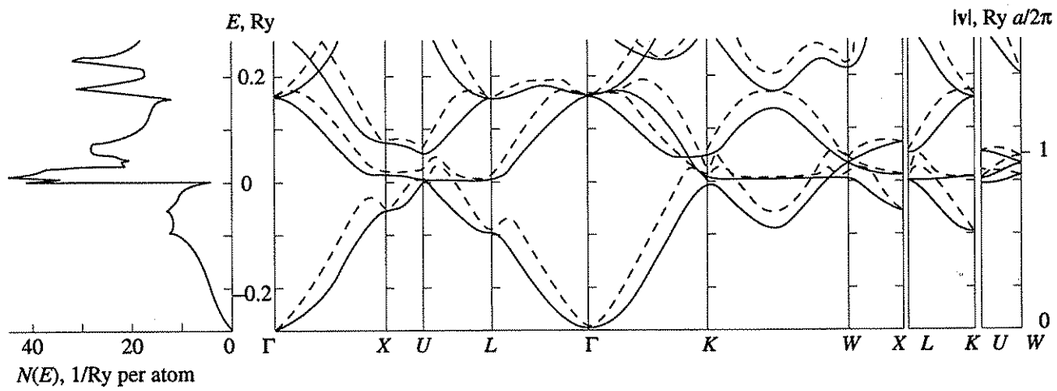

Fig. 3.2. *Same as in the previous figure, but for the fcc phase of strontium.*

k_B are the coordinates of two nearest van Hove singularity points on the line, and $\gamma \equiv E_a - E_b$ is small. Then the singularity contribution to $N(E)$ takes the form [70]

$$\delta N(E) = \begin{cases} \dfrac{\pi\Omega_0}{(2\pi)^3}\displaystyle\int_{k_a}^{k_b} dk_1 \bar{m}(k_1)\,\theta[E - E_a - \gamma\xi(k_1)] \\ \qquad \times \operatorname{sgn} m_2(k_1)_1, \quad m_2 m_3 > 0, \\ -\dfrac{\Omega_0}{(2\pi)^3}\displaystyle\int_{k_a}^{k_b} dk_1 \bar{m}(k_1) \ln|E - E_a - \gamma\xi(k_1)|, \\ \qquad m_2 m_3 < 0, \end{cases} \tag{3.2}$$

where $\bar{m} = [|m_2(k_1)m_3(k_1)|]^{1/2}$ and Ω_0 is the volume of the unit cell. For γ tending to zero, the van Hove singularity takes the form typical of the two-dimensional case. Notably, it may so happen that $\delta N(E) \sim -\ln(E - E_c)$, which is a *two-sided* singularity associated with the divergence of $N(E)$ and not only of $\partial N/\partial E$. Generally, the *P–N* line in bcc metals (such as Li, V, Cr, Fe, and Ba) [68, 115] quite often yields "giant" van Hove singularities. A special trait of Ca is that this singularity lies close to E_F.

In Sr, which has an fcc lattice, these lines do not have the property that $(\mathbf{v}_n)_\perp = 0$ by virtue of symmetry, and van Hove singularities are enhanced owing to a somewhat different cause. The point is that the Brillouin zone of an fcc crystal is approximated quite closely by a sphere. In the free-electron approximation, this sphere for divalent metals is almost identical to the Fermi sphere, which implies that in the zero approximation the energy is constant all along the boundary of the Brillouin zone. This is a prerequisite for the existence of lines of a nearly constant energy close to E_F at

the boundaries of the Brillouin zone in fcc Ca (and to a lesser degree in fcc Sr [70]).

In addition, one should expect narrow $N(E)$ peaks in metals with narrow energy bands. As an example, consider the results of band-theoretic calculations [121] for the δ phase of fcc plutonium (Figs. 3.4 and 3.5). To the narrow $N(E)$ peak above E_F (see Fig. 3.4), a multiplicity of almost "merged" van Hove singularities and a multiplicity of lines with a low electron velocity (see Fig. 3.5) correspond. The van Hove singularities closest to E_F are located near the points U and K ($E_c - E_F \approx 4 \times 10^{-4}$ Ry). As can be seen from Fig. 3.6, the Fermi surface neatly "fits" into the corresponding corners of the Brillouin zone.

Now let us sum up a few facts. In the general case, the root-type van Hove singularities are the only type of $N(E)$ singularities in a three-dimensional lattice. All of the stronger singularities result from their merger (degeneracy), which may be either the effect of a structural cause (for example, symmetry) or occur by chance. But then, as the examples given above show, such "chance" occurrences are not at all rare. A change in external parameters (for example, pressure) may, however, cause a different change in the position of the van Hove singularities that form, for example, an $N(E)$ peak. This will then cause a change not only in the distance from the peak to E_F, but also in the shape of the peak. Such a change is illustrated in Figs. 3.7 and 3.8, which give the values of $N(E)$ calculated for the various phases of Sr and Ba and for different lattice constants [122].

3.2. Density-of-States Peaks and Anomalies of Observables in the Single-Particle Approximation

Singularities in $N(E)$ that occur near E_F show up directly as anomalies in the electronic and lattice properties of metals. In turn, the singularities themselves can be detected through an experimental inquiry into such anomalies. For example, in the one-particle approximation, spin susceptibility χ and electronic heat capacity C_e are expressed in terms of $N(E)$ by the formulas [2]

$$\chi(T) = \mu_B^2 \int_{-\infty}^{\infty} dE N(E)\left(-\frac{\partial f(E)}{\partial E}\right), \tag{3.3}$$

$$C_e(T) = \frac{1}{T}\int_{-\infty}^{\infty} dE E^2 N(E)\left(-\frac{\partial f(E)}{\partial E}\right), \tag{3.4}$$

where $f(E) = [\exp E/T + 1]^{-1}$ is the Fermi distribution function, E is the energy reckoned from the chemical potential $\mu(T)$, and μ_B is the Bohr magneton. Consider the simplest case where, a short distance Δ from E_F, there is a peak of width $\Gamma \ll \Delta$, whose contribution to $N(E)$ is $a\delta(E - \Delta)$. Here, the corresponding contributions to $\chi(T)$ and $\gamma(T) \equiv C_e(T)/T$ are described by non-monotonic functions of temperature

$$\left.\begin{aligned} \chi(T) &= \frac{a}{4T\cosh^2(\Delta/2T)}, \\ \gamma(T) &= \frac{a\Delta^2}{4T^3\cosh^2(\Delta/2T)}, \end{aligned}\right\} \tag{3.5}$$

which have a maximum at $T \sim \Delta$. The anomalous behavior persists even in cases where the peak has a finite

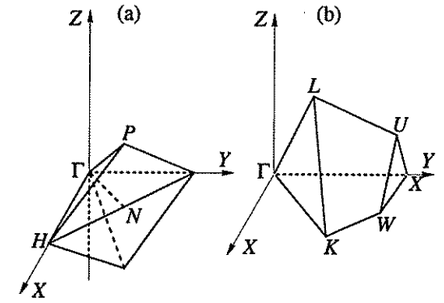

Fig. 3.3. *Irreducible part (1/48) of the Brillouin zone for the bcc structure (a), and 1/12th part of the Brillouin zone for the fcc structure (b).*

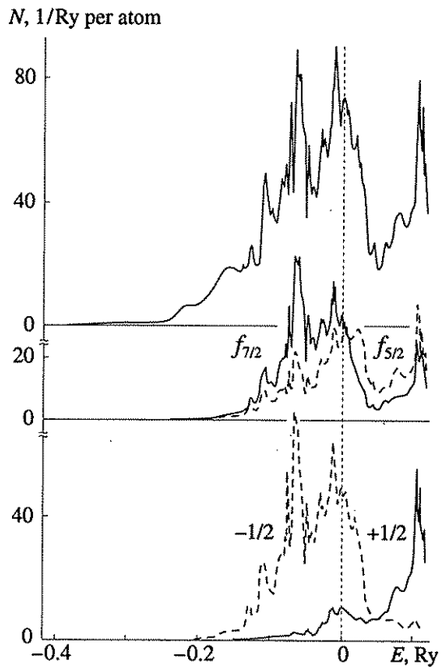

Fig. 3.4. *Total density of states and partial relativistic ($f_{5/2}$, $f_{7/2}$) and spin ($f_{+1/2}$, $f_{-1/2}$) contributions to electronic density of states in δ-Pu.*

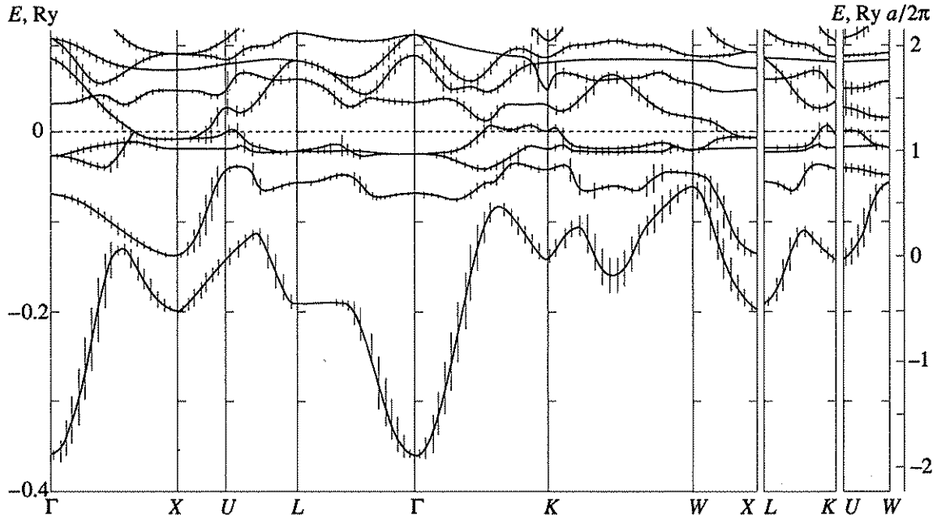

Fig. 3.5. *Dispersion curves E(k) and group velocities* $\mathbf{v}(k)$ *(vertical strokes) in δ-Pu;* $|\mathbf{v}(k)|$ *are drawn upward and downward from the corresponding E(k) curve in the units marked on the right of the scale.*

width. Model calculations of $\chi(T)$ for various forms of singularities in $N(E)$ (triangular, "twisted" triangular, jumplike, etc.) are given in [123]. When $N(E)$ has a two-dimensional van Hove singularity $\delta N(E) \sim -\ln(E - E_c)$, as, for example, in the Gor'kov model for compounds with A-15 structure [116, 117], one has

$$\chi(T) - \chi(0) \sim \eta\left(\frac{T}{\Delta}\right) \equiv \ln\frac{\Delta}{T} + \psi\left(\frac{1}{2}\right) - \mathrm{Re}\,\psi\left(\frac{1}{2} + i\frac{\Delta}{2\pi T}\right), \tag{3.6}$$

where $\psi(x) = \Gamma'(x)/\Gamma(x)$, and $\Gamma(x)$ is the gamma function. A graph of the function $\eta(T/\Delta)$ is given in [117, p. 275].

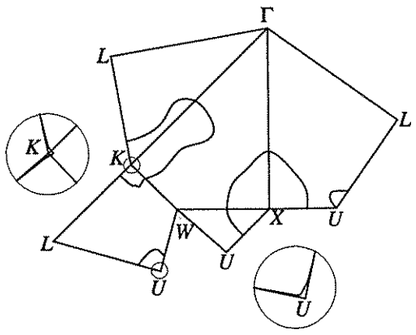

Fig. 3.6. *Section through the irreducible part of the Brillouin zone by the Fermi surface for δ-Pu. In the neighborhood of the points U and K (shown on an exaggerated scale), the Fermi surface almost exactly fits into the Brillouin zone.*

In the case at hand, the temperature dependences of the kinetic coefficients likewise turn out to be anomalous. For example, in the case of elastic scattering the electrical conductivity $\sigma(T)$ and the thermo-emf $S(T)$ are defined by the expressions [124]

$$\sigma(T) = \int_{-\infty}^{\infty} dE\sigma(E)\left(-\frac{\partial f(E)}{\partial E}\right), \tag{3.7}$$

$$S(T) = \frac{1}{eT\sigma(T)}\int_{-\infty}^{\infty} dEE\sigma(E)\left(-\frac{\partial f(E)}{\partial E}\right), \tag{3.8}$$

where $\sigma(E)$ is the conductivity function proportional to $N(E)$. Then, the anomalous part of $\sigma(T)$ is proportional to the anomalous part of $\chi(T)$ and has a singularity of the same character. The temperature dependence of $S(T)$ will likewise be nonmonotonic.

If one considers the electronic properties of a metal as a function of pressure, deformation, or impurity concentration for T tending to zero and for the $N(E)$ peak approaching E_F, then (3.3), (3.4), (3.7), and (3.8) will imply that χ, γ, and σ demonstrate anomalies of the same character as $N(E_F)$, and S, of the same character as $\partial N(E_F)/\partial E_F$, that is, far stronger anomalies. Among other things, this implies that the thermo-emf is subject to strong anomalies [of the form $(E_F - E_c)^{-1/2}\theta(\pm(E_F - E_c))$], even if an ordinary root-type van Hove singularity approaches E_F for $E = E_c$ (the Lifshitz's electronic topological transition [125]). These anomalies were first predicted by Vaks *et al.* [126] and were observed in a number of systems (see, for example, [127, 128]).

As $N(E)$ peaks approach E_F, this may give rise to anomalies not only in electronic but also in lattice properties. For example, by differentiating the band energy E_b with respect to deformations u_i under the assumption of noninteracting electrons, one can obtain the following expression for the band contribution to the elastic constants C_{ik} for $T = 0$ [129, 122]:

$$C_{ik}^{(b)} \equiv \frac{\partial^2 E_b}{\partial u_i \partial u_k} = \frac{1}{\Omega_0}\sum_{\lambda}\left[\theta(-\varepsilon_\lambda)\frac{\partial^2}{\partial u_i \partial u_k}(\varepsilon_\lambda + E_F) - \delta(\varepsilon_\lambda)\frac{\partial\varepsilon_\lambda}{\partial u_i}\frac{\partial\varepsilon_\lambda}{\partial u_k}\right], \tag{3.9}$$

where Ω_0 is the atomic volume and ε_λ is the one-particle energy reckoned from E_F. Owing to the second term in (3.9), the function $C_{ik}^{(b)}(E_F)$ contains the same singularities as $N(E)$ does. At reduced temperatures, the $C_{ik}(T)$ singularity behaves as $\chi(T)$, thereby rendering the temperature dependence $C_{ik}(T)$ nonmonotonic. Notably, the Gor'kov model for compounds with A-15 structure gives $C_{ik}(T) \sim \eta(T/\Delta)$, and for $\Delta = 0$ (when the $N(E)$ singularity occurs exactly at E_F),

$$\delta C_{ik}(T) \sim \ln T/E_F + \text{const}. \tag{3.10}$$

This explains the observed "softening" of the shear modulus with decreasing temperature that leads to a structural (martensitic) transformation (see [117]).

Thus, the observed nonmonotonic behavior of electronic and lattice properties with temperature may indicate the presence of narrow $N(E)$ peaks (or other singularities) near E_F. As an example of the experimentally observed minimum in C_{ik}, which might be associated with narrow $N(E)$ peaks, we can mention the change in the bulk modulus B in $CeBe_{13}$, observed by Lenz *et al.* [130]. If the peak occurs right at E_F ($\Delta = 0$), the temperature dependences turn monotone and are now determined by the peak's width Γ rather than by Δ.

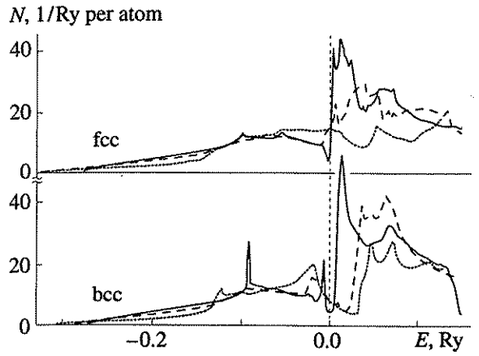

Fig. 3.7. *Electronic density of states in the bcc and fcc phases of Sr. The full, dashed, and dotted lines correspond to the compressions u = 0, 0.25, and 0.50, respectively.*

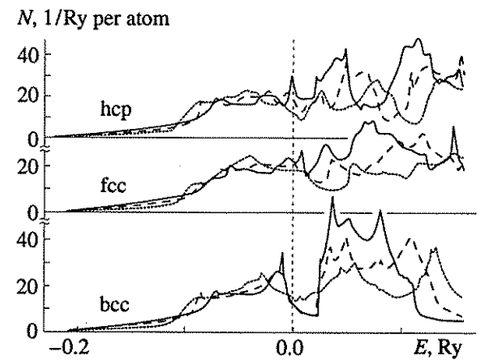

Fig. 3.8. *Electronic density of states in the bcc, fcc, and hcp phases of Ba. The full, dashed, and dotted lines correspond to the compression u = 0, 0.2, and 0.35, respectively.*

3.3. Screening Anomalies

Sometimes it may prove advantageous to analyze the $N(E)$ structure on a relatively large energy scale. Then, as the basic "structural element," one takes not a van Hove singularity but the entire $N(E)$ peak (which may contain several van Hove singularities) located a distance Δ from E_F: $\Gamma \lesssim \Delta \ll W$ (where Γ is the width of the peak and W is the width of the conduction band). This relationship between the parameters holds for most alloys and compounds, especially for *d* and *f* metals, compounds with A-15 structure [117, 118], the intermetallic NiTi [131], dilute PdFe alloys [131], to say nothing of heavy-fermion systems [132], mixed-valence systems [92], and other compounds of 4*f* and 5*f* elements [133]. The influence of $N(E)$ peaks "as an entity" on the various electronic and lattice properties of metals and alloys was qualitatively analyzed in [39 - 41], [134], and [135]. Here, we will briefly discuss their principal results. Transitions from narrow $N(E)$ peaks to E_F (or vice versa) or between filled and empty peaks (in which case Δ is the spacing between the peaks) give rise to an anomalous frequency dispersion of permittivity or polarization operator $\Pi(\mathbf{r}_1, \mathbf{r}_2; \omega)$ (screening anomalies) at $\omega \sim \Delta \ll E_F$. We will denote the corresponding contribution by $\hat{\Pi}_s$.

Consider the singularities that arise in the electronic spectrum owing to screening anomalies. The corresponding first-order-in-$\hat{\Pi}_s$ contribution to the self-energy part $\hat{\Sigma}$ takes the form [compare with (2.67)]

$$2\pi i\Sigma(\mathbf{r}, \mathbf{r}', E) = \int dr_1 dr_2 d\omega G(\mathbf{r}, \mathbf{r}'; E - \omega) \times v_{\text{eff}}(\mathbf{r}, \mathbf{r}_1) v_{\text{eff}}(\mathbf{r}_2, \mathbf{r}') \Pi_s(\mathbf{r}, \mathbf{r}_2; \omega). \tag{3.11}$$

Here,

$$G(\mathbf{r}, \mathbf{r}'; \varepsilon) = \sum_{\lambda} \frac{\psi_\lambda(\mathbf{r})\psi_\lambda^*(\mathbf{r}')}{E - E_\lambda + i\delta \operatorname{sgn} E_\lambda}, \quad (3.12)$$

$\psi_\lambda(\mathbf{r})$ and E_λ are the one-electron wave and energy functions, and $v_{\text{eff}}(\mathbf{r}, \mathbf{r}')$ is the Coulomb potential with allowance for normal screening (minus the singular contribution $\hat{\Pi}_s$).

Using a spectral representation for $\hat{\Pi}$, we may write the contribution $\hat{\Pi}_s$ as

$$\Pi_s(\mathbf{r}_1, \mathbf{r}_2; \omega) = \sum_{\nu} \frac{A_\nu(\mathbf{r}_1, \mathbf{r}_2)}{\omega_\nu^2 - \omega^2 - i\delta}. \quad (3.13)$$

The eigenstates $|\nu\rangle$ may be a pair of electron-hole states $|\lambda_1, \lambda_2\rangle$ ($E_{\lambda_1} < 0$, $E_{\lambda_2} > 0$), or they may be of many-electron origin (collective degrees of freedom, such as in ion excitation with a strong correlation, caused by, for example, the splitting of rare-earth terms in a crystal field, see Sec. 2.5; excitons, paramagnons, etc.). Inserting (3.12) and (3.13) in (3.11) and noting (2.69), one observes that for $|E| \ll E_F$ a singular contribution $\hat{\Sigma}_s$ occurs

$$\Sigma_s(\mathbf{r}, \mathbf{r}'; E) = \sum_{\lambda} \Sigma_\lambda^{(s)}(E)\psi_\lambda(\mathbf{r})\psi_\lambda^*(\mathbf{r}'),$$

such that

$$\left.\frac{\partial \Sigma_\lambda^{(s)}(E)}{\partial E}\right|_{E=0} = -\delta(E_\lambda) \times \int d\mathbf{r}_1 d\mathbf{r}_2 v_{\text{eff}}(\mathbf{r}_1, \mathbf{r}_2)\Pi_s(\mathbf{r}_1, \mathbf{r}_2; 0)v_{\text{eff}}(\mathbf{r}_2, \mathbf{r}_1). \quad (3.14)$$

Thus, the singularity at the discontinuity of the distribution function at E_F, $z_\lambda^* = [1 - \partial\Sigma_\lambda(E)/\partial E]^{-1}|_{E=0}$, is of the same order as in $\hat{\Pi}_s(\omega = 0)$. The singularity in $\hat{\Sigma}$ at $E = 0$ is weaker

$$\Sigma_s(\mathbf{r}, \mathbf{r}'; 0) = G(\mathbf{r}, \mathbf{r}'; 0) \times \int d\mathbf{r}_1 d\mathbf{r}_2 v_{\text{eff}}(\mathbf{r}_1, \mathbf{r}_2)v_{\text{eff}}(\mathbf{r}_2, \mathbf{r}')\delta S(\mathbf{r}_1, \mathbf{r}_2), \quad (3.15)$$

where

$$S(\mathbf{r}_1, \mathbf{r}_2) = \langle n(\mathbf{r}_1)n(\mathbf{r}_2)\rangle - \langle n(\mathbf{r}_1)n(\mathbf{r}_2)\rangle = \int_{-\infty}^{\infty} \frac{d\omega}{2\pi}\Pi(\mathbf{r}_1, \mathbf{r}_2; i\omega) = \sum_{\nu} \frac{A_\nu(\mathbf{r}_1, \mathbf{r}_2)}{2\omega_\nu}$$

is the static correlator of electron density $\hat{n}(\mathbf{r})$.

In the case of free electrons, $|\lambda\rangle = |\mathbf{k}\rangle$ is a plane wave with a wave vector $\mathbf{k}$. The singular contribution to the effective mass from (3.14) may then be written as

$$\frac{m^*}{m} \approx \frac{1}{Z^*} = 1 + \frac{\pi e^2}{2k_F^2 \Omega_0}\overline{\Pi}_s(0), \quad (3.16)$$

where $\overline{\Pi}_s(\omega) = \sum_{\mathbf{q}} \Pi_s(\mathbf{q}, \omega)$ is the average taken over the Brillouin zone [134] [the singularity in $\partial\Sigma(k_F, 0)/\partial k_F$ is weaker than in Z^*].

As will be shown shortly, $\overline{\Pi}_s$ defines the average anomalous contribution to the frequency of short-wave phonons, whereas (3.16) [similar to the exact equation (3.14)] implies that the singularities appearing in electronic and phonon spectra because of screening anomalies are the same in character. Moreover, $\overline{\Pi}_s$ characterizes the screening of a local static disturbance, which is why contributions $\overline{\Pi}_s(0)$ must show up in, for example, Raman and Mössbauer spectra, thereby determining singularities in the effective electric-field gradient. Thus, the expression (3.16) establishes the relation between anomalous contributions to various observables: the electronic effective mass at the Fermi surface, quadrupole splitting in Raman or Mössbauer spectra, etc.

We now turn to the anomalous contributions to the thermodynamic potential Ω with particular reference to the free-electron case. It is convenient to use a known expression involving permittivity $\varepsilon(\mathbf{q}, \omega)$:

$$\Omega = \Omega_0 + \int_0^1 \frac{d\lambda}{\lambda} \sum_{\mathbf{q}} \left\{ \frac{1}{2\pi} \int_{-\infty}^{\infty} \frac{d\omega}{1 - \exp(-\omega/T)} \operatorname{Im} \varepsilon_\lambda^{-1}(\mathbf{q}, \omega) + \frac{2\pi n e^2}{\mathbf{q}^2} \right\}, \quad (3.17)$$

where $\varepsilon_\lambda = 1 + v_c(\mathbf{q})\lambda\Pi_\lambda(\mathbf{q}, \omega)$ and, in computing $\hat{\Pi}$, $e^2 \to \lambda e^2$; and T is the temperature. Proceeding as in [134], it is an easy matter to derive from (3.17) the singular contribution to $\hat{\Sigma}$:

$$\tilde{\Omega}_s \approx -\frac{\beta}{4} \int_0^{\omega_c} d\omega\omega\overline{\Pi}_s(\omega), \quad (3.18)$$

where $\omega_c \sim E_F$ is the cutoff energy and $\beta = me^2/\pi k_F$ is the usual parameter of electron–electron interaction. If $N(E)$ has a narrow peak at a distance of Δ from E_F (see [39, 40]), then

$$\overline{\Pi}_s(\omega) \sim -\ln|\omega - \Delta| \quad (3.19)$$

and, as (3.16) and (3.18) imply,

$$\delta m^* \sim (Z^*)^{-1} \sim -\ln|\Delta|, \quad \delta\overline{\Omega} \sim \Delta^2 \ln|\Delta|. \quad (3.20)$$

Similarly, in the case of filled and empty narrow $N(E)$ peaks spaced Δ apart (a "two-peak" situation), we have

$$\overline{\Pi}_s(\omega) \sim \Delta(\Delta^2 - \omega^2)^{-1} \quad (3.21)$$

and, accordingly,

$$\delta m^* \sim (Z^*)^{-1} \sim \Delta^{-1}, \quad \delta\overline{\Omega} \sim -\Delta\ln|\Delta| \quad (3.22)$$

[compare with (2.71) and (2.72)]. The treatment in this section is to the first order in $\hat{\Pi}_s$. The higher order situation was discussed in Sec. 2.5.

We now turn to the temperature dependence of anomalous contributions associated with screening anomalies. Substituting in (3.17) the expression for $\Pi_\lambda(\mathbf{q}, \omega)$ in the random-phase approximation, integrating with respect to ω, and isolating the singular contribution yield an explicit expression for $\tilde{\Omega}_s$ [39 - 41]

$$\tilde{\Omega}_s \approx -\sum_{\lambda, \lambda'} f_{\lambda'}(1 - f_\lambda) K_{\lambda\lambda'} \Phi(E_\lambda - E_{\lambda'}), \quad (3.23)$$

where

$$K_{\lambda, \lambda'} = \sum_{\mu, \nu} \delta(E_\mu)\delta(E_\nu)|\langle\mu\lambda'|v_{\text{eff}}|\nu\lambda\rangle|^2, \quad (3.24)$$

$$\Phi(x) = \int d\varepsilon d\varepsilon' \frac{f(\varepsilon)f(\varepsilon')\tilde{C}(\varepsilon)\tilde{C}(\varepsilon')}{(\varepsilon + \varepsilon')^2 - x^2} = \pi^2 T^2 \operatorname{Re} \int_0^{\infty} \frac{dt \sin xt}{\sinh^2(\pi^2 T(t - i/W))}, \quad (3.25)$$

where $\lambda \to \lambda'$ are "dangerous" transitions yielding a singular contribution to $\hat{\Pi}$, and $\tilde{C}(\varepsilon)$ is a smooth function of divergence truncation for ε, ε' tending to infinity [for definiteness, it is chosen that $\tilde{C}(\varepsilon) = e^{\varepsilon/W}$, where W is of the order of conduction-band width]. The singular contribution (3.3) to the potential Ω leads to contributions to the elastic constants

$$\delta C_{ik} = \frac{\partial^2 \tilde{\Omega}_s}{\partial u_i \partial u_k} \quad (3.26)$$

(where u_i are the components of the deformation tensor), which, as will be shown shortly, vary with temperature in a nonmonotonic manner. For $T = 0$, these contributions, as immediately follows from (3.20) and (3.22), are on the order of

$$\delta C_{ik} \sim \ln\left|\frac{\Delta}{W}\right| \frac{\partial\Delta}{\partial u_i}\frac{\partial\Delta}{\partial u_k}, \quad (3.27)$$

when a filled or an empty N(E) peak approaches the Fermi level (a "one-peak" situation), and

$$\delta C_{ik} \sim -\frac{1}{\Delta}\frac{\partial\Delta}{\partial u_i}\frac{\partial\Delta}{\partial u_k}, \quad (3.28)$$

when a filled and an empty $N(E)$ peak move closer together (a two-peak situation). Thus, the approach of two narrow $N(E)$ peaks to E_F and, especially, their moving closer together, reduces the elastic constants, that is, "softens" the lattice.

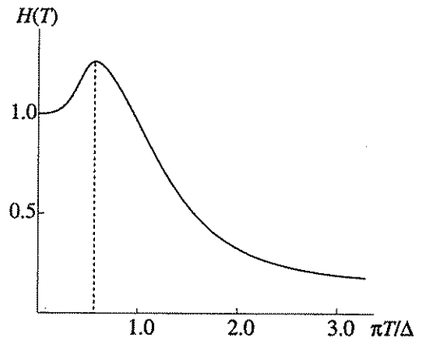

Fig. 3.9. *Function H(T) from (3.29).*

As (3.25) implies, the temperature dependence of the contributions δC_{ik} to the elastic constants is defined as

$$\left.\begin{aligned} \delta C_{ik}(T) &\sim -H\left(\frac{\pi T}{\Delta}\right), \\ H(x) &= \frac{1}{x}\int_0^{\infty} \frac{d\tau\tau^2 \sin^2(\tau/x)}{\sinh^2\tau}, \end{aligned}\right\} \quad (3.29)$$

in the case of a two-peak situation, and

$$\delta C_{ik}(T) \sim -\tilde{H}\left(\frac{\pi T}{\Delta}, \tilde{W}\right) \quad (3.30)$$

$$\tilde{H}(x, \tilde{W}) = \operatorname{Re}\int_0^{\infty} d\tau \frac{\tau\cos(\tau/x)}{\sinh^2(\tau - ix/\tilde{W})}, \quad \tilde{W} \equiv \frac{W}{\Delta},$$

in the case of a one-peak situation [41]. As is seen from Fig. 3.9, $\delta C_{ik}(T)$ has a minimum at $T \simeq 0.2\Delta$ according to (3.29) and at $T \simeq 0.3\Delta$ according to (3.30).

Similarly, one can use the local-spin-density functional theory to consider "anomalous" contributions to the paramagnetic susceptibility $\chi(T)$ [41]. A useful general representation for χ was obtained by Liu *et al.* [136]

$$\chi(T) = \frac{\chi_0(T)}{1 - I(T)\chi_0(T)}, \quad (3.31)$$

where $\chi_0(T)$ is the spin susceptibility for noninteracting electrons (3.3),

$$I(T) = -\int d\mathbf{r}d\mathbf{r}'\gamma(\mathbf{r}, T)\frac{\delta^2\Omega_{xc}}{\delta m(\mathbf{r})\delta m(\mathbf{r}')}\gamma(\mathbf{r}', T) \quad (3.32)$$

is the Stoner exchange parameter, Ω_{xc} is the exchange-correlation contribution to the $\tilde{\Omega}$ potential, $m(\mathbf{r})$ is the spin density, and

$$\gamma(\mathbf{r}, T) = \frac{1}{\chi_0(T)}\sum_{\nu}\left(-\frac{\partial f_\nu}{\partial\varepsilon_\nu}\right)|\psi_\nu(\mathbf{r})|^2. \quad (3.33)$$

By inserting the contribution Ω_s to Ω_{xc} in (3.32), it is possible to show, similarly to the derivation of (3.29),

that $I(T)$ contains nonmonotonic temperature-dependent contributions $I_s(T)$

$$\frac{I_s(T)}{I_s(0)} = H\left(\frac{\pi T}{\Delta}\right) \tag{3.34}$$

in a two-peak situation, and

$$\frac{I_s(T)}{I_s(0)} \propto \tilde{H}\left(\frac{\pi T}{\Delta}, W\right) \tag{3.35}$$

in a one-peak situation, if $\delta\Delta/\delta m(\mathbf{r}) \neq 0$. The latter condition means that one of the $N(E)$ peaks must be associated with the local magnetic moment. Then

$$I_s(0) \sim \begin{cases} \ln\left|\dfrac{W}{\Delta}\right| - \text{in the one-peak case,} \\ \Delta^{-1} - \text{in the two-peak case.} \end{cases} \tag{3.36}$$

As was pointed out in Sec. 3.2, in the case of a narrow $N(E)$ peak, $\chi(T)$ has a maximum [and $C_{ik}(T)$ has a minimum] even in the one-particle approximation. However, consideration of $I(T)$ as given by (3.34) and (3.35) [and, similarly, many-particle anomalous contributions to (3.29) and (3.30)] shifts the temperature of the maximum of χ (the minimum of C_{ik}) toward the lower temperatures.

On the whole, screening anomalies change $C_{ik}(T)$, $\chi(T)$, and other properties qualitatively in the same way as the one-particle effects associated with $N(E)$ peaks do. However, they extend the domain of existence for anomalies [for example, in the one-particle approximation of the δ-like $N(E)$ peak model, it does not affect the observable properties at $T = 0$ if $\Delta \neq 0$], shift the maxima (minima) toward the lower temperatures, and may alter the mathematical character of the singularity. To illustrate the latter assertion and to obtain an idea about the numerical coefficients in anomalous contributions, we will consider the case where an ordinary van Hove singularity occurs at E_F (an electronic topological transition) [134].

The most important physical result one obtains when one takes into account screening anomalies is the fact that the singularity in the thermodynamic potential at $T = 0$ and, as a consequence, in the corresponding observable properties becomes two-sided, albeit asymmetric. Thus, if a singularity in $N(E)$ has the form

$$\delta N(E) = -A\sqrt{z - E}\,\theta(z - E) \tag{3.37}$$

(where $z = E_c - E_F$), then the singularity in the Ω potential, if one allows for the one-particle band contribution and (3.18), takes the form [134]

$$\delta\tilde{\Omega} = \frac{4}{15}Az^{5/2}\theta(z) + \frac{4\pi}{105}\beta\tilde{\Gamma}N(E_F)A(-z)^{7/2}\theta(-z), \tag{3.38}$$

where

$$\tilde{\Gamma} = \overline{\left|\langle n, \mathbf{k}_0 - \mathbf{q}|e^{i\mathbf{qr}}|\,(n, \mathbf{k}_0)\rangle\right|^2},$$

$\mathbf{k}_0$ is the van Hove singularity point in the nth band, and the overscribed bar denotes averaging over the Brillouin zone with respect to $\mathbf{q}$. In the weak interaction approximation, we have $\tilde{\Gamma} \approx 1$.

3.4. Phonon-Spectrum and Anharmonic-Effect Singularities Caused by Screening Anomalies

Thus far, we completely neglected lattice vibrations. Meanwhile, electron–phonon interaction in a situation where the electronic subsystem has excitations with energies $\Delta \ll E_F$ (or even $\Delta \lesssim \bar{\omega}$, where $\bar{\omega}$ is the characteristic phonon frequency) is a nontrivial and interesting case. The basis for an inquiry into the effects of electron–phonon interaction is the Born–Oppenheimer adiabatic approximation (for a consistent derivation of this approximation for metals, see [138]).

In this approach, one considers perturbations in the adiabatic smallness parameter $\kappa = (m/M)^{1/4}$ (where m is the mass of an electron, and M is the mass of an ion). As Migdal [138] showed for the first time, in a layer of a thickness of the order of $\bar{\omega} \sim \kappa^2 E_F$, the renormalization of the electronic spectrum near E_F is not small ($m^*/m = 1 + \lambda$, where λ is the electron–phonon interaction constant, $\lambda \sim \kappa$). Because, however, this layer is thin, the effects of electron–phonon interaction make small contributions in terms of κ to such integral properties as the total energy (and, as a consequence, elastic constants, etc.) [46]. If, however, a significant proportion of the electron spectral density is concentrated in that layer (which corresponds to the case analyzed in [135], i.e., $\Delta \lesssim \bar{\omega}$), one might, it would seem, expect the adiabatic approximation to fail. True, strong nonadiabatic effects may well occur in both the phonon and the electronic spectra in such a case. An example of the former is the splitting of phonon dispersion curves owing to hybridization with the excitation of rare-earth ions associated with the term effects, or the term splitting in a crystal field; such a splitting, for example, was observed in $CeAl_2$ (see review in [91]). The nonadiabatic rearrangement of the electronic spectrum in cases where the width Γ of the electronic peak and the distance Δ from the peak to E_F are comparable with $\bar{\omega}$ was investigated in detail by various methods by Hewson [139] and by Hewson and Newns [140]. According to them, if Γ and Δ are smaller than or almost equal to $\bar{\omega}$ (that is, if a significant part of an $N(E)$ peak lies in a "nonadiabatic" layer), the peak width can strongly (exponentially) decrease owing to polaron effects. If, on the other hand, Δ or Γ is greater than $\bar{\omega}$, the phonon renormalization of the peak width will be relatively small.

The anomalies that arise in phonon spectra owing to electron–phonon interaction in systems with narrow $N(E)$ peaks near E_F were investigated for various specific classes of such systems, including the A-15 compounds [118], mixed-valence systems [141], and heavy-fermion compounds [142].

For purposes of this review, we will limit ourselves to a general analysis of the one-peak situation within the simple semiphenomenological consideration reported in [135] (some of these results were later discussed by Liu [143] with reference to Ce). We denote the state that forms an $N(E)$ peak by $|\nu\rangle$ and band states by $|\mu\rangle$, and take into account electron–phonon interactions of the "hybridization" type

$$\tilde{H}_{e\text{-ph}} = \sum_{\mathbf{q},\mu,\nu} \lambda_{\mathbf{q}}(\hat{b}_{\mathbf{q}}^{+} + \hat{b}_{\mathbf{q}})\,\hat{c}_{\mu}^{+}\hat{c}_{\nu} + \text{h.c.}, \tag{3.39}$$

where $\hat{b}_{\mathbf{q}}^{+}$, and $\hat{b}_{\mathbf{q}}$ are the operators of phonon creation and annihilation with momentum $\mathbf{q}$ and frequency $\omega_{\mathbf{q}}$; $\hat{c}_{\mu}^{+}$ are the electron creation operators; and $\lambda_{\mathbf{q}}$ is the electron–phonon interaction constant. The phonon-frequency correction $\delta\omega_{\mathbf{q}}$ due to the interaction (3.39) is $\delta\omega_{\mathbf{q}}^2/2\omega_{\mathbf{q}}$,

$$\delta\omega_{\mathbf{q}}^2 = -\lambda_{\mathbf{q}}^2\Pi(\mathbf{q}, \omega_{\mathbf{q}}), \tag{3.40}$$

where $\Pi(\mathbf{q}, \omega_{\mathbf{q}})$ is the contribution to the electron polarization operator due to $\mu \rightleftarrows \nu$ transitions. Similar to (3.39), we can isolate the singular contribution to $\Pi(\mathbf{q}, \omega_{\mathbf{q}})$ in the random-phase approximation

$$\left.\begin{aligned} \Pi(\mathbf{q}, \omega) &\simeq B(\mathbf{q})\ln\left[\frac{W^2}{\Delta^2 - \omega^2 - i_0}\right], \\ B(\mathbf{q}) &= \sum_{\mu}\left|\langle\nu|e^{i\mathbf{qr}}|\mu\rangle\right|^2\delta(\varepsilon_{\mu}). \end{aligned}\right\} \tag{3.41}$$

At $\Delta \sim \bar{\omega}$, the contribution (3.41) cannot generally be treated in the adiabatic approximation [46] [$\Pi(\mathbf{q}, \omega_{\mathbf{q}}] \to \Pi(\mathbf{q}, 0)$). All of this contribution to $\omega_{\mathbf{q}}$ is, however, small because of the small overlap between the wave functions $|\nu\rangle$ and $|\mu\rangle$ in $B(\mathbf{q})$ [which is a necessary condition for the $N(E)$ peak to be narrow]. Thus, in the case at hand, the adiabatic approximation for the phonon spectrum is satisfied not because the parameter κ is small, but because this overlap [that is, $B(\mathbf{q})$] is small. Moreover, $B(\mathbf{q}) \sim \Gamma/W$, where Γ is the peak width because Γ is likewise proportional to the square of the overlap of the functions $|\nu\rangle$ and $|\mu\rangle$. The contribution of "dangerous" electron transitions to $\omega_{\mathbf{q}}$ appearing in (3.40) and (3.41) softens the phonon spectra, $\delta\omega_{\mathbf{q}} \sim -\ln|W/\Delta|$ [see (3.40) and (3.41)], but not the elastic constants C_{ik} because $\Pi(\mathbf{q}, \omega_{\mathbf{q}}) \sim \mathbf{q}^2$; the singular contribution to C_{ik} is determined by the higher order interactions (see Sec. 3.3). For specific systems (such as A-15 compounds), this softening of phonons was calculated microscopically by Weber [118].

At $\omega \to \Delta \gg \Gamma$, the task of determining the singular contribution to $\Pi(\mathbf{q}, \omega_{\mathbf{q}})$ is formally equivalent to the problem of the "edge singularity" in X-ray spectra where, as was first shown by Mahan and, more fully, by Nosieres and de Dominisis (see [96]), one needs to consider electron–electron interactions of the higher orders. Then, according to Mahan [96], instead of (3.41) we have

$$\Pi(\mathbf{q}, \omega) = \sum_{l} A_l(\mathbf{q})\frac{1}{\alpha_l}\left[\left(\frac{W}{\Delta - \omega}\right)^{\alpha_l} + \left(\frac{W}{\Delta + \omega}\right)^{\alpha_l} - 2\right], \tag{3.42}$$

$$\alpha_l = \frac{2\delta_l}{\pi} - 2\sum_{l=0}^{\infty}(2l + 1)\left(\frac{\delta_l}{\pi}\right)^2. \tag{3.43}$$

Here, δ_l is the phase of scattering at the potential of the hole that is formed as an electron moves from the $N(E)$ peak to the Fermi level, and $A_l(\mathbf{q})$ are the coefficients related to the screening effect of electrons at E_F with an orbital moment l. In the d- or f-resonance model, where account is taken of scattering only with $l = 2, 3$, Friedel's sum rule $\frac{2}{\pi}\sum_{l}(2l + 1)\,\delta_l = 1$ implies that $\alpha = [2(2l + 1)]^{-1}$; that is, α is positive, but small. In the case of strong s–p scattering (a small ionic radius), α may be significantly greater, $\alpha \simeq 1/2$. The contribution (3.42) to phonon damping $\gamma_{\mathbf{q}}$ is defined by

$$\operatorname{Im}\Pi(\mathbf{q}, \omega_{\mathbf{q}}) \sim |\omega_{\mathbf{q}} - \Delta|^{-\alpha}\theta(\omega_{\mathbf{q}} - \Delta). \tag{3.44}$$

Equations (3.42) and (3.44) imply that, for $\alpha > 0$, both $\gamma_{\mathbf{q}}(\omega)$ and the density of phonon states $g(\omega)$ increase as ω tends to Δ. The singular contribution to $g(\omega)$ is proportional to $|\omega - \Delta|^{-\alpha}$, with ω tending to Δ. As follows from the above reasoning, the conclusion that a strong damping takes place when ω is greater than Δ as ω tends to Δ holds not only for phonons but also for other excitations in the corresponding frequency interval, including, for example, local excitations associated with the splitting of the f level in a crystal field. It is relevant to note the experimental fact that local excitations in $CeAl_3$ (a heavy-fermion compound) strongly damp at temperatures down to room temperature in contrast to "normal" systems, such as $PrAl_3$ and $NdAl_3$. This might be explained on the basis of (3.44) by assuming that one of the sublevels in the f level in $CeAl_3$ is located near E_F, so the local excitation energy is the same as Δ (the distance from another sublevel to E_F). This supposition appears rather natural for heavy-fermion systems.

When one takes into account electron–phonon interaction, the Ω potential receives a contribution defined by the diagram of Fig. 3.10, where the wavy line represents Green's function for phonons [20].

$$\delta\Omega = -\frac{1}{2}T\sum_{\mathbf{q},\omega}\Pi(\mathbf{q}, i\omega)\frac{\lambda_{\mathbf{q}}^2\omega_{\mathbf{q}}^2}{\omega_{\mathbf{q}}^2 + \omega^2}, \quad \omega = 2\pi nT, \quad n = 0, \pm 1. \tag{3.45}$$

Then, in view of (3.41), one obtains

$$\delta\Omega = -\frac{1}{2}\sum_{\mathbf{q}}\lambda_{\mathbf{q}}^2 B(\mathbf{q})\omega_{\mathbf{q}}^2 \times\left[\frac{\coth\omega_{\mathbf{q}}/2T}{2\omega_{\mathbf{q}}}\ln\left|\frac{E_F^2}{\Delta^2-\omega_{\mathbf{q}}^2}\right| + \int_{\Delta}^{\infty}\frac{dx}{\omega_{\mathbf{q}}^2-x^2}\coth\frac{x}{2T}\right] = \begin{cases} -\frac{1}{2}\sum_{\mathbf{q}} B(\mathbf{q})\omega_{\mathbf{q}}\lambda_{\mathbf{q}}^2\ln\left(\frac{E_F}{\Delta+\omega_{\mathbf{q}}}\right), & T=0, \\ -T\sum_{\mathbf{q}} B(\mathbf{q})\lambda_{\mathbf{q}}^2\ln\left|\frac{E_F}{\Delta}\right|, & T\gg\Delta,\theta_D, \end{cases} \quad (3.46)$$

where θ_D is the Debye temperature. Equation (3.46) implies that anharmonic effects, including potential anharmonism, may be great at small Δ, because every variation $\delta\Omega$ in terms of displacements enhances the singularity.

A rise in temperature should be accompanied by a broadening of $N(E)$ peaks because of electron–ion interaction [96], and this results in an increase in the effective values of Δ: $d\Delta/dT > 0$. If so, the softening of phonon spectra should increase with decreasing temperature; that is, peaks should "grow up" in $g(\omega)$ at $\omega \sim \Delta$ [at high T, such singularities will most likely be masked by a broadening of $N(E)$ peaks]. Such behavior was observed in reality in, for example, Chevrel phases for which the presence of narrow $N(E)$ peaks near E_F is a typical occurrence [144]. Interestingly, the anharmonic contribution to the lattice specific heat turns out, according to (3.46), to be negative (if $\left|\frac{d\ln\Delta}{d\ln\Delta}\right| \lesssim 1$). This agrees with the experimental data on A-15 compounds [145].

The mean-square atomic displacement $\langle x^2(T)\rangle$, which can be calculated similarly to $\delta\Omega$, is

$$\delta\langle x^2(T)\rangle = \begin{cases} \frac{1}{2}\sum_{\mathbf{q}}\frac{B(\mathbf{q})\lambda_{\mathbf{q}}^2}{\omega_{\mathbf{q}}+\Delta}, & T=0, \\ 2T\sum_{\mathbf{q}}\frac{B(\mathbf{q})}{\omega_{\mathbf{q}}}\lambda_{\mathbf{q}}^2\ln\left|\frac{E_F}{\Delta}\right|, & T\gg 0,\theta_D. \end{cases} \quad (3.47)$$

Equation (3.47) implies that if $\Delta \ll E_F$, then $\langle x^2\rangle$ is abnormally great. In keeping with Linderman's criterion of the constancy of $\langle x^2(T)\rangle$, this must depress the melting point T_m. The cause of such an occurrence may be, for example, the addition of substances with narrow quasilocal levels near the matrix E_F. Quite possibly, this relative increase in $\langle x^2\rangle$ and the enhancement of anharmonic effects at small Δ (because of which the anomalous contributions to $\langle x^4\rangle$ are considerably greater than to $\langle x^2\rangle^2$) explain the very large displacements of vanadium atoms that Stanndenmann and Testardi [146] observed in V_3Si. According to them, this behavior, when interpreted in the language of the interatomic potential, implies that it has two minima.

3.5. The Effect of the Density-of-States Peaks on the Structural and Magnetic Stability of Metals and Alloys: Specific Examples

As Secs. 3.2 - 3.4 demonstrated, the approach to a narrow $N(E)$ peak has several consequences. Notably, this softens the elastic constants and phonon frequencies, accentuates anharmonic effects, and enhances both the Pauli spin susceptibility and the Stoner exchange parameter I. On the whole, these occurrences may be construed as the display of a tendency toward structural and magnetic instability. A qualitative insight into this tendency can be obtained from simple considerations. The variation of the total energy in the case of the "reoccupancy" δn_e of the electronic states takes the form

$$\delta E = \frac{1}{2}\left(\frac{\partial n}{\partial\mu}\right)^{-1}(\delta n_e)^2, \quad (3.48)$$

where n is the number of particles, and μ is the chemical potential; in the one-electron approximation $\partial n/\partial\mu = N(E_F)$. Therefore, when $N(E_F)$ is large, δE is small, and the system resides, as it were, in a state of "indifferent" equilibrium that can be disturbed by an exchange interaction (thereby resulting in magnetic instability) and by other contributions to the energy, leading to changes in the crystal structure. The large $N(E_F)$ may be of a widely differing origin.

In the bcc phase of iron, for example, ferromagnetism apparently arises owing to the merger, noted in Sec. 3.1, of van Hove singularities at the high-symmetry P–N line, which, according to (3.2), results in the logarithmic divergence of $N(E_F)$ in the hypothetical magnetic phase. According to the band-theoretic calculations [68], nonmagnetic bcc Fe has an $N(E)$ peak near E_F. In this case, $E_F = 0.859$ Ry, $E_P = 0.851$ Ry, and $E_N = 0.848$ Ry; that is, in (3.2), $\gamma = 0.003$ Ry. Thus, it is the quasi-two-dimensional character of the corresponding van Hove singularity in iron that leads to ferromagnetism. As to the 4*d*- and 5*f*-transition metals, this peak would probably occur at E_P in Ru and Os, which are the analogs of Fe, or even a little earlier (that is, in Tc and Re), if they had a bcc structure (see the band-theoretic calculations of a hypothetical bcc phase in Ir in [72]). One may, therefore, suppose that the behavior of the $N(E)$ peak associated with the P–N line in the bcc structure at the end of the corresponding rows of the Periodic System results in magnetic instability for the 3*d* metals, where I is relatively large, and in the overall loss of stability by the bcc structure for the 4*d* and 5*d* metals, where it cannot be stabilized at the expense of magnetism. Thus, an analysis of "geometrical" motifs in the $N(E)$ structure presented in Sec. 3.1 permits one to add more detail to the general idea about the increasingly more localized behavior of *d* electrons toward the end of the 3*d* row as the cause of ferromagnetism in iron [26], and about

changes in the character of chemical bonding in the series of *d* metals discussed in Sec. 2.2.

Dilute Pd–Fe and Pd–Ni alloys give an interesting example of the increase in the Stoner exchange parameter that may be associated with the effects in question. From calculations of $N(E)$ for these alloys [131] (Fig. 3.11), one can say that a two-peak situation (that is, an almost completely filled band peak typical of pure Pd and an empty Fe impurity peak) exists in the Pd–Fe alloy and a one-peak situation in the Pd–Ni alloy. The impurities Fe and Ni in Pd possess magnetic moments, and one can, according to (3.36), expect that I will increase by as much as $-c\ln|\Delta|$ (where c is the impurity concentration) in Pd–Ni and by a considerably greater amount ($\sim c\Delta^{-1}$) in Pd–Fe. This difference between the two systems correlates with the experimental fact [147] that an almost ferromagnetic Pd becomes ferromagnetic when alloyed with 2.8 at % Ni or with a mere 0.1 at % Fe. The increase in the Stoner exchange parameter for Pd alloyed with Ni was directly verified by Ohlsen and Nordberg [148] in their experiments concerned with the de Haas–Van Alfphen effect.

We now turn to examples demonstrating the involvement of the above effects in structural instability. An interesting example of local instability of electronic origin is supplied by an analysis of the dynamics of CuO chains in $YBa_2Cu_3O_7$ [149]. This system has an $N(E)$ peak with $\Delta \approx -0.2$ eV, traceable to the *p* states of the oxygen atoms in the chains; when the oxygen atoms are shifted by an amount Q, the peak diffuses owing to an increased hybridization with the states of the CuO_2 planes. The simplest model Hamiltonian describing this situation takes the form

$$\hat{H} = \sum_{\mathbf{k}}\varepsilon_{\mathbf{k}}C_{\mathbf{k}}^{+}C_{\mathbf{k}} + \Delta a^{+}a + \lambda Q\sum_{\mathbf{k}}(a^{+}C_{\mathbf{k}} + C_{\mathbf{k}}^{+}a) + \frac{CQ^2}{2} + \frac{\mathcal{P}^2}{2M}, \quad (3.49)$$

where Q and $\mathcal{P}$ are the coordinate and momentum of the oxygen atom, and $\varepsilon_{\mathbf{k}}$ is the spectrum of itinerant electrons; the hybridization of the itinerant ($C_{\mathbf{k}}$) and localized (a) states is proportional to Q. As is shown in [149], for

$$|\Delta| < \Delta_0 \equiv W\exp\left(-\frac{C}{2N(E_F)\lambda^2}\right) \quad (3.50)$$

(where W is of the order of conduction band width), the ion acquires a two-well effective potential – a fact that seems to check with the experimentally observed large displacements of oxygen ions in the chains.

Many-well potentials should apparently arise near martensitic phase transitions, which, as Kurdyumov [150] argues, are characterized by relatively low barriers for the displacement of atoms. The only "first-principles" study, done by Chen *et al.* [58], confirmed such a picture for pressure-induced bcc–hcp transitions in Ba. The graph in Fig. 3.12 relates the total energy E to tetragonal deformations γ_3 and additional shear deformation with a doubled period in the [110] direction that transform the bcc to the hcp lattice. As this happens, one of the shear moduli, $C' \equiv \partial^2 E/\partial\gamma_3^2$, becomes negative near the transition (the premartensitic softening of the constants). Vaks *et al.* [122] showed that this softening (likewise observable experimentally) is actually caused by an increase of the band contribution (3.9) in bcc Ba with increasing pressure because E_F occurs at an $N(E)$ peak. Thus, the martensitic phase transition in Ba may likewise be regarded as an example of structural destabilization that occurs because of the density-of-states effects. Similar effects were observed in Ca and Sr [122] and, in a weaker form, in Li, thus explaining why the phase diagrams of Li and Na under pressure differ in shape [62].

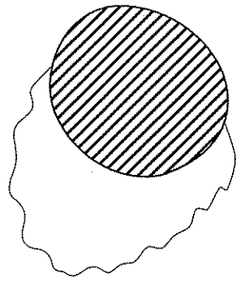

Fig. 3.10.

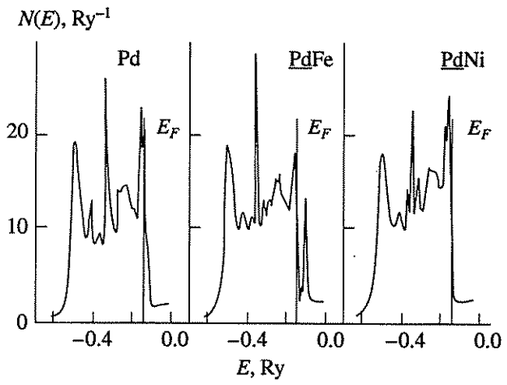

Fig. 3.11. *Electronic density of states in Pd, $Pb_{0.95}Fe_{0.05}$, and $Pb_{0.95}Ni_{0.05}$ (borrowed from [131]).*

A number of martensitic transitions are characterized by premartensitic anomalies either in shear modulus or in the frequency of phonons with a large momentum q. An illustrative example of this kind is the softening of C' in A-15 compounds at $T \approx 20$ - 30 K [117] accompanied by sudden anomalies in shear modulus and phonon spectra (see, for example, [151]). These anomalies are

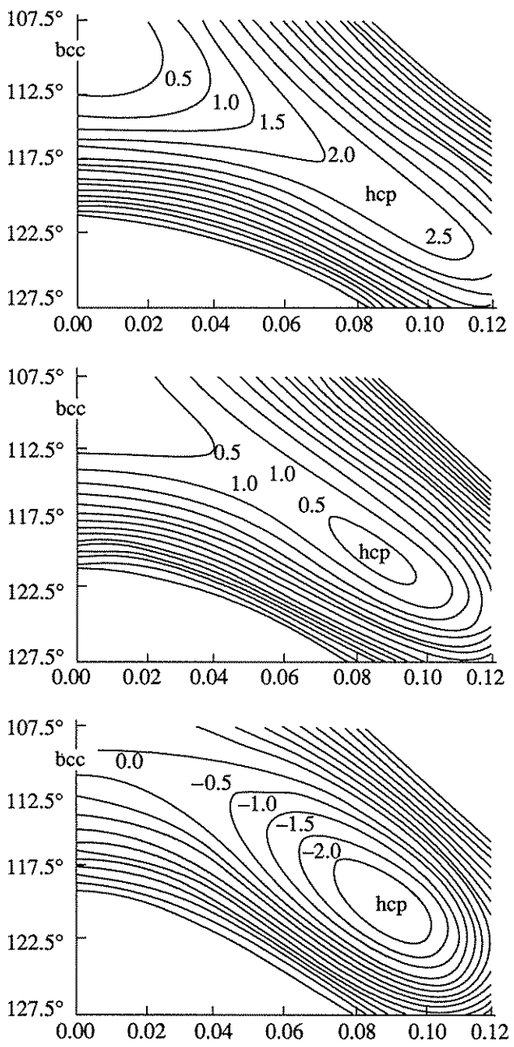

Fig. 3.12. *Contour maps of the calculated total energy of Ba for a bcc–hcp transition. The variable along the axis of abscissas represents the displacement corresponding to a phonon of the Σ_4 branch at the Brillouin zone boundary (point N_4) in units of $\sqrt{2}a$, where a is the edge of the unit cube. The variable along the axis of ordinates is the angle of shear deformation. The energy (in Ry) is reckoned from the energy of the bcc structure. The bcc–hcp transition is shown to occur upon compression: atomic volume Ω_0 (reckoned downward) is 421.771 a.u., 334.572 a.u., and 287.398 a.u. (according to [58]).*

obviously of electronic origin (related to specific features in the band structure) and were interpreted both within the Gor'kov model [116, 117] and on the basis of microscopic calculations [118]. Another interesting example of "pretransition" anomalies is the softening of transverse phonons near $\mathbf{q} = \frac{2\pi}{a}(\frac{1}{3}, \frac{1}{3}, 0)$ on approach to the martensitic transition in NiTi [152]. It is natural to assume that the stronger the softening (in the high-temperature phase), the higher the transition temperature T_M. The calculations Anisimov *et al.* [131] did for NiTi-base alloys confirm the existence of a correlation between the approach (or recession) of the $N(E)$ peak to (or from) E_F and the increase (or decrease) in T_M upon alloying. This is indirect evidence that the proximity of the peak to E_F and the softening of phonon spectra are interrelated events.

On the whole, the issue of electronic mechanisms involved in or responsible for structural (including martensitic) transformations in metals and alloys appears to be among the most interesting and important in the theory of such transformations. At present, however, little has been done to investigate it.

The subsequent chapters deal with the properties of strong electron–electron interaction systems where the problem of whether electrons show localized or itinerant behavior is especially acute. Indeed, one may even question the validity of the Bloch picture for some states. We will begin our discussion of this group of matters from the problem of localized magnetic moments in ferromagnetic metals.

3.6. Concluding Remarks

To a "pure" theorist, the inclusion of this chapter in a review dealing with the *problem* of localized and itinerant behavior of electrons may at first glance appear far-fetched, for all phenomena in question are described in the language of Bloch (band) states. Even narrow electronic density-of-states peaks, intuitively associated with localization in real space, may appear to be due to the merger of van Hove band singularities in consequence of lattice geometry. The demonstration of this (see Sec. 3.1) is among the most important results of this chapter. One must, however, reckon with the fact that experimental physicists and metal scientists often use the terminology related to electron localization in an attempt to give a qualitative description of anomalies in the properties of many transition-metal alloys and compounds (tungsten–rhenium, titanium–iron, etc.). In this connection, we showed that it would be more appropriate to use the language of singularities (electronic density-of-states peaks). When located near the Fermi level, such singularities give rise to anomalies in physical properties. This chapter briefly described specific mechanisms involved in this relationship. Thus, the results of this chapter are of interest above all for an interpretation of specific experimental findings.

4. LOCALIZED MAGNETIC MOMENTS AND MAGNETISM OF THE TRANSITION METALS IN THE SPIN-DENSITY-FUNCTIONAL METHOD

The problem of magnetism in the iron group metals is discussed. The phenomena in question reveal most distinctly both localized and itinerant traits in the behavior of the same 3*d* electrons. Moreover, while the characteristics of magnetic excitations and exchange interaction in the ground state of ferromagnetic metals can be calculated quite accurately within the present-day band theory, the magnetic and electric properties observed at finite temperatures and, especially, in the paramagnetic state are, to a considerable degree, caused by the presence of localized magnetic moments.

4.1. The Problem of Magnetic-Moment Localization in the Iron Group Metals

In Secs. 2 and 3, the localized and itinerant behavior of electrons in a metal was mainly discussed in connection with their lattice properties. As noted in the introduction, historically this problem goes back to attempts to gain insight into the contradictory properties of the magnetic metals of the iron group.

Basically, the snag is that some properties of these metals can be understood only if their valence electrons are assumed to have a "band" character, while others, if the electrons are "atomlike." Among the properties in the former group, one may above all mention the large linear term in the heat capacity and the results of studies into the de Haas–Van Alfphen effect, definitively demonstrating the essential role of *d* electrons in the formation of the Fermi surface and the density-of-states at E_F [26]. In the latter group, the most outstanding are properties such as the Curie–Weiss law of magnetic susceptibility; the temperature, momentum, and energy dependences of neutron scattering cross sections, which are most conveniently interpreted if one assumes the existence of localized magnetic moments; photoemission [27, 153] and optical data on the spontaneous "spin" splitting at above the Curie point T_C; and, finally, data on the Fermi surface at elevated temperatures obtained by the positron annihilation method [154]. Even the Curie–Weiss law is usually accepted as confirming the existence of local magnetic moments [26, 28, 155], although some investigators hold opposite views [24, 156] (not backed, though, by estimates of microscopic parameters). However, the observed spontaneous spin splitting poses even more radical difficulties for the acceptance of a purely band picture. As is noted in the introduction, the latter is in effect based on Landau's theory of Fermi liquid, in which the pivotal postulate is the existence of a reciprocal one-to-one correspondence between particles and quasiparticles [18]. The band theory assigns to each state of a particle a quasimomentum $\mathbf{k}$, a band index n, and a spin projection σ, and in the paramagnetic state, the energy cannot depend on σ from symmetry considerations. Therefore, the splitting of the energy spectrum above T_C suggests the existence of a quantum number other than σ, that is, the absence of a reciprocal one-to-one correspondence between particles (labeled, among things, with a spin index as well) and quasiparticles.

Recently, a quantitative approach was proposed toward the problem of local magnetic moments in magnetic metals. Based on calculations of a real electronic structure, it is the subject-matter of this chapter. To describe the spontaneous spin splitting and other anomalous properties of the paramagnetic phase, we use an "alloy analogy" traceable, in effect, to Slater's idea [38] and developed in detail within what are known as spin-fluctuation theories in Hubbard's model; they are reviewed in detail in [28]. With this approach most consistently set forth by Gyorffy *et al.* [36], the problem of local magnetic moments is tackled in two steps. First, one considers the electronic structure of a metal with a "frozen" distribution of local moments on lattice sites, then one averages the distribution of these moments (in, for example, the coherent potential approximation). At first glance, this procedure is quite justified owing to the existence of a small parameter, T_C/W (where $W \simeq 5$ eV is the width of the energy *d* band), in terms of which the dynamics of spins may be taken to be slow (an analog of the adiabatic approximation of electron–phonon interaction).

As noted in Sec. 3.5, however, the *d* metals seem to owe their ferromagnetism not to the entire *d* band, but to a relatively small group of states (arranged along the *P–N* line of the Brillouin zone in the case of bcc Fe). They form an $N(E)$ peak with a width Γ of a few tenths of an electron volt, so T_C/Γ is not at all small. Therefore, we believe, the alloy analogy remains rather untenable. Moreover, such a description itself is rather heuristic in the sense that it does not yet suggest how one can improve the approximations used by, for example, considering higher order effects in terms of some explicit small parameters.

Thus, despite its sixty-year history, the problem of local magnetic moments still exists and, we believe, is far from being resolved. On the other hand, the headway recently made in its understanding is impressive indeed. It is, above all, associated with the development of microscopic approaches based on calculations of a real electronic structure within what is known as the spin-density-functional method.

4.2. The Formulation of the Spin-Density-Functional Method and Conditions for Spin Polarization

As already noted, the current stage in the evolution of solid-state theory is, in particular, characterized by the possibility of calculating various crystal properties from first principles, that is, by specifying solely the position and charge of atoms in the lattice. This possibility is achieved with rapid advances in computers and computational techniques. The underlying ideology of the latter is provided by the spin density functional (SDF) formalism [29 - 31], usually combined with a so-called local approximation (the LSDF formalism). With this method, one is in a position to "split" the task

of describing the properties of a system of interacting electrons in the external field of the lattice of nuclei into two subtasks, one of calculating the properties of a spatially homogeneous system of interacting electrons (which can at present be handled by, for example, the quantum Monte Carlo method [23]), and the other of solving a *single-particle* Schrödinger-type equation with a certain self-consistent potential (the Kohn–Sham equation [31]). Its idea goes back to Slater's $X\alpha$-method [38]. Taking a cue from Gunnarsson and Lundquist [30] and from Perdew and Zunger [158], the general scheme of the LSDF method can be set forth as follows.

Consider a many-particle system described by the Hamiltonian

$$\hat{H} = \hat{T} + \hat{U}_{ee} + \hat{V}; \tag{4.1}$$

$$\hat{T} = -\frac{1}{2}\int \mathbf{dr}\psi_\alpha^+(\mathbf{r})\nabla^2\psi_\alpha(\mathbf{r}); \tag{4.2}$$

$$U_{ee} = \frac{1}{2}\int \mathbf{dr}\mathbf{dr}'\psi_\alpha^+(\mathbf{r})\psi_\beta^+(\mathbf{r})\frac{1}{|\mathbf{r}-\mathbf{r}'|}\psi_\beta(\mathbf{r}')\psi_\alpha(\mathbf{r}); \tag{4.3}$$

$$V = \int \mathbf{dr}V_{\alpha\beta}(\mathbf{r})\psi_\alpha^+(\mathbf{r})\psi_\beta(\mathbf{r}), \tag{4.4}$$

where $\psi_\alpha^+(\mathbf{r})$ and $\psi_\alpha(\mathbf{r})$ are the field operators of electron creation and annihilation at the point $\mathbf{r}$ with a spin projection $\alpha = \pm$ (summation over the repeated spin indices is presumed); $V_{\alpha\beta}(\mathbf{r}) = V(\mathbf{r})\delta_{\alpha\beta} - \mathbf{B}(\mathbf{r})\vec{\sigma}_{\alpha\beta}$ is the external potential (possibly including the external magnetic field $\mathbf{B}(r)$ that acts upon the spin variables); $\hat{T}$, $\hat{U}_{ee}$, and $\hat{V}$ are the Hamiltonians of the kinetic energy, Coulomb interaction of electrons, and interaction with the external field, respectively (use is made of atomic units, $\hbar = m = |e| = 1$). Let $|\phi\rangle$ be the exact wave function of the ground state ($\langle\phi|\phi\rangle = 1$), and

$$\rho_{\alpha\beta}(\mathbf{r}) = \langle\Phi|\psi_\beta^+(\mathbf{r})\psi_\alpha(\mathbf{r})|\Phi\rangle \tag{4.5}$$

is the single-particle density matrix. The rationale of the SDF method is that the ground-state energy $E = \langle\Phi|\hat{H}|\Phi\rangle$ is regarded as $E[\hat{\rho}]$, that is, as a functional of $\rho_{\alpha\beta}(\mathbf{r})$. The latter is sought as

$$\rho_{\alpha\beta}(\mathbf{r}) = \sum_\nu f_\nu \psi_{\nu\alpha}^*(\mathbf{r})\psi_{\nu\beta}(\mathbf{r})\mathbf{dr}, \tag{4.6}$$

where $0 \le f_\nu \le 1$, and $\psi_{\nu\alpha}(\mathbf{r})$ is so far an arbitrary orthonormal set

$$\sum_\alpha \int d\mathbf{r}\psi_{\nu\alpha}^*(\mathbf{r})\psi_{\nu'\alpha}(\mathbf{r}) = \delta_{\nu\nu'}. \tag{4.7}$$

The constraints imposed on f_ν arise from the properties of the density matrix (all of its eigenvalues must range between 0 and 1) [157]. In explicit form, the functional $E[\hat{\rho}]$ is written as

$$E[\hat{\rho}] = T[\hat{\rho}] + V[\hat{\rho}] + U_H[\hat{\rho}] \neq E_{xc}[\hat{\rho}], \tag{4.8}$$

where

$$T[\hat{\rho}] = -\frac{1}{2}\sum_\nu f_\nu \int \mathbf{dr}\psi_{\nu\alpha}^*(\mathbf{r})\nabla^2\psi_{\nu\alpha}(\mathbf{r}), \tag{4.9}$$

$$V[\hat{\rho}] = \sum_\nu \int \mathbf{dr}\, V_{\alpha\beta}(\mathbf{r})\,\psi_{\nu\alpha}^*(\mathbf{r})\psi_{\nu\beta}(\mathbf{r}), \tag{4.10}$$

$$U_H[\hat{\rho}] = \frac{1}{2}\int \mathbf{dr}\mathbf{dr}'\frac{n(\mathbf{r})n(\mathbf{r}')}{|\mathbf{r}-\mathbf{r}'|}, \tag{4.11}$$

$$n(\mathbf{r}) = \mathrm{Tr}\,\hat{\rho}(\mathbf{r}) = \sum_\nu f_\nu \psi_{\nu\alpha}^*(\mathbf{r})\psi_{\nu\alpha}(\mathbf{r}), \tag{4.12}$$

and U_H is the classical electrostatic energy of the electron gas of density $n(\mathbf{r})$. The term E_{xc} is the exchange-correlation energy. Of course, unless a specific method of calculating E_{xc} is suggested, the problem is in no way simplified.

In a homogeneous electron gas, the total energy E and, in consequence, E_{xc} are related to $\rho_{\alpha\beta}$ through the invariants

$$n = \mathrm{Tr}\hat{\rho}, \quad m = |\mathrm{Tr}\hat{\rho}\vec{\sigma}| \tag{4.13}$$

(the charge and spin density, respectively) of Pauli's $\vec{\sigma}$ matrix. At present, E_{xc} in a homogeneous electron gas can be calculated most rigorously by what is known as the quantum Monte Carlo method. Here, the ground state energy is calculated by a direct variational method, which involves integration over the coordinates of a large number of electrons, using an antisymmetric trial function that takes care of correlation between their positions [23]. The numerical dependences $E(n, m)$ thus obtained are then approximated by an analytical expression (for the nonmagnetic case, see, for example, [158]). The LSDF approximation postulates (and this is a crucial point) that the exchange-correlation energy density at the point $\mathbf{r}$ is a function of $n(\mathbf{r})$ and $m(\mathbf{r})$ at that point, and functionally this dependence takes the same form as in a homogeneous electron gas

$$E_{xc} = \int d\mathbf{r}n(\mathbf{r})\varepsilon_{xc}(n(\mathbf{r}), m(\mathbf{r})), \tag{4.14}$$

where ε_{xc} is the exchange-correlation energy in a homogeneous gas of density n and of spin density m per particle. Then the relation (4.8) is completely defined, and one finds $\psi_{\nu\alpha}(\mathbf{r})$ and then f_ν so as to minimize the total energy or, more accurately, the thermodynamic potential $\Omega = E - \mu N$ (where μ is the chemical potential and N is the number of particles). Next, one inserts (4.9) - (4.11) and (4.14) in (4.8) and varies $E(\rho)$ for a fixed f_ν and subject to the additional condition of the orthonormality of the function $\psi_{\nu\alpha}(\mathbf{r})$. As a result of tedious, but standard manipulations (see [158]), one obtains equations for $\psi_{\nu\alpha}(\mathbf{r})$, usually called the Kohn–Sham equations

$$\{-\frac{1}{2}\nabla^2 + \int \mathbf{dr}'\frac{n(\mathbf{r}')}{|\mathbf{r}-\mathbf{r}'|}\delta_{\alpha\beta} + V_{\alpha\beta} + V_{\alpha\beta}^{xc}\}\,\psi_{\nu\beta}(\mathbf{r}) = \varepsilon_\nu\psi_{\nu\alpha}(\mathbf{r}), \tag{4.15}$$

where

$$V_{\alpha\beta}^{xc}(\mathbf{r}) = \frac{\delta E_{xc}}{\partial\rho_{\alpha\beta}(\mathbf{r})} = \frac{\partial\,[n\varepsilon_{xc}(n, m)]}{\partial n}\delta_{\alpha\beta} + \frac{1}{m}\frac{\partial\,[n\varepsilon_{xc}(n, m)]}{\partial m}\sigma_{\alpha\beta}\mathrm{Tr}(\hat{\rho}\hat{\sigma}) \tag{4.16}$$

is the exchange-correlation potential. If, then, one varies $E[\rho]$ with respect to f_ν, it will, as is shown by Perdew and Zunger [158], be the same as the Fermi distribution function of ε_ν for $T = 0$

$$f_\nu = \begin{cases} 1, & \varepsilon_\nu < \mu, \\ 0, & \varepsilon_\nu > \mu, \end{cases} \tag{4.17}$$

and

$$\varepsilon_\nu = \frac{\delta E}{\delta f_\nu} \tag{4.18}$$

is the energy of a quasiparticle in the sense of Landau's theory of Fermi liquid [18]. For purely formal reasons, it is convenient to express the total energy E as a sum of the energies of occupied states, E_{sp}, and a remainder of what are called "doubly counted" terms E_{dc}

$$E = E_{sp} - E_{dc}; \tag{4.19}$$

$$E_{sp} = \sum_\nu f_\nu\varepsilon_\nu; \tag{4.20}$$

$$E_{dc} = U_H + \int \mathbf{dr}\mathrm{Tr}\left[\hat{\rho}\frac{\partial E_{xc}}{\partial\rho}\right] - E_{xc} = U_H + \int \mathbf{dr}\{n\frac{\partial\,(n\varepsilon_{xc})}{\partial n} + m\frac{\partial\,(n\varepsilon_{xc})}{\partial m} - n\varepsilon_{xc}\}. \tag{4.21}$$

In the absence of an external magnetic field ($V_{\alpha\beta} = V\delta_{\alpha\beta}$), equations (4.15) always have so-called spin-limited solutions: $\nu \equiv \lambda\sigma$ (where λ are the orbital quantum numbers and $\sigma = \pm$), $\psi_{\lambda\sigma\alpha} = \delta_{\alpha\sigma}\psi_\lambda$, and $\varepsilon_{\lambda\sigma} \equiv \varepsilon_\lambda$. (Here, $\rho_{\alpha\beta} = 1/2n\delta_{\alpha\beta}$, $m = 0$). Sometimes, however, there may be an instability in spin polarization. If, in the case of a self-consistent solution of the nonlinear equations (4.15) [subject to (4.16), (4.13), and (4.6)], one specifies for the initial iteration $\varepsilon_{n+} \neq \varepsilon_{n-}$ and $\psi_{n+} \neq \psi_{n-}$, these differences in the self-consistent process will build up, tending to certain finite values. Such a situation arises if the obvious loss in E_{sp} (in the absence of an external magnetic field) in consequence of spin polarization is made up for by a gain in E_{dc}. The point is that, by virtue of Pauli's principle, the wave function Φ of a many-electron system is antisymmetric under the permutation of the spatial coordinates of any two electrons with parallel spins. For this reason, such electrons are, on average, spaced wider apart than electrons with antiparallel spins, and this leads to a gain in the Coulomb repulsion energy upon spin polarization. Consider, as an example, the most important case of spin polarization along a certain axis, say, z axis. Then

$$\hat{\rho} = \begin{pmatrix} n_+ & 0 \\ 0 & n_- \end{pmatrix}, \quad \hat{V}^{xc} = \begin{pmatrix} V_+^{xc} & 0 \\ 0 & V_-^{xc} \end{pmatrix}, \tag{4.22}$$

and $n_\pm = 1/2(n \pm m)$. A "Fermi hole" of radius $\sim(n_\pm)^{-1/2}$ then comes about around each electron with spin $\pm$, and this leads to a gain in energy, $V_\pm^{xc} \sim (n_\pm)^{1/3}$ [38]. With large parameters $r_s = (4\pi/3n)^{1/3}$ (small n), this gain upon spin polarization can exceed the loss in kinetic energy [see (3.48), where $\delta n_e \equiv m$]. As Ceperley and Adler [23] demonstrated, in a homogeneous electron gas, this can happen at unattainably high values of $r_s \sim 10^2$. Because E_{xc} seems to be a smooth function of r_s, one may hope that if one uses the local approximation, E_{xc} will be of the same order of magnitude in an inhomogeneous gas as in a homogeneous gas for r_s corresponding to an average density $n(r)$. At the same time, the real values of $N(E_F)$ may be considerably greater than in a free-electron gas with the same r_s (see Sec. 3.5), thus leading, in accord with (3.48), to a substantial decrease in δE. In fact, it is this occurrence that makes ferromagnetism possible at the observable values of r_s. Numerous band-theoretic calculations under the LSDF approximation (see, for example, [68, 115]) do explain the existence of ferromagnetism in Fe, Co, and Ni, antiferromagnetism in Cr and Mn, and the absence of spontaneous spin polarization in the other d metals. The LSDF method can be used not only to calculate ferromagnetic and antiferromagnetic polarization in the entire crystal, but also the magnetic moments of impurities. As a rule, the results of such calculations show good agreement with experiment [159].

4.3. Exchange Interactions, Magnetic Structure Stability, and Magnetic-Moment Localization

We now turn to spin fluctuations, that is, magnetic excitations above the ground state of a system, using the LSDF approach. As early as the 1950s, Herring and Kittel noticed the important fact that in any ferromagnet, with either localized or itinerant electrons, spin waves exist and any weakly inhomogeneous spin density distribution can be described with the aid of Heisenberg's efficient classical Hamiltonian

$$H_{ex} = -\sum_{ij}{}' J_{ij}\mathbf{e}_i\mathbf{e}_j, \tag{4.23}$$

where $\mathbf{e}_i$ is the unit vector in the direction of magnetization at the ith site, and J_{ij} are the exchange parameters [26, 155, 160]. Liechtenstein *et al.* [37] and Liechtenstein *et al.* [161] demonstrated that in the LSDF method the latter can be calculated, no matter what specific model one chooses to represent the nature of ferromagnetism. From a technical point of view, the pivotal point in [37] and [161] is the use of the "local

force theorem" according to Andersen [162, 34], extended in [37] to the case of spin polarization. By this theorem, given the first-order variation of charge and spin density $\delta n(\mathbf{r})$ and $\delta m(\mathbf{r})$, the total-energy variation δE is equal to $\delta^* E_{sp}$ for a fixed self-consistent potential; the variation $\delta_1 E_{sp}$ is exactly balanced out by variations of the latter [see (4.19) and (4.21)]:

$$\delta E = \delta^* E_{sp}. \tag{4.24}$$

To prove (4.24), we first calculate the variation of the sum of single-particle state energies E_{sp} caused by the variation of the potential in (4.15)

$$\delta_1 E_{sp} = \sum_{\nu} f_{\nu} \sum_{\alpha\beta} \int \mathbf{dr} \psi^*_{\nu\alpha}(\mathbf{r})$$

$$\times \{ \int \frac{\mathbf{dr}'}{|\mathbf{r}-\mathbf{r}'|} \delta n(\mathbf{r}') \delta_{\alpha\beta} + \delta V^{xc}_{\alpha\beta} \} \psi_{\alpha\beta}(\mathbf{r}) \tag{4.25}$$

$$= \int d\mathbf{r} d\mathbf{r}' \frac{n(\mathbf{r}) \delta n(\mathbf{r}')}{|\mathbf{r}-\mathbf{r}'|} + \int d\mathbf{r} \mathrm{Tr} \{ \hat{\rho} \delta V^{xc} \}.$$

The first term in (4.25) is the variation of $U_H[n(\mathbf{r})]$, (4.11). In view of (4.16), the integrand in the second term can be written as

$$\mathrm{Tr} \{ \hat{\rho} V^{xc} \} = \frac{\partial^2 (n\varepsilon_{xc})}{\partial n^2} n\delta n + \frac{\partial^2 (n\varepsilon_{xc})}{\partial m^2} m\delta m$$

$$+ \frac{\partial^2 (n\varepsilon_{xc})}{\partial n \partial m} (m\delta m + n\delta n) \tag{4.26}$$

$$+ \sum_{\alpha\beta} \frac{\partial (n\varepsilon_{xc})}{\partial m} \rho_{\alpha\beta} \delta \left(\frac{1}{m} \hat{\vec{\sigma}}_{\alpha\beta} \mathrm{Tr} \left(\hat{\vec{\sigma}} \hat{\rho} \right) \right).$$

Direct calculation will prove that the last term in (4.26) vanishes. Then, substituting (4.26) in (4.25) and comparing the result with the result of varying (4.21) yields

$$\delta_1 E_{sp} = \delta E_{dc}. \tag{4.27}$$

Thus, the variation of the sum of occupied-state energies caused by changes in the self-consistent potential is exactly made up for by the variation δE_{dc}, which proves (4.24). The variation δE_{sp} can be expressed in terms of changes in the integral $[n(\varepsilon)]$ and differential $[N(\varepsilon) = dn(\varepsilon)/d\varepsilon]$ densities of states

$$\delta^* E_{sp} = \int_{-\infty}^{E_F} d\varepsilon \varepsilon \delta^* N(\varepsilon) = -\int_{-\infty}^{E_F} d\varepsilon \delta^* n(\varepsilon), \tag{4.28}$$

where account is taken of the fact that magnetic excitations do not change the number of particles.

The specific exchange parameters in (4.23) can be calculated by the multiple scattering method (the KKR method, see, for example, [52] and [165]). With this method, the description of the atomic state at the ith site in terms of the single-center scattering matrix $\hat{t}_i$ is naturally separated from that of the lattice structure by introducing a Green's function for an "empty" lattice, $\hat{G}_{ij}$ (all quantities are matrices in a space of spin quantum numbers $\alpha = \pm$ or $\uparrow\downarrow$, and orbital quantum numbers $L = lm$). Then [52, 165]

$$n(\varepsilon) = n_0(\varepsilon) + \frac{1}{\pi} \mathrm{Im} \mathrm{Tr} \ln \hat{T}(\varepsilon). \tag{4.29}$$

Here, $n_0(\varepsilon)$ is the integrated density of states in the empty lattice and $\hat{T}(\varepsilon)$ is the total scattering matrix (the scattering path operator), defined by the matrix equation

$$(T^{-1})_{iL\alpha, jL'\beta} = (t_i^{-1})_{L\alpha, L'\beta} \delta_{ij} - G_{iL, jL'} \delta_{\alpha\beta}. \tag{4.30}$$

To calculate J_{ij} from (4.23), consider the disturbance associated with the rotation of $\mathbf{e}_i$, $\mathbf{e}_j$ through small angles $\pm\theta/2$ from the direction of magnetization in the crystal. Then, by (4.23), we have

$$\delta E_{ex} = J_{ij} \theta^2. \tag{4.31}$$

On the other hand, the $\hat{t}$ matrix on the ith site has a spinor structure [164]

$$t_i = \frac{1}{2}(t_{i\uparrow} + t_{i\downarrow}) + \frac{1}{2}(t_{i\uparrow} - t_{i\downarrow})(\mathbf{e}_i \vec{\sigma}), \tag{4.32}$$

determined by the requirement that it should be diagonal (with eigenvalues $t_{i\uparrow}$ and $t_{i\downarrow}$), so that the quantization axis is directed along the vector $\mathbf{e}_i$. From (4.32), one can find the changes δt_i, δt_j caused by changes $\delta \mathbf{e}_i$, $\delta \mathbf{e}_j$. Note that with the perturbation in question $\delta m(\mathbf{r}) \sim \theta^2 \sim \delta E_{ex}$, so in calculating δE_{ex} by the LSDF method, one may use the local force theorem (4.24). Then δE_{ex} can be expressed in terms of $\delta \hat{t}_i$, $\delta \hat{t}_j$ by (4.28) - (4.30). By comparing the result with (4.31), one obtains an exact expression for J_{ij} in the LSDF method

$$J_{ij} = \frac{1}{4\pi} \int_{-\infty}^{E_F} d\varepsilon \mathrm{Tr}_L \{ (t_{i\uparrow}^{-1} - t_{i\downarrow}) T_{ij}^{\uparrow} (t_{j\uparrow}^{-1} - t_{j\downarrow}) T_{ji}^{\downarrow} \}, \tag{4.33}$$

where all terms refer to the ground ferromagnetic state.

A really observable characteristic for weakly excited magnetic states is the spin stiffness tensor D_{ab} (for cubic structures, it reduces to a scalar) defined according to a phenomenological theory [155, 160] by

$$\delta E_{ex} = \frac{M_0}{2} D_{ab} \mathbf{q}_a \mathbf{q}_b. \tag{4.34}$$

Here, M_0 is the saturation magnetization in Bohr magnetons and $\mathbf{q}$ is the wave vector (the inclination of the vector $\mathbf{e}_i$ is $\mathbf{qR}_i$, where $\mathbf{R}_i$ is the lattice vector). By considering such a perturbation in the LSDF method, one can derive, similar to (4.33), the expression

$$D_{ab} = \frac{1}{2\pi M_0} \sum_{\mathbf{k}} \int_{-\infty}^{E_F} d\varepsilon$$

$$\times \mathrm{Im} \mathrm{Tr}_L \{ (t_{\uparrow}^{-1} - t_{\downarrow}^{-1}) \frac{\partial T^{\uparrow}(\mathbf{k})}{\partial k_a} (t_{\uparrow}^{-1} - t_{\downarrow}^{-1}) \frac{\partial T^{\downarrow}(\mathbf{k})}{\partial k_b} \}$$

$$= \frac{2}{M_0} \sum_j J_{0j} R_{ja} R_{jb}, \tag{4.35}$$

which agrees with (4.33) and (4.23). To simplify matters, we consider here a case where all atoms in the lattice are the same, 0 is the site with $\mathbf{R}_0 = 0$, and the sum of $\mathbf{k}$ in (4.31) is taken over the Brillouin zone. In theory, the expression (4.35) is as exact as the multiple scattering method (4.30) itself and the local force theorem, and admits a direct comparison with experiment. As an example, we give the results Liechtenstein *et al.* [37] obtained for $D_{ab} = D\delta_{ab}$ in α-Fe and Ni by (4.33) and (4.35). They used the cluster multiple scattering method and considered two coordination shells to obtain: $D = 294$ meV Å^2 for α-Fe and 386 meV Å^2 for Ni (the experimental values are 280 and 400, respectively).

Figure 4.1 gives calculated results from [161] for $D(E_F)$ in α-Fe. Of course, the value of this function has a direct physical significance only for a real value of E_F; yet, the dependence of D on E_F is rather instructive from a qualitative point of view. This dependence reflects the tendency of ferromagnetism to instability ($D < 0$) when the band is about half filled, and toward stability near the edge of the band. Naturally, it is assumed that spin polarization as such does exist. Qualitatively, such a tendency exists among the magnetic d metals (and alloys): Cr and Mn are antiferromagnets, while Fe, Co, and Ni are ferromagnets. We will go back to this tendency a bit later in connection with the hcp phase of Co.

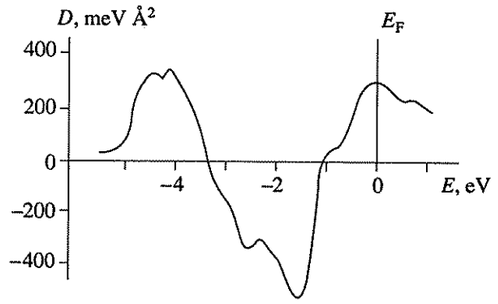

Fig. 4.1. *Spin-wave stiffness in the bcc phase of iron, calculated as a function of Fermi energy [161].*

An important characteristic of exchange interactions is the total exchange interaction parameter. Introduced in [166], it defines the interaction of a given site 0 with all of its environment J_0. To calculate it, one should first calculate the change in energy as the vector $\mathbf{e}_0$ at the selected ith site rotates through a small angle θ relative to the magnetization of the crystal. Then [37, 166]

$$J_0 = \lim_{\theta \to 0} [\delta E(\theta)/\theta^2] = -\frac{1}{4\pi} \int_{-\infty}^{E_F} d\varepsilon \mathrm{Tr} \{ (t_{0\uparrow}^{-1} - t_{0\downarrow}^{-1}) \tag{4.36}$$

$$\times (T_{00}^{\uparrow} - T_{00}^{\downarrow}) + (t_{0\uparrow}^{-1} - t_{0\downarrow}^{-1}) T_{00}^{\uparrow} (t_{0\uparrow}^{-1} - t_{0\downarrow}^{-1}) T_{00}^{\downarrow} \}.$$

If in (4.36) one passes to the limit of an isolated atom ($G_{ij} \to 0$, $\hat{T}_{00} \to \hat{t}_{00}$), then J_0 will tend to 0. Thus, the exchange parameter J_0 characterizes "intersite" exchange interactions and is only indirectly related to Hund's "intrasite" exchange that determines the splitting $t_{0\uparrow}^{-1} - t_{0\downarrow}^{-1}$. Moreover, using (4.30), (4.33), and (4.36), one can show that

Fig. 4.2. *Exchange integral J_0 plotted against Fermi energy for impurities (Fe, Ni) in the hcp phase of cobalt and for metallic cobalt [167].*

$$J_0 = \sum_{j \neq 0} J_{0j} \tag{4.37}$$

is in full agreement with (4.23). From a purely computational point of view, however, (4.36) is much simpler than (4.37) or (4.33). Notably, it permits computation of J_0 not only for pure metals, but also for impurities. The values of J_0 calculated by Anisimov *et al.* [167] for the hcp phase of Co and for the impurities Fe and Ni in Co are given in Fig. 4.2.

The negative values of J_0 imply the instability of the chosen magnetic configuration toward spin rotation, as they lead in this case to a reduction in the total energy. For example, the results given in Fig. 4.2 indicate that when the impurity states are filled almost half full, the impurity spin tends to be antiparallel to the magnetization of the matrix. The results calculated for pure cobalt demonstrate the already discussed tendency of mag-

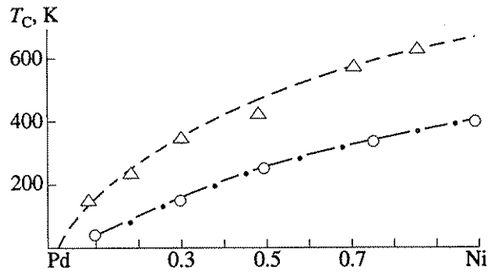

Fig. 4.3. *Concentrational dependence of the Curie temperature in Ni–Pd alloys: triangles, experiment; open circles, calculation [37].*

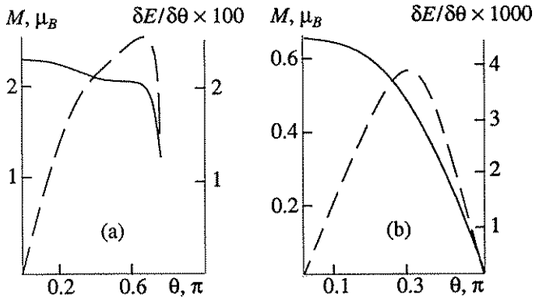

Fig. 4.4. *Magnetic moment in Bohr magnetons (the full curve) and the first derivative of energy with respect to angle of rotation in Ry (the dashed curve) according to calculations in [168]: (a) Fe, (b) Ni.*

netic metals to antiferromagnetism as their states approach the "half-full" mark.

In calculating an equilibrium magnetic structure, a necessary (but not a sufficient) condition for the selected structure to actually correspond to an energy minimum is the convergence of the self-consistency procedure to nonzero magnetic moments, which implies stability (at least local) with respect to changes in the magnitude of magnetic moments. As to the condition $J_0 > 0$, it implies stability with respect to their small rotations. Thus, the calculation of J_0 is an efficient tool for a theoretical inquiry into the stability of magnetic structures. An illustrative example is the theoretical proof derived by Anisimov *et al.* [167] in calculating the stability of experimentally observed magnetic structures in the magic square

$$MnPt_3(FM);\quad MnPd_3(AFM);$$

$$FePt_3(AFM);\quad FePd_3(FM).$$

In all of these compounds, calculations yielded $J_0 > 0$ for "regular" and $J_0 < 0$ for "irregular" structures.

By using both the molecular field and classical spin approximations, the Curie temperature T_C can be expressed in terms of J_0 as

$$T_C = \frac{2}{3}J_0. \tag{4.38}$$

Although this expression is not very exact, it yields useful estimates of T_C for the pure metals and alloys for which the T matrix can be determined in, say, the coherent-potential approximation. As an illustration, Fig. 4.3 gives calculated [37] and experimental concentrational dependences of $T_C(x)$ for disordered $Ni_{1-x}Pd_x$ alloys.

Thus, if one limits oneself to weakly excited states of a magnet, one can calculate their properties without resort to any model considerations, that is, with almost a complete disregard of the degree of localization of "magnetic" electrons. Information about the latter can be derived by considering excitations with rotations of magnetic moments through finite angles [168]. To prove this, let us consider the "impurity" problem for the case where at some selected site 0 the vector $\mathbf{e}_0$ is turned through an angle θ relative to the z axis [this is specified in terms of the spinor structure of the $\hat{t}$ matrix by (4.32)]. Suppose the vector $\mathbf{e}_0$ is turned through a small angle $\delta\vec{\theta}$. Then $\delta\mathbf{e}_0 = \delta\vec{\theta} \times \mathbf{e}_0$, and, by virtue of (4.29) and (4.30), the variation of the integrated density of states $n(\varepsilon)$ takes the form

$$\delta n(\varepsilon) = \frac{1}{\pi}\mathrm{Im}\mathrm{Tr}_{i,L,\sigma}(\delta \ln \hat{T}(\varepsilon))$$

$$= \frac{1}{\pi}\mathrm{Im}\mathrm{Tr}_{i,L,\sigma}\left[-\hat{T}(\varepsilon)\delta\hat{T}^{-1}(\varepsilon)\right] \tag{4.39}$$

$$= -\frac{1}{\pi}\mathrm{Im}\mathrm{Tr}_{i,L,\sigma}[\hat{T}_{00}(\varepsilon)\delta\hat{t}_0^{-1}(\varepsilon)].$$

Inversion of the matrix (4.32) readily yields

$$\hat{t}_0^{-1} = \frac{1}{2}(t_{0\uparrow}^{-1} + t_{0\downarrow}^{-1}) + \frac{1}{2}(t_{0\uparrow}^{-1} - t_{0\downarrow}^{-1})(\mathbf{e}_0 \cdot \vec{\sigma}); \tag{4.40}$$

$$\delta\hat{t}_0^{-1} = \frac{1}{2}(t_{0\uparrow}^{-1} - t_{0\downarrow}^{-1})\,\delta\mathbf{e}_0 \cdot \vec{\sigma} \equiv (\delta\vec{\theta} \times \vec{\Delta}_0) \cdot \vec{\sigma}, \tag{4.41}$$

where $\vec{\Delta} \equiv \frac{1}{2}(t_{0\uparrow}^{-1} - t_{0\downarrow}^{-1})\,\mathbf{e}_0$. By presenting $\hat{T}_{00}(\varepsilon)$ in spinor form

$$T_{00}(\varepsilon) = T_{00}^{(0)}(\varepsilon) + \mathbf{T}_{00}^{(1)}(\varepsilon)\vec{\sigma}, \tag{4.42}$$

and substituting (4.41) and (4.42) in (4.39) and then in (4.28), one finds the expression for the variation of total energy with the angle of the moment

$$\frac{\delta E}{\delta\theta} = \frac{2}{\pi}\mathrm{Im}\int_{-\infty}^{E_F} d\varepsilon \mathrm{Tr}_L[\vec{\Delta}_0(\varepsilon) \times \mathbf{T}_{00}^{(1)}(\varepsilon)]. \tag{4.43}$$

By applying self-consistent solutions of the impurity problem for different angles θ of the vector $\mathbf{e}_0$ with respect to the direction of magnetization of the crystal, it is possible to determine the angular dependence of the magnetic moment for site 0, $M_0(\theta)$ and, by (4.43), the dependence $\partial E/\partial\theta$. If the Heisenberg model is

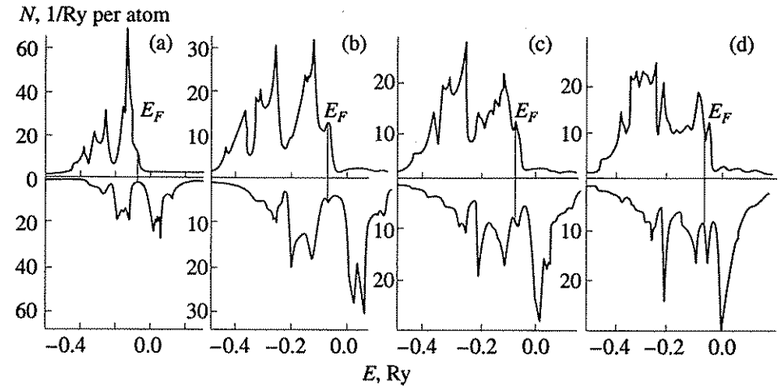

Fig. 4.5. *Electronic density of states for an Fe atom in a metal with the magnetic moment turned through θ = 0 (a), θ = 0.2π (b), θ = 0.35π (c), and θ = 0.5π (d).*

applicable not only at small deviations (completely localized magnetic moments), then

$$M_0(\theta) = \text{const}, \quad \partial E/\partial\theta = 2J_0 \sin\theta. \tag{4.44}$$

The angle θ, at which noticeable deviations from (4.44) are observed, is exactly the one that can serve as a quantitative measure of whether the behavior of magnetism in a given substance is localized or itinerant.

Figure 4.4 gives the results that Turzhevskii *et al.* [168] calculated by the LMTO method (a linearized version of the KKR method) for Fe and Ni. In each instance, there is a critical angle θ_c, at which M_0 vanishes. At $0 \lesssim \theta_c$, the dependence $\partial E/\partial\theta$ begins to deviate strongly from a sinusoid. In quantitative terms, however, the situation for Fe and Ni is entirely different. Whereas for Fe, $\theta_c \simeq 0.7\pi$, in the case of Ni, the relations (4.44) are severely violated even at $\theta \approx 0.2$ or 0.3π (and $\theta_c \lesssim \pi/2$).

Deviations from the Heisenberg behavior at large θ are traceable to the fact that at such angles significant changes occur in the atom's electronic structure itself (see the corresponding local density-of-states graphs shown in Fig. 4.5 after Turzhevskii *et al.* [168]).

Thus, in Ni, the magnetism is far more "band-type" than in Fe. One will draw the same conclusion when one considers localized magnetic moments in the paramagnetic phase of these metals, which we proceed to do in the next section.

4.4. Spin Splitting and Localized Magnetic Moments in the Paramagnetic Region

The problem of localized magnetic moments in the paramagnetic phase of the iron-group metals was clearly stated and partly solved within the spin-fluctuation theories proposed by Hubbard, Hasegawa, Moriya, and other physicists in the late 1970s. These theories are reviewed in detail by Hohenberg [29]. Before we proceed to consider the problem within the framework of the LSDF method, it is worthwhile discussing their approaches at least in brief. As a rule, the spin-fluctuation theories are formulated within the framework of Hubbard's model [4], which takes into account solely the Coulomb electron repulsion U at one site

$$\hat{H} = \sum_{ij\sigma}{}' t_{ij}c_{i\sigma}^{+}c_{j\sigma} + U\sum_i n_{i\uparrow}n_{i\downarrow}, \tag{4.45}$$

where $\hat{c}_{i\sigma}^{+}$ and $\hat{c}_{i\sigma}$ are the electron creation and annihilation operators at the ith site with the spin projection σ; $\hat{n}_{i\sigma} = \hat{c}_{i\sigma}^{+}\hat{c}_{i\sigma}$; the primed sum is taken over $i \neq j$. By the functional integration method, one can reduce the many-particle problem described by the Hamiltonian (4.45) to the problem of motion of a system of noninteracting electrons in random fields that fluctuate in space and time.

To demonstrate, suppose the Hamiltonian of a large canonical ensemble $\hat{\mathrm{H}} = \hat{H} - \mu\hat{N}$ can be written as

$$\hat{\mathrm{H}} = \hat{\mathrm{H}}_0 - \sum_\alpha a_\alpha \hat{Q}_\alpha^2. \tag{4.46}$$

Here, $\hat{\mathrm{H}}_0$ is the Hamiltonian of noninteracting electrons, $\hat{Q}_\alpha$ are the operators bilinear in $c_{i\sigma}^{+}$ and $c_{i\sigma}$, and a_α are numerical factors. Then, using the Hubbard–Stratonovich identity

$$\exp\hat{A}^2 = \int_{-\infty}^{\infty}\frac{d\xi}{\sqrt{\pi}}\exp(-\xi^2 + 2\xi\hat{A}), \tag{4.47}$$

valid for any operator $\hat{A}$, one can write the statistical sum $Z = \mathrm{Tr}\exp(-\beta\hat{\mathrm{H}})$ ($\beta \equiv T^{-1}$) as a functional integral [28]

$$Z = \int \Pi D\xi_\alpha(\tau)\exp\left[-\int_0^\beta d\tau\sum_\alpha\frac{\varepsilon_\alpha^2(\tau)}{a_\alpha}\right. \tag{4.48}$$

$$\left.\times\,\mathrm{Tr}\left\{\exp(-\beta\hat{\mathrm{H}}_0)\,T_\tau\exp\left[-2\sum_\alpha\int_0^\beta d\tau\varepsilon_\alpha(\tau)\hat{Q}_\alpha(\tau)\right]\right\},\right.$$

where T_τ is the chronological ordering symbol, and $Q_\alpha(\tau) = e^{\tau\hat{H}_0}\hat{Q}_\alpha e^{-\tau\hat{H}_0}$. The expression under the trace sign (Tr) in (4.48) is nothing more than the statistical sum of the system of noninteracting electrons in external alternating fields, $\varepsilon_\alpha(\tau)$, adjoint to the operators $\hat{Q}_\alpha$. As a rule, one uses what is known as a statistical approximation where $\varepsilon_\alpha(\tau) \to \varepsilon_\alpha \equiv \int_0^\beta d\tau\varepsilon(\tau)/\beta$. This is formally equivalent to neglecting the noncommutative property of the operators $\hat{Q}_\alpha(\tau)$ at different instants of time or, if $\hat{Q}_\alpha$ are spin operators, to replacing them by classical vectors. Then the results come to depend on the choice of a particular representation of (4.46).

In the Hubbard model, it is most convenient to use the representation

$$U\sum_i \hat{n}_{i\uparrow}\hat{n}_{i\downarrow} = \frac{U}{4}\sum_i \hat{n}_i^2 - U\sum_i (\hat{\mathbf{s}}_i\mathbf{m}_i)^2, \qquad (4.49)$$

where $\mathbf{m}_i$ is an arbitrary unit vector, $\hat{n}_i$ and $\hat{\mathbf{s}}_i$ are the operators of the total number of particles and of spin at the ith site. Ordinarily, charge density fluctuations are neglected. This is equivalent to using the saddle-point method in (4.48) over the field adjoint to the operator $\hat{n}_i$. Following that, the procedure reduces to the renormalization of the chemical potential. As a result, from (4.48) we obtain [28]

$$Z = \left(\frac{2\beta}{\pi U}\right)^{N/2}\int\prod_j d\hat{\varepsilon}_j \exp\left[-\frac{\beta}{U}\sum_j \hat{\varepsilon}_j^2\right]\tilde{Z}[\hat{\varepsilon}_j], \qquad (4.50)$$

$$\tilde{Z}[\hat{\varepsilon}_j] = \mathrm{Tr}\exp\{-\beta\hat{H}[\hat{\varepsilon}_j]\},$$

$$\hat{H}[\varepsilon_j] = \sum_{ij\sigma}(t_{ij} - \mu\delta_{ij})\hat{c}_{i\sigma}^+\hat{c}_{j\sigma} + \sum_j \hat{\varepsilon}_j\hat{c}_{j\alpha}^+\vec{\sigma}_{\alpha\beta}\hat{c}_{j\beta}. \qquad (4.51)$$

We thus reduced the problem of calculating Z for a system of interacting particles in the crystal to finding $\tilde{Z}$ for a certain disordered alloy with random magnetic fields $\hat{\varepsilon}_i$ (the alloy analogy). The latter can be further reduced to calculating the average electronic Green's function, and this can in turn be calculated in, for example, the coherent potential approximation [165].

As is noted in Sec. 4.1, the existence of localized magnetic moments in a paramagnetic phase is most unambiguously confirmed by the Curie–Weiss law for magnetic susceptibility χ, on the one hand, and by spin splitting in the energy spectrum, on the other. Let us explain the relationship between the two phenomena in terms of the alloy analogy.

In the functional integration method, χ can be estimated [28] as

$$\chi \sim \frac{\langle\hat{\varepsilon}^2\rangle}{T}. \qquad (4.52)$$

Then, if the probability distribution for the length of the vector $\hat{\varepsilon}_i$ has a maximum at $\hat{\varepsilon} = 0$, then $\langle\hat{\varepsilon}^2\rangle \sim T$ (Gaussian fluctuations) and $\chi = \text{const}$. If, on the other hand, it has a maximum at $|\hat{\varepsilon}| = \varepsilon_0 \neq 0$, then $\chi \sim \hat{\varepsilon}_0^2/T$ (Curie's law). In the latter case, the mean Green's function will have two poles spaced $2\varepsilon_0$ apart (at least within narrow bands), in agreement with (4.51).

Note that the Curie–Weiss law for $\chi(T)$ admits, in theory, alternative interpretations arising from specific features of the band structure [24], interaction with phonons [156], etc. By contrast, spin splitting observed in the energy spectrum at $T > T_C$ [25, 27, 153, 154] (where T_C is the Curie temperature) appears to bear out the existence of local magnetic moments unambiguously. From the standpoint of the general many-particle quantum theory, this is a very crucial fact – it implies the violation of the fundamental postulate in Landau's theory of Fermi liquid [18] about a reciprocal one-to-one correspondence between particles and quasiparticles. Indeed, whereas the state of particles (electrons) is characterized by a quasimomentum $\mathbf{k}$ and a spin projection σ, in the case of quasiparticles, σ must be replaced by some other quantum number; otherwise no splitting of the spectrum would occur in the paramagnetic phase. In this sense, the very term "spin splitting" appears somewhat arbitrary. Moreover, the strong spatial inhomogeneity of spin density in the presence of localized magnetic moments implies the inapplicability of the condition $q \ll k_P$, where q is the characteristic electron scattering momentum.

The alloy analogy can be readily extended from the Hubbard model to real calculations in the LSDF method [30]. (The idea of the alloy analogy seems to have been advanced for the first time by Slater [38].) With it, one models a paramagnet by an "alloy" in which half of the atoms has upward-directed magnetic moments and the other half, downward-directed magnetic moments. Then one carries out a self-consistent calculation by the coherent-potential method. While, according to [36], this leaves the magnetic moment in α-Fe almost unchanged in comparison with the ground state (1.9 μ_B and 2.2 μ_B, respectively), in the paramagnetic phase of nickel, M_0 is negligibly small. This fully checks with the conclusion drawn in the previous section about the comparative localization of magnetic moments in Fe and Ni. Note that the calculation by Gyorffy *et al.* for α-Fe (but not for Ni) gives in the paramagnetic phase not only a nonzero M_0, but also a nonzero spin splitting. Experimentally, this was also observed in Ni [153, 154]. In this respect, the theory set forth by Gyorffy *et al.* [36] is not satisfactory enough.

Thus, the degree of magnetic-moment localization is a problem that can be solved in quantitative terms for each specific metal. At the same time, the influence of local magnetic moments on the energy spectrum, thermodynamic, and kinetic properties of an electron liquid remains a fairly complex question. It is part of the more general problem that has as its objective to describe

strongly correlated systems. That is what will be taken up in the next chapter.

CONCLUSION

The magnetism of the iron group metals is a phenomenon in which the dual (localized versus itinerant) nature of electrons in a metal stands out with especial clarity from an experimental point of view. As to the purely band-theoretic approach, it covers important traits of the *d* metals, such as the participation of *d* electrons in the formation of the Fermi surface and the "Fermi-liquid" character of their contribution to the low-temperature properties, such as the electronic heat capacity of a metal. At the same time, it is at variance with other, likewise reliably established experimental facts, above all the conservation of the spin splitting of the spectrum in the paramagnetic phase, and agrees with difficulty with the Curie–Weiss law. All of these properties are, however, evidence in support of the localized character of magnetic moments. In this chapter (see Sec. 4.3), we showed that the interaction characteristics (exchange parameters) of these moments can be calculated within the present-day band theory based on the spin-density-functional method in good agreement with experiment. However, in contrast to Heisenberg magnets, both the exchange parameters and the magnitudes of the magnetic moments are generally strong functions of their angle of rotation.

A qualitative description of the properties of ferromagnets at finite temperatures (including those in the paramagnetic region) within the spin density functional method remains a problem not yet fully resolved. On the whole, although it is good in describing many, but not all, properties of the iron group metals, one does not see at present how this approach can be improved in cases where it falls short of the goal.

REFERENCES

1. Hedin, L. and Lundquist, S., Effects of Electron–Electron and Electron–Phonon Interactions of the One-Electron States of Solids, *Solid State Physics*, New York: Academic, 1969, vol. 23, pp. 2 - 182.
2. Vonsovsky, S.V. and Katsnelson, M.I., *Quantum Solid-State Physics*, Berlin: Springer, 1989, 2nd ed.
3. Bloch, F., Quantum Mechanik von Elektronen in Kristallgitter, *Z. Phys.*, 1928, vol. 52, pp. 555 - 570.
4. Hubbard, J., Electron Correlations in Narrow Energy Bands, *Proc. Roy. Soc.*, 1963, vol. A276, pp. 238 - 257.
5. Peierls, R., Theorie Elektrische Leitfähigkeit und Thermoleitfähigkeit von Metalle, *Ann. Phys.*, 1930, vol. 4, pp. 619 - 630.
6. Harrison, W., *Pseudopotentials in the Theory of Metals*, New York: W.A. Benjamin, 1966.
7. Heine, W., Cohen, M., and Weire, D., The Pseudopotential Concept, *Solid State Physics*, New York: Academic, 1970, vol. 24.
8. Schubin, S.P. and Vonsovsky, S.V., On the Electron Theory of Metals, *Proc. Roy. Soc.*, 1934, vol. A145, pp. 159 - 180.
9. Schubin, S.P. and Wonsowsky, S.W., Zur Elektronentheorie der Metalle: I, *Phys. Z. UdSSR*, 1935, vol. 7, pp. 292 - 328.
10. Schubin, S.P. and Wonsowsky, S.W., Zur Elektronentheorie der Metalle: II, *Phys. Z. UdSSR*, 1936, vol. 10, pp. 348 - 377.
11. Shubin, S.P., *Izbrannye Trudy po Teoreticheskoi Fizike* (Selected Works on Theoretical Physics), Sverdlovsk, 1991.
12. De Boer, J.H. and Verwey, E.J.W., Semiconductors with Partially and Completely Filled Bands, *Proc. Phys. Soc.*, 1937, vol. A49, pp. 59 - 69.
13. Mott, N.F., The Basis of the Theory of Metals with Special Reference to the Transition Metals, *Proc. Phys. Soc.*, 1949, vol. A62, pp. 416 - 422.
14. Svirskii, M.S. and Vonsovskii, S.V., On the Possible Spontaneous Ionization of Interacting Electrons in Crystal, *Fiz. Met. Metalloved.*, 1957, vol. 4, pp. 392 - 399.
15. Vonsovskii, S.V., Svirskii, M.S., and Svirskaya, L.M., On the Theory of Spontaneous Ionization of a Crystal with Interacting Electrons. I. Polar Model: Hubbard's Approximation, *Phys. Met. Metallogr.*, 1992, vol. 74, no. 4, pp. 344 - 351.
16. Vonsovskii, S.V., Svirskii, M.S., and Svirskaya, L.M., On the Theory of Spontaneous Ionization of a Crystal with Interacting Electrons. II. Polar Model: Allowing for the Effects of Transfer Processes, Electrostatic and Exchange Interaction in Couples and in Neighboring Crystal Lattice Sites, *Phys. Met. Metallogr.*, 1992, vol. 74, no. 4, pp. 352 - 359.
17. Vonsovskii, S.V., Svirskii, M.S., and Svirskaya, L.M., On the Theory of Spontaneous Ionization of a Crystal with Interacting Electrons. III. Polar Model: Insulating and Conducting States, *Phys. Met. Metallogr.*, 1992, vol. 74, no. 6, pp. 565 - 572.
18. Landau, L.D., The Theory of Fermi Liquid, *Zh. Eksp. Teor. Fiz.*, 1958, vol. 30, pp. 1058 - 1064; Vibrations of Fermi Liquid, *Zh. Eksp. Teor. Fiz.*, 1958, vol. 32, pp. 59 - 66.
19. Silin, V.P., On the Theory of Degenerate Electron Liquid, *Zh. Eksp. Teor. Fiz.*, 1957, vol. 33, pp. 495 - 500; On the Theory of Anomalous Skin Effect in Metals, *Zh. Eksp. Teor. Fiz.*, 1957, vol. 33, pp. 1282 - 1286; On Optical Properties of Metals in the Infrared Region, *Zh. Eksp. Teor. Fiz.*, 1958, vol. 34, pp. 707 - 713; Vibrations of Degenerate Electron Liquid, *Zh. Eksp. Teor. Fiz.*, 1958, vol. 35, pp. 1243 - 1250.
20. Abrikosov, A.A., Gor'kov, L.P., and Dzyaloshinskii, I.E., *Methods of Quantum Field Theory in Statistical Physics*, New York: Dover, 1975.
21. Platzman, P.M. and Wolff, P.A., *Waves and Interactions in Solid State Plasmas*, New York: Academic, 1973.
22. Silin, V.P., The Theory of Degenerate Electron Liquid and Electromagnetic Waves in Metals, *Fiz. Met. Metalloved.*, 1970, vol. 29, pp. 681 - 734.
23. Ceperley, D.M. and Adler, B.J., Ground State of the Electron Gas by a Stochastic Method, *Phys. Rev. Lett.*, 1980, vol. 45, pp. 566 - 568.
24. Irkhin, Yu.P., *sd*-Hybridization and Paramagnetic Susceptibility of the Transition Metals, *Pis'ma Zh. Eksp. Teor. Fiz.*, 1980, vol. 32, pp. 205 - 209.

25. Guletskii, P.G., Knyazev, Yu.V., Kirillova, M.M., and Sandratskii, L.M., Effect of Spin Disordering on Optical Properties of Iron, *Fiz. Met. Metalloved.*, 1989, vol. 67, pp. 279 - 286.
26. Herring, C., Exchange Interactions among Itinerant Electrons, *Magnetism*, Rado, G.T. and Suhl, H., Eds., New York: Academic, 1966, vol. IV.
27. Clauberg, R., Haines, E.M., and Feder, R., Effects of Short-Range Magnetic Order on Photoemission and Inverse Photoemission Spectra in Iron, *Z. Phys. B.*, 1985, vol. 62, pp. 31 - 41.
28. Moriya, T., *Spin Fluctuations in Itinerant Electron Magnetism*, Berlin: Springer, 1985.
29. Hohenberg, P. and Kohn, W., Inhomogeneous Electron Gas, *Phys. Rev. B*, 1964, vol. 136, pp. 864 - 871.
30. Gunnarsson, O. and Lundquist, B.J., Exchange and Correlation in Atoms, Molecules, and Solids in Spin Density Functional Formalism, *Phys. Rev. B*, 1976, pp. 4274 - 4296.
31. *Theory of the Inhomogeneous Electron Gas*, Lundquist, S. and March, N.H., Eds., New York: Plenum, 1983.
32. Rajagopal, A.K., The Density Functional Approach, *Advances in Chemical Physics*, Prigogine, I. and Rice, S.A., Eds., New York: Wiley, 1980, vol. 41, pp. 59 - 200.
33. Malozemoff, A.P., Williams, A.R., and Moruzzi, V.L., "Band-Gap Theory" of Strong Ferromagnetism: Application to Concentrated Crystalline and Amorphous Fe- and C-Metalloid Alloys, *Phys. Rev. B*, 1984, vol. 29, pp. 1620 - 1631.
34. Methfessel, M. and Kübler, J., Bond Analysis of Heats of Formation: Application to Some Group VIII and Ib Hydrides, *J. Phys. F: Metal Phys.*, 1982, vol. 12, pp. 141 - 162.
35. Christensen, N.E., "Force Theorem" and Elastic Constants of Solids, *Solid State Commun.*, 1984, vol. 49, pp. 701 - 706.
36. Gyorffy. B.L., Pindor, A.J., Staunton, J., *et al.*, Electronic Structure of Metallic Ferromagnets above the Curie Temperature, *J. Phys. F: Metal Phys.*, 1985, vol. 15, pp. 1337 - 1386 and 1387 - 1404.
37. Liechtenstein, A.I., Katsnelson, M.I., Antropov, V.P., and Gubanov, V.A., Local Spin Density Functional Approach to the Theory of Exchange Interactions in Ferromagnetic Metals and Alloys, *J. Magn. Magn. Mater.*, 1987, vol. 67, pp. 65 - 74.
38. Slater, J., *The Self-Consistent Field for Molecules and Solids*, New York: McGraw-Hill, 1974.
39. Katsnel'son, M.I. and Trefilov, A.V., On Electronic Phase Transitions due to Correlation Effects, *Pis'ma Zh. Eksp. Teor. Fiz.*, 1984, vol. 40, pp. 303 - 309; Density of States and Anomalies of Electronic and Lattice Properties of Metals and Alloys, *Usp. Fiz. Nauk*, 1988, vol. 154, pp. 523 - 525.
40. Katsnelson, M.I. and Trefilov, A.V., Anomalies in Properties of Metals and Alloys due to Electron Correlations, *Phys. Lett. A*, 1985, vol. 109, pp. 109 - 112.
41. Vonsovsky, S.V., Katsnelson, M.I., and Trefilov, A.V., Anomalies in Properties of *d*- and *f*-Metals and Alloys due to Charge Density Fluctuations, *J. Magn. Magn. Mater.*, 1986, vol. 61, pp. 83 - 87.
42. Mott, N.F., *Metal–Insulator Transitions*, London: Taylor & Francis, 1974.
43. Anderson, P.W., 50 Years of the Mott Phenomenon: Insulators, Magnets, Solids, and Superconductors as Aspects of Strong-Repulsion Theory, *Frontiers and Borderlines in Many-Particle Physics* (Enrico Fermi Int. School of Physics, 104), Amsterdam: North Holland, 1988.
44. Stewart, G.P., Heavy Fermion Systems, *Rev. Mod. Phys.*, 1984, vol. 56, pp. 755 - 787.
45. Lee, P.A., Rice, T.M., Serene, J.W., *et al.*, Theories of Heavy-Electron Systems, *Commun. Cond. Mat. Phys.*, 1986, vol. 12, pp. 99 - 161.
46. Brovman, E.T. and Kagan, Yu.M., Phonons in the Nontransition Metals, *Usp. Fiz. Nauk*, 1974, vol. 112, pp. 369 - 426.
47. Wilson, A.H., The Theory of Electronic Semiconductors, *Proc. Roy. Soc. A*, 1931, vol. 133, pp. 458 - 470; vol. 134, pp. 277 - 290.
48. Schubin, S.P., On the Theory of Liquid Metals, *Phys. Z. UdSSR*, 1939, vol. 5, pp. 81 - 105.
49. Lifshitz, I.M., Azbel', M.Ya., and Kaganov, M.I., *Elektronnaya Teoriya Metallov* (An Electron Theory of Metals), Moscow: Nauka, 1971.
50. Schoenberg, D., *Magnetic Oscillations in Metals*, Cambridge: Cambridge University, 1984.
51. Phillips, J.C. and Kleinman, L., New Method for Calculating Wave Function in Crystals and Molecules, *Phys. Rev.*, 1959, vol. 116, pp. 287 - 294.
52. Ziman, J., The Calculation of Bloch Functions, *Solid State Physics*, New York: Academic, 1971, vol. 26.
53. Fermi, E., Sulmoto dei Neutroni nelle sostaze idragenate, *Ric. Scientifica*, 1936, vol. 7(2), pp. 13 - 52.
54. Bachelet, G.B., Hamann, D.R., and Schluter, M., Pseudopotentials that Work: from H to Pu, *Phys. Rev. B*, 1982, vol. 26, pp. 4199 - 4228.
55. Zein, N.E., Kamyshenko, V.V., and Samolyuk, G.D., First-Principles Pseudopotentials for Simple Metals, *Fiz. Tverd. Tela*, 1990, vol. 32, pp. 1846 - 1853.
56. Cohen, M., Pseudopotential and Total Energy Calculations, *Phys. Scr.*, 1982, vol. T1, pp. 5 - 10.
57. Ho, K.M., Fu, C.L., Harmon, B.N., *et al.*, Vibrational Frequencies and Structural Properties of Transition Metals via Total Energy Calculations, *Phys. Rev. Lett.*, 1982, vol. 49, pp. 673 - 676.
58. Chen, Y., Ho, K.M., and Harmon, B.N., First-Principles Study of the Pressure-Induced BCC–HCP Transition in Ba, *Phys. Rev. B*, 1988, vol. 37, pp. 283 - 288.
59. Migdal, A.V., *Teoriya Konechnykh Fermi Sistem i Svoistva Atomnykh Yader* (Theory of Finite Fermi Systems and Properties of Atomic Nuclei), Moscow: Nauka, 1983.
60. Geldart, D.J. and Taylor, R., Wave-Number Dependence of the Static Screening Functions of Interacting Electrons: I. Lowest-Order Hartree-Fock Corrections. II. Higher Order Exchange and Correlation Effects, *Can. J. Phys.*, 1970, vol. 48, pp. 155 - 166.
61. Cracknell, A.P. and Wong, K.C., *The Fermi Surface*, Oxford: Oxford University, 1973.
62. Vaks, V.G., Katsnelson, M.I., Koreshkov, V.G., *et al.*, An Experimental and Theoretical Study of Martensitic Phase Transitions in Li and Na under Pressure, *J. Phys.: Condens. Matter*, 1989, vol. 1, pp. 5319 - 5336.

63. Vaks, V.G. and Trefilov, A.V., On the Theory of Atomic Properties of the Alkali Metals, *Fiz. Tverd. Tela*, 1977, vol. 19, pp. 244 - 258.
64. Vaks, V.G., Kravchuk, S.P., and Trefilov, A.V., Description of the Atomic Properties of the Alkali Metals: Dependence of Its Accuracy on the Pseudopotential Used, *Fiz. Met. Metalloved.*, 1977, vol. 44, pp. 1151 - 1161.
65. Vaks, V.G., Zarochentsev, E.V., Kravchuk, S.P., *et al.*, Thermal Expansion and Grüneisen Parameters in Alkali Metals, *Phys. Status Solidi B*, 1978, vol. 85, pp. 749 - 759.
66. Vaks, V.G., Kravchuk, S.P., and Trefilov, A.V., Martensitic Phase Transitions and Phase Diagrams of Lithium and Sodium under Low Pressure, *Fiz. Met. Metalloved.*, 1977, vol. 19, pp. 3396 - 3399.
67. Bratkovskii, A.M., Vaks, V.G., and Trefilov, A.V., The Theory of Melting of Alkali Metals, *Zh. Eksp. Teor. Fiz.*, 1984, vol. 86, pp. 2141 - 2157.
68. Moruzzi, V.L., Janak, J.P., and Williams, A.R., *Calculated Electronic Properties of Metals*, New York: Plenum, 1978.
69. Fomichev, S.V., Katsnelson, M.I., Koreshkov, V.G., and Trefilov, A.V., On the Effect of Three-Body Interactions and Proximity of the Fermi Level to the Brillouin Zone Faces on Elastic Moduli of Simple Metals, *Phys. Status Solidi B*, 1990, vol. 161, pp. 153 - 164.
70. Katsnel'son, M.I., Peschanskikh, G.V., and Trefilov, A.V., On the Character of Electronic Density-of-States Singularities and Their Effect on Elastic Constants in the Alkaline-Earth Metals, *Fiz. Tverd. Tela*, 1990, vol. 32, pp. 470 - 479.
71. Vaks, V.G., Kapinos, V.G., Osetskii, Yu.N., *et al.*, Application of Interionic Potentials Derived from Model Pseudopotential for Modeling Point Defects and Radiation Effects in Cu, Fe, Ni, Ti, and Zr, *Fiz. Tverd. Tela*, 1989, vol. 31, no. 3, pp. 139 - 149.
72. Greenberg, B.A., Katsnelson, M.I., Koreshkov, V.G., *et al.*, On the Possibility of Description of Lattice Properties of Iridium in Terms of Pseudopential Theory, *Phys. Status Solidi B*, 1990, vol. 158, pp. 441 - 456.
73. Ho, K.M., Louie, S.G., Chelikowsky, J.R., and Cohen, M.L., Self-Consistent Pseudopotential Calculation of the Electronic Structure of Nb, *Phys. Rev. B*, 1977, vol. 15, pp. 1755 - 1759.
74. Katsnel'son, M.I., Soldatov, A.A., and Trefilov, A.V., On the Polarizability of Ion Cores in Metals, *Fiz. Met. Metalloved.*, 1985, vol. 59, pp. 883 - 888.
75. Landau, L.D. and Lifshitz, E.M., *Statisticheskaya Fizika* (Statistical Physics), Moscow: Nauka, 1976.
76. Dorfman, Ya.G., *Diamagnetizm i Khimicheskaya Svyaz'* (Diamagnetism and Chemical Bonding), Moscow: Nauka, 1961; see translated version: Dorfman, Ya.G., Diamagnetism and Chemical Bond, New York: American Elsevier, 1965.
77. Band, I.M., Listengarten, M.A., Trzhaskovskaya, M.V., and Fomichev, V.I., *RAINE Program Package on the Relativistic Atom: Interaction of Electromagnetic Radiation and the Nucleus with Atomic Electrons*, Leningrad: Nuclear Physics Institute, 1976, Preprint 289.
78. Nieminen, R.M. and Puska, M.J., Core Polarizabilities in Metals, *Phys. Scr.*, 1982, vol. 25, pp. 952 - 956.
79. Sharma, J.C., Shanker, J., and Goyal, S.C., Electronic Polarizabilities of Ions, *J. Phys. Chem. Solids*, 1977, vol. 38, pp. 327 - 328.
80. Shanker, J., Sharma, J.C., and Sharma, H.P., Analysis of the Electronic Polarizabilities of Ions in Alkaline Earth Chalcogenides, *J. Phys. Chem. Solids*, 1978, vol. 39, pp. 129 - 132.
81. Berestetskii, V.B., Lifshitz, E.M., and Pitaevskii, L.P., *Kvanotvaya Elektrodinamika* (Quantum Electrodynamics), Moscow: Nauka, 1980.
82. Katsnel'son, M.I. and Trefilov, A.V., The Effect of van der Waals and Born–Mayer Interactions of Ion Cores on the Atomic Properties of the Alkali Metals, *Fiz. Tverd. Tela*, 1988, vol. 30, pp. 3299 - 3310.
83. Rehr, J.J., Zaremba, E., and Kohn, W., Van der Waals Forces in the Noble Metals, *Phys. Rev. B*, 1975, vol. 12, pp. 2062 - 2066.
84. Mon, K.K., Ashkroft, N.W., and Chester, C.V., Core Polarization and the Structure of Simple Metals, *Phys. Rev. B*, 1979, vol. 19, pp. 5103 - 5122.
85. Sturm, K., Core Polarization in the Dielectric Response of Simple Metals, *Solid State Commun.*, 1983, vol. 48, pp. 29 - 32.
86. Mahanty, J. and Taylor, R., Effects of the Space-Dispersion in Dynamical Screening in Metals, *Phys. Rev. B*, 1978, vol. 17, pp. 554 - 559.
87. Slater, J.C., *Electronic Structure of Molecules*, New York: McGraw-Hill, 1963.
88. Heitler, W. and London, F., Wechselwirkung von Neutral Atome und Homopolaren Bindung in Quantum Mechanik, *Z. Phys.*, vol. 44, pp. 455 - 470.
89. Benedek, R., Core Overlap Interaction in Metals, *Phys. Rev. B*, 1977, vol. 15, p. 2902 - 2913.
90. Upadhayaya, J.C., Wang, S., and Moore, R.A., Van der Waals and Repulsive Interactions in the Crystal Structure of Heavy Alkali Metals, *Can. J. Phys.*, 1980, vol. 58, pp. 905 - 911.
91. Fulde, F. and Loewenhaupt, M., Magnetic Excitations in Crystal Field Split 4*f* Systems, *Adv. Phys.*, 1985, vol. 34, pp. 589 - 662.
92. Lawrence, J.M., Riseboreugh, P.S., and Parks, R.D., Valence Fluctuation Phenomena, *Rep. Prog. Phys.*, 1981, vol. 44, pp. 1 - 84.
93. Engelberg, S. and Schrieffer, J.R., Coupled Electron-Phonon Systems, *Phys. Rev.*, 1963, vol. 131, pp. 993 - 1003.
94. Irkhin, V.Yu. and Katsnelson, M.I., Interaction of Conduction Electrons with Local Excitation: The Infrared Divergencies, *Z. Phys. B*, 1988, vol. 70, pp. 371 -378.
95. Anderson, P.W., A Poor Man's Derivation of Scaling Laws for the Kondo Problem, *J. Phys. C*, 1970, vol. 3, pp. 2436 - 2441.
96. Mahan, C., *Many-Particle Physics*, New York: Plenum, 1981.
97. Khomskii, D.I., The Problem of Intermediate Valence, *Usp. Fiz. Nauk*, 1979, vol. 129, pp. 443 - 485.
98. Wachter, P. and Travaglini, G., Intermediate Valence and Hybridization Model: A Study of SmB_6, "Gold" SmS, and YbB_{12}, *J. Magn. Magn. Mater.*, 1985, vol. 47/48, pp. 423 - 428.
99. Kikoin, K.A., On the Nature of the "Gold" Phase of Samarium Sulfide, *Zh. Eksp. Teor. Fiz.*, 1983, vol. 85, pp. 1000 - 1016.

100. Irkhin, V.Yu. and Katsnel'son, M.I., On the Theory of Intermediate-Valence Semiconductors, *Zh. Eksp. Teor. Fiz.*, 1986, vol. 90, pp. 1080 - 1091; Intermediate-Valence Semiconductors in a Magnetic Field, *Fiz. Tverd. Tela*, 1987, vol. 29, pp. 1461 - 1466.
101. Moshchalkov, V.V. and Brandt, N.B., Nonmagnetic Kondo Lattices, *Usp. Fiz. Nauk*, 1986, vol. 149, pp. 585 - 634.
102. Johansson, B., The α–γ Transition in Cerium is a Mott Transition, *Philos. Mag. B*, 1974, vol. 30, pp. 469 - 482.
103. Finkel'shtein, L.D., On the Nature of Tetravalent Ce in the Metal and in its Metallic Compounds, *Fiz. Met. Metalloved.*, 1984, vol. 57, pp. 402 - 405.
104. Wielizka, D., Wesver, I.H., Lynch, D.W., and Ohlson, C.G., Photoemission Studies of α–γ Phase Transition in Ce: Changes in the 4*f* Character, *Phys. Rev. B.*, 1983, vol. 26, pp. 7056 - 7059.
105. Kornstädt, U., Lässer, R., and Lengeler, B., Investigation of the α–γ Transition in Cerium by Compton Scattering, *Phys. Rev. B*, 1980, vol. 21, pp. 1898 - 1901.
106. Podloucky, R. and Glötzel, D., Band Structure, Cohesive Properties, and Compton Profile of α- and γ-Cerium, *Phys. Rev. B*, 1983, vol. 27, pp. 3390 - 3405.
107. Karaziya, R.I., The Collapse of the Excited Electron Orbit and Peculiarities of Atomic Spectra, *Usp. Fiz. Nauk*, 1981, vol. 135, pp. 79 - 115.
108. Kamyshenko, V.V., Katsnel'son, M.I., Liechtenstein, A.I., and Trefilov, A.V., The Collapse of *f* Electrons and Intermediate Valence in Cerium and Uranium Compounds, *Fiz. Tverd. Tela*, 1987, vol. 29, pp. 3581 - 3585.
109. El'yashevich, M.A., *Spektry Redkikh Zemel'* (Spectra of the Rare Earths), Moscow: Gostekhizdat, 1953.
110. Barth, U. and Hedin, L., A Local Exchange-Correlation Potential for the Spin Polarized, *J. Phys. C*, 1972, vol. 5, pp. 1629 - 1642.
111. Abbati, I., Braicovich, L., and Michelis, B., Temperature Dependence of Core Photoemission in $Ce_{24}Co_{11}$, *Solid State Commun.*, 1985, vol. 55, pp. 1081 - 1083.
112. Schlapbach, L., Hüfner, S., and Riesteres, T., Core Level Spectroscopy of Heavy-Fermion Ce Compounds, *J. Phys. C*, 1986, vol. 19, p. L63 - L66.
113. Radtsig, A.A. and Smirnov, B.M., *Parametry Atomov i Atomnykh Ionov. Spravochnik* (A Handbook of the Parameters of Atoms and Atomic Ions), Moscow: Energoizdat, 1986.
114. van Hove, L., The Occurrence of Singularities in the Elastic Frequency Distribution of a Crystal, *Phys. Rev.*, 1953, vol. 89, pp. 1189 - 1196.
115. Papacostantopoulos, D.A., *Handbook of Band Structure of Elemental Solids*, New York: Plenum, 1986.
116. Gor'kov, L.P., On Singularities in the Electronic Spectrum of Compounds with a β-Tungsten Structure, *Pis'ma Zh. Eksp. Teor. Fiz.*, 1974, vol. 20, pp. 571 - 574.
117. Vonsovsky, S.V., Izyumov, Yu.A., and Kurmaev, E.Z., *Superconductivity of Transition Metals, Their Alloys, and Compounds*, Berlin: Springer, 2nd ed., 1982.
118. Weber, W., The Electron–Phonon Interactions in A-15 Structure, *The Electron Structure of Complex System Compounds*, New York: Plenum, 1984.
119. Jan, J.P. and Skriver, H.L., The Electron Structure of Calcium, *J. Phys. F: Metal Phys.*, 1981, vol. 11, pp. 805 - 820.
120. Blaha, P. and Callaway, J., Electronic Structure and Fermi Surface of Calcium, *Phys. Rev. B*, 1985, vol. 32, pp. 7664 - 7669.
121. Antropov, V.P., Katsnel'son, M.I., Liechtenstein, A.I., *et al.*, Electronic Structure, Magnetism, and Lattice Property Anomalies in the Various Phase of Plutonium, *Fiz. Tverd. Tela*, 1990, no. 9, pp. 2782 - 2790.
122. Vaks, V.G., Katsnelson, M.I., Likhtenstein, A.I., *et al.*, Pre-Transition Softening and Anomalous Pressure Dependence of Shear Constants in Alkali and Alkaline-Earth Metals due to Band Structure Effects, *J. Phys.: Condens. Matter*, 1991, vol. 3, pp. 1409 - 1425.
123. Rozenfel'd, E.V. and Irkhin, Yu.P., The Effect of State-Density Singularities on the Paramagnetic Susceptibility of the Transition Metals, *Fiz. Met. Metalloved.*, 1984, vol. 57, pp. 837 - 851.
124. Mott, N.F. and Jones, H., *The Theory of the Properties of Metals and Alloys*, New York: Dover, 1958.
125. Lifshitz, I.M., On Anomalies in the Electronic Characteristics of a Metal in the High-Pressure Region, *Zh. Eksp. Teor. Fiz.*, 1960, vol. 38, pp. 1569 - 1576.
126. Vaks, V.G., Trefilov, A.V., and Fomichev, S.V., On Singularities in the Electrical Resistance and Thermo-EMF of Metals under Phase Transitions (2.5 Order), *Zh. Eksp. Teor. Fiz.*, 1981, vol. 80, pp. 1613 - 1631.
127. Egorov, V.S. and Fedorov, A.I., Thermo-EMF in Lithium–Magnesium Alloys in Transitions of 2.5 Order, *Zh. Eksp. Teor. Fiz.*, 1983, vol. 85, pp. 1647 - 1657.
128. Overcash, D.R., Davis, T., Cook, J.W., and Skonce, M.J., Stress-Induced Electronic Transition (2.5 Order) in Al, *Phys. Rev. Lett.*, 1981, vol. 46, pp. 287 - 290.
129. Ohto, Y. and Shimizu, M., Influence of Shear Strain on the Electronic Structure of Vanadium, *J. Phys. F: Metal Phys.*, 1983, vol. 18, pp. 761 - 777.
130. Lenz, D., Schmidt, H., Ewert, S., Boksch, W., Pott, R., and Wohlleben, D., The Anomalous Bulk Modulus of $CeBe_{13}$, *Solid State Commun.*, 1984, vol. 52, pp. 759 - 763.
131. Anisimov, V.I., Katsnel'son, M.I., Liechtenstein, A.I., and Trefilov, A.V., The Effect of Electronic Density-of-States Peaks on the Structural and Magnetic Instability of Alloys, *Pis'ma Zh. Eksp. Teor. Fiz.*, 1987, vol. 45, pp. 285 - 288.
132. Fulde, P., Introduction to the Theory of Heavy Fermions, *J. Phys. F: Metal Phys.*, 1988, vol.18, pp. 601 - 639.
133. Proc. Int. Conf. on Anomalous Rare Earth and Actinides (Grenoble, 1986), *J. Magn. Magn. Mater.*, 1987, vol. 63 - 64; Proc. 9th Int. Conf. on Crystal-Field Effects and Heavy-Fermion Physics (Frankfurt, 1987), *J. Magn. Magn. Mater.*, 1988, vol. 76 - 77.
134. Katsnelson, M.I. and Trefilov, A.V., Anomalies of Electronic and Lattice Properties of Metals and Alloys Caused by Screening Anomalies, *Physica B*, 1990, vol. 163, pp. 182 - 187.
135. Katsnel'son, M.I. and Trefilov, A.V., Anomalies in Phonon Spectra due to Charge Density Fluctuations, *Pis'ma Zh. Eksp. Teor. Fiz.*, 1985, vol. 42, pp. 393 - 396.
136. Liu, K.L., MacDonald, A.H., Daams, J.M., *et al.*, Spin Density Functional Theory of the Temperature-Dependent Spin Susceptibility, *J. Magn. Magn. Mater.*, 1979, vol. 22, pp. 43 - 57.
137. Ihlemann, J. and Barner, K., Elastic Anomalies and Phonon Damping in a Metallic High Spin–Low Spin System, *J. Magn. Magn. Mater.*, 1984, vol. 46, pp. 40 - 48.
138. Migdal, A.B., Interaction of Electrons with Lattice Vibrations in a Metal, *Zh. Eksp. Teor. Fiz.*, 1958, vol. 34, pp. 1438 - 1446.
139. Hewson, A.C., A Scaling Approach to Locally Coupled Electron-Phonon Systems, *J. Phys. C*, 1981, vol. 14, pp. 2747 - 2758.
140. Hewson, A.C. and Newns, D.M., Polaronic Effects in Mixed- and Intermediate-Valence Compounds, *J. Phys. C*, 1977, vol. 12, pp. 1665 - 1683.
141. Grewe, N. and Entel, F., Lattice Dynamics in Mixed Valence Rare Earth Compounds, *Z. Phys. B*, 1979, vol. 33, pp. 331 - 340.
142. Thalmeier, P., Theory of Elastic Properties of Heavy-Fermion Compounds, *J. Phys. C*, 1987, vol. 20, pp. 4449 - 4466.
143. Liu, S.H., Pseudo-Excitons in Mixed-Valence Metals, *Phys. Rev. B*, 1989, vol. 39, pp. 1403 - 1406.
144. *Superconductivity in Ternary Compounds: I. Structural, Electronic, and Lattice Properties*, Fisher, F. and Marple, M.B., Eds., Berlin: Springer, 1982.
145. Knapp. G.S., Bader, S.D., Culbert, H.V., *et al.*, Heat Capacity of V_3X Compounds and the Relationship between T_C and Anharmonicity, *Phys. Rev. B*, 1975, vol. 11, pp. 4331 - 4339.
146. Stanndenmann, J.L. and Testardi, L.R., X-Ray Determination of Anharmonicity in V_3S, *Phys. Rev. Lett.*, 1979, vol. 43, pp. 40 - 43.
147. Ododo, J.C., Percolation Concentration and Saturation of the Pd Moment in Ferromagnetic Pd Alloys, *J. Phys. F: Metal Phys.*, 1983, vol. 13, pp. 1291 - 1310.
148. Ohlsen, H. and Nordberg, L., Effect of Nickel Impurities on the Conduction Electron Zeeman Splitting in Palladium, *J. Phys. F: Metal Phys.*, 1987, vol. 17, pp. 885 - 892.
149. Izyumov, Yu.A. and Katsnel'son, M.I., On the Dynamics of Oxygen Ions in $YPa_2C_3O_7$, *Fiz. Met. Metalloved.*, 1988, vol. 66, pp. 1083 - 1089.
150. Kurdjumov, G.V., Martensitic Transformations, *Problemy Sovremennoi Fiziki* (Problems of Modern Physics), Leningrad: Nauka, 1980, pp. 396 - 407.
151. Axe, J.D. and Shirane, C., Inelastic, Neutron-Scattering Study of Acoustic Phonon in Nb_3Sn, *Phys. Rev. B*, 1973, vol. 8, pp. 1965 - 1977.
152. Moire, F., Allain, J., and Renker, R., Observation of a Soft-Phonon Mode and a Pre-Martensitic Phase in the Intermetallic Compound $Tu_{50}Ni_{47}Fe_3$ Studied by Inelastic Neutron Scattering, *J. Phys. F: Metal Phys.*, 1984, vol. 14, pp. 2517 - 2523.
153. Kisker, K., Photoemission and Finite Temperature Ferromagnetism of Fe and Ni, *J. Magn. Magn. Mater.*, 1984, vol. 45, pp. 23 - 32.
154. Genoval, P., Manuel, A.A., Walker, E., and Petar, M., Spin-Polarized 2D ACAR in Nickel across the Curie Temperature, *J. Phys.: Condens. Matter*, 1991, vol. 3, pp. 4201 - 4212.
155. Vonsovsky, S.V., *Magnetism*, New York: Wiley & Sons, 1974, vol. I, p. 474; vol. II, p. 794.
156. Silin, V.P., Magnetodeformation Relation and the Equation of State in the Spin Fluctuation Theory of Magnetism, *Fiz. Met. Metalloved.*, 1990, vol. 69, pp. 60 - 67.
157. Landau, L.D. and Lifshitz, E.M., *Kvantovaya Mekhanika. Nerelyativistskaya Teoriya* (Quantum Mechanics: Nonrelativistic Theory), Moscow: Nauka, 1974,
158. Perdew, J.P. and Zunger, A., Self-Interaction Correction to Density Functional Approximation for Many-Electron Systems, *Phys. Rev. B*, 1981, vol. 23, pp. 5048 - 5079.
159. Dederichs, P.H., Zeller, R., Akai, H., *et al.*, *Ab Initio* Calculations for Impurities in Cu and Ni, *Philos. Mag. B*, 1985, vol. 51, pp. 137 - 150.
160. Kittel, C., *Quantum Theory of Solids*, New York: Wiley & Sons, 1963.
161. Liechtenstein, A.I., Katsnelson, M.I., and Gubanov, V.A., Exchange Interactions and Spin-Wave Stiffness in Ferromagnetic Metals, *J. Phys. F: Metal Phys.*, 1984, vol. 14, pp. L125 - L128.
162. Mackintosh, A.R. and Andersen, O.K., The Electronic Structure of Transition Metals, *Electron on Fermi Surface*, Springford, M., Ed., London: Cambridge University, 1980, pp. 149 - 220.
163. Gilat, G., Possible Effects of van Hove Singularities on Specific Heat of Solids, *Phys. Rev. Lett.*, 1969, vol. 23, pp. 78 - 81.
164. Oguchi, T., Terakura, K., and Hamada, N., Magnetism of Iron above the Curie Temperature, *J. Phys. F: Metal Phys.*, 1983, vol. 1, pp. 145 - 160.
165. Ziman, J.M., *Model of Disorder: The Theoretical Physics of Homogeneously Disordered Systems*, London: Cambridge University, 1979.
166. Liechtenstein, A.I., Katsnelson, M.I., and Gubanov, V.A., Local Spin Excitations and Curie Temperature of Iron, *Solid State Commun.*, 1985, vol. 54, pp. 327 - 329.
167. Anisimov, V.I., Antropov, V.P., Gubanov, V.A., *et al.*, The Band Theory of Magnetism in Metals and Alloys, *Usp. Fiz. Nauk*, 1988, vol. 155, pp. 721 - 724.
168. Turzhevskii, S.A., Liechtenstein, A.I., and Katsnel'son, M.I., On Localization of Magnetic Moments and Non-Heisenberg Character of Exchange Interactions in Metals and Alloys, *Fiz. Tverd. Tela*, 1990, vol. 32, no. 7, pp. 1952 - 1960.